

**DEVELOPMENT AND ANALYSIS OF A DRUM-SHAPED
COMPACT MICROSTRIP ANTENNA**

A thesis submitted by

JACOB GEORGE

in partial fulfilment of the requirements for the degree of
DOCTOR OF PHILOSOPHY

DEPARTMENT OF ELECTRONICS
FACULTY OF TECHNOLOGY, COCHIN UNIVERSITY OF SCIENCE AND TECHNOLOGY
COCHIN 682 022, INDIA

JUNE 1998

*To my Parents, my Brother
and
to my Teachers*

CERTIFICATE

This is to certify that this thesis entitled "**DEVELOPMENT AND ANALYSIS OF A DRUM-SHAPED COMPACT MICROSTRIP ANTENNA**" is a bona fide record of the research work carried out by Mr. Jacob George under my supervision in the Department of Electronics, Cochin University of Science and Technology. The results presented in this thesis or part of it have not been presented for any other degree.



Dr. P. MOHANAN
(Supervising Teacher)
Reader

Cochin 682 022
26th June 1998

Department of Electronics
Cochin University of Science and Technology

DECLARATION

I hereby declare that the work presented in this thesis entitled "**DEVELOPMENT AND ANALYSIS OF A DRUM-SHAPED COMPACT MICROSTRIP ANTENNA**" is based on the original work done by me under the supervision of Dr. P. Mohanan, in the Department of Electronics, Cochin University of Science and Technology, and that no part thereof has been presented for the award of any other degree.

Cochin 682 022
26th June 1998



JACOB GEORGE

Acknowledgements

I would like to express my deepest sense of gratitude to my research guide, Dr. P. Mohanan, Reader, Department of Electronics, Cochin University of Science and Technology, Kerala, India, for his excellent guidance, constant encouragement and affection through out the course of this work. It has been really a pleasure and privilege working under him.

I am deeply indebted to Dr. K.G. Nair, former Head of the Department of Electronics for his timely suggestions and encouragements which were indispensable for the successful completion of this work.

I would like to thank Dr. C.S. Sridhar, former Head and Dr. P.R.S. Pillai, Head, Department of Electronics for their valuable suggestions and helps during my research.

Let me express my deep felt sense of gratitude to Dr. C.K. Aanandan, Lecturer, Department of Electronics for his valuable suggestions and encouragements.

Sincere thanks are due to Dr. K. Vasudevan, Dr. K.T. Mathew and Dr. K.A. Jose, faculty members, Department of Electronics for their invaluable suggestions and help. My sincere thanks are due to Dr. E.J. Zachariah, Joint Director, STIC, Cochin for the help and encouragements extended to me.

The help and valuable advices extended to me by Dr. Ramesh Garg, Professor, Department of Electronics and Electrical Communication Engineering, IIT, Kharagpur, for the theoretical analysis is gratefully acknowledged.

During different phases of my research work, I was enjoying financial support from different Government funding agencies. The financial assistance I received from Department of Electronics (DoE), University Grants Commission (UGC) and Council for Scientific and Industrial Research (CSIR) are acknowledged.

I take this opportunity to place on record the cooperation, help and encouragements I received from my friends Mr. Paul V. John, STIC, CUSAT and Mr. Deepukumar M. Nair, Corning Inc., USA.

I would like to acknowledge with thanks the splendid cooperation from Dr. K.K. Narayanan, Lecturer in Physics, S.D. College, Alapuzha, Dr. U. Raveendranath, Lecturer, Department of Electronics, CUSAT, Mr. Sebastian Mathew, Lecturer in Physics, K.E. College, Mannanam, Mr. Joe Jacob, Lecturer in Physics, Newman College, Thodupuzha, Dr. Thomaskutty Mathew, Lecturer in Physics, Christ College, Irinjalakkuda, Dr. D. Saji Stephen, Lecturer in Physics, University College, Trivandrum, Mr. Anandakumar V., Lecturer in Physics, NSS College, Nenmara, Mr. V.P. Joseph, Lecturer in Physics, Christ College, Irinjalakkuda and Mr. Bijukumar S, Research Scholar, Department of Electronics, CUSAT.

The encouragements and cooperation I received from Dr. J. Jagannath Bhatt and Dr. R. Sumangala, Scientist officers, STIC are thankfully acknowledged. A special expression of gratitude is reserved for Mr. G. Gireesh, Research Scholar, STIC.

My acknowledgements would be incomplete, if a mention is not made of the kind cooperation and affection extended to me by Mrs. Beena Aanandan, former Librarian, Department of Electronics. It is with great pleasure that I acknowledge the helps rendered by Mr. Suresh, Librarian, Mr. P.M. Ibrahimkutty and other non-teaching staff members.

Jacob George

CONTENTS

Chapter I

INTRODUCTION

I

- I.1 Microstrip antennas 2
 - I.1.1 Radiation from a microstrip antenna 3
 - I.1.2 Excitation techniques 4
 - I.1.2.1 Microstrip feed 4
 - I.1.2.2 Coaxial feed 5
 - I.1.2.3 Buried feed 6
 - I.1.2.4 Slot feed 7
 - I.1.3 Broadband microstrip antennas 7
 - I.1.4 Compact microstrip antennas 8
 - I.1.5 Models/Techniques used in the analysis of microstrip antennas 8
 - I.1.5.1 Transmission line model 9
 - I.1.5.2 Cavity model 9
 - I.1.5.3 Method of moments 9
 - I.1.5.4 Finite element method 10
 - I.1.5.5 Finite difference time domain method 10
 - I.1.5.6 Green's function method 10
 - I.1.5.7 Segmentation technique 11
- I.2 Outline of the present work 11
- I.3 Chapter organisation 12

- 2.1 Microstrip antennas-brief review 14
- 2.2 Compact microstrip antennas 26

- 3.1 Fabrication of microstrip antennas 33
 - 3.1.1 Photolithographic technique 34
 - 3.1.2 Fast fabrication process 34
- 3.2 Excitation techniques 36
- 3.3 Measurement of return loss, resonant frequency and bandwidth 36
- 3.4 Measurement of radiation pattern 37
- 3.5 Measurement of gain 39
- 3.6 Measurement of electric field intensity 39
- 3.7 Theoretical analysis of the antenna 40

- 4.1 Resonant modes and excitation techniques 44
 - 4.1.1 Resonant modes 44
 - 4.1.2 Excitation techniques 45
- 4.2 Characteristics of the TM_{01} mode 49
 - 4.2.1 Resonant frequency variation with respect to central width (W) 49
 - 4.2.2 Impedance bandwidth 63
 - 4.2.3 Radiation pattern 63
 - 4.2.4 Gain 78
 - 4.2.5 Mode identification through near field probing 78
- 4.3 Characteristics of TM_{10} mode 82
 - 4.3.1 Resonant frequency 82
 - 4.3.2 Impedance bandwidth 87
 - 4.3.3 Radiation pattern 87

- 5.1 Introduction 93
- 5.2 Analysis 93
 - 5.2.1 Magnetic wall model formation 94
 - 5.2.2 Segmentation 95
 - 5.2.3 Multiport connection method 100
 - 5.2.4 Resonant frequency 102
 - 5.2.5 Electric field variation 107
 - 5.2.6 Aperture model development 113
 - 5.2.7 Determination of radiation pattern 116

- 5.2.8 Determination of power radiated 120
- 5.2.9 Stored energy in the cavity 125
- 5.2.10 Quality factor 127
- 5.2.11 Input Impedance 127

Chapter 6

CONCLUSIONS 136

- 6.1 Inferences from experimental investigations 136
- 6.2 Inferences from theoretical investigations 138
- 6.3 Some possible applications of the proposed antenna 139
- 6.4 Scope for further work in the field 140

Appendix A

COMPACT DUAL FREQUENCY MICROSTRIP ANTENNA 141

- A.1 Introduction 141
- A.2 Design details and experimental setup 142
- A.3 Experimental results and discussion 142
- A.4 Conclusions 146

Appendix B

BROADBAND DUAL FREQUENCY MICROSTRIP ANTENNA 147

- B.1 Introduction 147
- B.2 Design and experimental details 148
- B.3 Results 149
- B.4 Theoretical analysis 151
- B.5 Conclusions 153

Appendix C

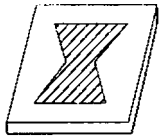
DIELECTRIC RESONATOR LOADED MICROSTRIP ANTENNA FOR ENHANCED IMPEDANCE BANDWIDTH AND EFFICIENCY 154

- C.1 Introduction 154
- C.2 Design details and experimental setup 155
- C.3 Experimental results and discussion 156
- C.4 Conclusions 158

REFERENCES 160

INDEX 170

LIST OF PUBLICATIONS OF THE AUTHOR 175



INTRODUCTION

In 1886, Heinrich Rudolph Hertz, the father of electromagnetics, in his Karlsruhe laboratory, generated, transmitted and received electromagnetic energy by means of an end loaded half-wave dipole as transmitter and a resonant square loop antenna as receiver. This was the birth of a new field called antennas. "*Antennas are like electronic eyes and ears*" [18]. They act as interface between free space and circuitry. According to Institute of Electrical and Electronics Engineers (IEEE) an antenna is defined as "*a means for radiating or receiving radio waves*" [4]. Hertz has observed that when sparks were produced at a gap at the centre of a dipole, sparking also observed at a gap in the nearby loop. This was a memorable event in the history of science and this invention triggered talented scientists all over the world to generate and transmit electromagnetic waves efficiently.

In 1897, J.C. Bose, the talented Indian Scientist, experimented at very short waves with

a new type of antenna called electromagnetic horn. The works of Hertz and Bose, inspired Guglielmo Marconi and he erected large monoconical wire antennas for longwave transatlantic communication. In 1901, he succeeded in transmitting the first wireless signal across the Atlantic. Since then, many researchers around the world conducted brain storming work towards the development of various types of antennas to meet different applications. The early history of electromagnetic waves before 1900 is well reviewed by Ramsay [12].

According to Prof. J.D. Kraus[18, 5], antennas can be classified on the basis of the material from which it is made of as

- a. antennas made of conductors of wire or tubing
- b. antennas made of sheet conductors
- c. antennas made of dielectrics
- d. array antennas

Different types of helices, linear conductor antennas and loops are coming in group (a). Category (b) consists of reflectors, guiding, slotted and microstrip antennas. Group (c) is constituted by lenses, polyrods and slabs. The last group is divided into driven, parasitic, adaptive, interferometric and digital beam forming arrays.

The rapid developments in the present day communication systems (personal communication systems, mobile satellite communication systems, etc.) demand planar low profile and conformal antennas. Microstrip antennas are satisfying all the above requirements and therefore they are fast replacing conventional antennas in the above areas.

1.1 MICROSTRIP ANTENNAS

The microstrip antenna concept was first proposed by Deschamps [19] in 1953. Since then, it took nearly 20 years for the first practical microstrip antennas to come up. The first practical

microstrip antennas were developed by Howell [22] and Munson [23] in the early 1970's and this set the pace of research and development in the area of microstrip antennas all over the world.

The basic configuration of a microstrip antenna is shown in Figure 1.1. It consists of a planar radiating structure of any geometrical shape over a ground plane separated by a thin dielectric substrate. Commonly used microstrip radiating geometries are rectangular and circular. However, other shapes are also considered depending upon the application. These antennas have got many advantages like light weight, low volume, low profile planar configuration that can be made conformal, low fabrication cost, etc., compared to conventional microwave antennas. However, they have some serious drawbacks like narrow bandwidth, low gain, radiation in one half plane, poor isolation between the feed and the radiating element, etc.

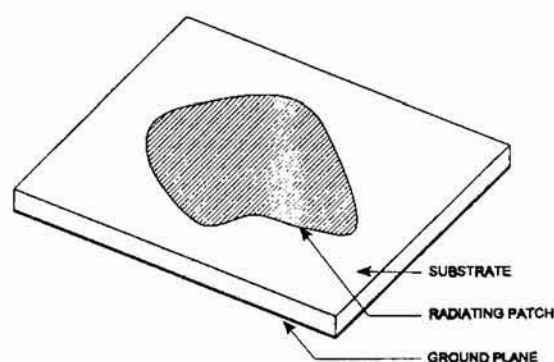


FIGURE 1.1 Basic microstrip antenna configuration

1.1.1 Radiation from a Microstrip Antenna

The radiation from microstrip antennas occurs from the fringing fields between the edge of the microstrip antenna conductor and the ground plane. For a rectangular microstrip antenna fabricated on a thin dielectric substrate and operating in the fundamental mode, there is no field variation along the width and thickness. The fields vary along the length, that is about half a wavelength long. These electric field configurations are shown in Figure 1.2.

The radiation mechanism may be explained by resolving the fringing fields at the open circuited edges into normal and tangential components with respect to the ground plane. The normal components are out of phase (as the patch is half wavelength long) and hence the far field produced by them cancel each other. Whereas, the tangential components are in phase and the resulting fields are combined to give maximum radiation in the broadside direction.

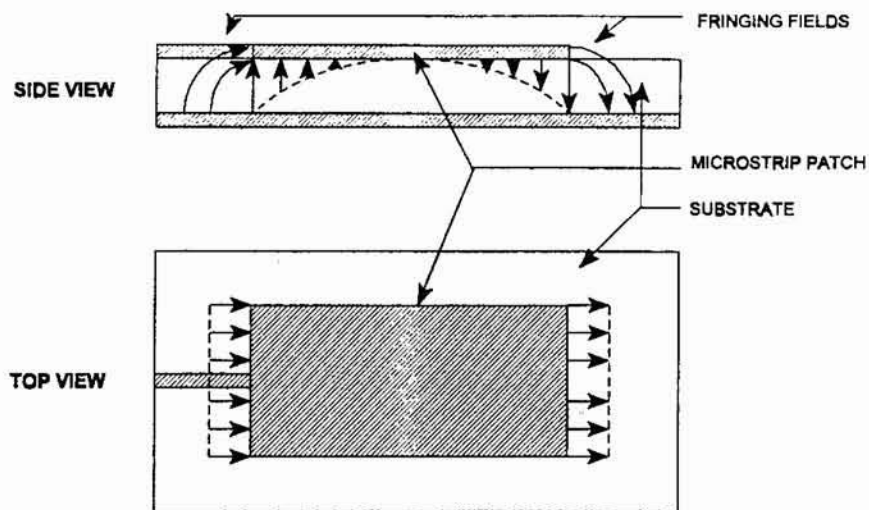


FIGURE 1.2. Field variation along the length and width of a rectangular microstrip antenna

1.1.2 Excitation techniques

The selection of an appropriate feeding mechanism to couple power to a microstrip antenna is as important as the selection of a suitable geometry for a particular application. A variety of feeding mechanisms are available and some important techniques are explained here.

1.1.2.1 Microstrip feed

This is the simplest way to feed electromagnetic power to a microstrip antenna. Here, the antenna and the feed line are fabricated simultaneously on the same side of the substrate as shown in Figure 1.3 and this makes it very attractive in array environments. The most undesirable feature

of this feeding mechanism is the spurious radiation from bends, transitions, junctions, etc. These radiations adversely affect the side-lobe level and cross-polarisation characteristics of the antenna. This drawback may be compensated by suitably selecting a high dielectric constant substrate. In fact, this will reduce the radiation efficiency of the antenna. A compromise between the two is to be made depending upon the applications.

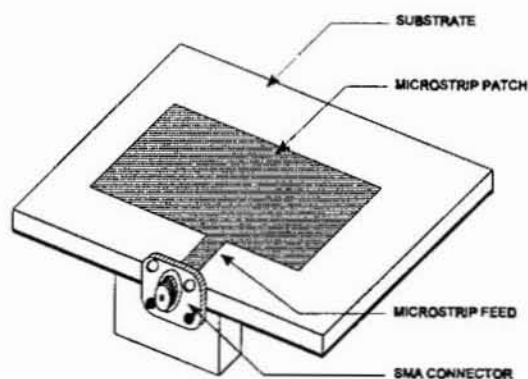


FIGURE 1.3. Microstrip feeding arrangement

1.1.2.2 Coaxial feed

It is a convenient method of feeding a single patch. Here, the coaxial connector is attached to the backside of the printed circuit board and the centre conductor is attached to the antenna at the desired point. The coaxial (probe) feeding arrangement is shown in Figure 1.4. Here, as the feed lies behind the radiating surface, there is no question of unwanted radiation from the feed for thin substrates. In fact, for thick substrates, the coupling between adjacent feeds may deteriorate the performance. In array environment, the complete antenna and feeding arrangement cannot be etched simultaneously. This increases the feeding complexity, especially in large arrays. At high frequencies, it becomes very difficult to realise these types of feeding as it involves drilling

holes through the substrate and proper soldering of the centre conductor to the patch.

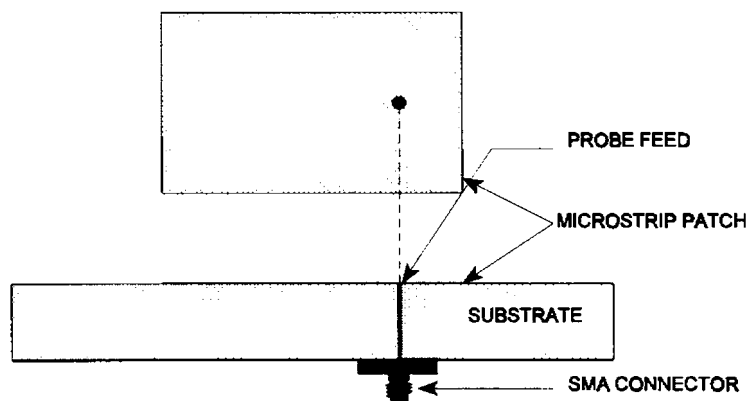


FIGURE 1.4 Coaxial(probe) feeding of a microstrip antenna

1.1.2.3 Buried feed (electromagnetic coupling)

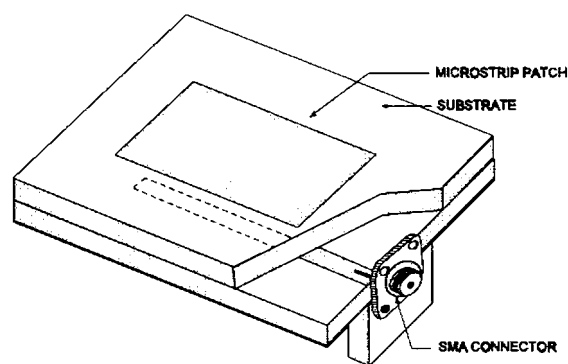


FIGURE 1.5 Buried feeding arrangement

In this type of feeding, the antenna and the feed are placed at different levels. i.e., the feed system is a covered microstrip line and the radiating element is etched on the covering substrate immediately above the open-ended feed line. The radiating element is thus parasitically coupled to the feed line. The system can be considered as a microstrip patch on a double layered substrate sharing a common ground plane with the feed as shown in Figure 1.5. Like the microstrip feed

system, this arrangement also suffers from spurious radiation from the feed network. This may be minimised by using substrates of high dielectric constant for the feedline.

1.1.2.4 Slot feed (aperture coupling)

This feeding arrangement utilises a common ground plane to separate the feed and the radiating geometry. The coupling between the two is provided by a slot etched on the ground plane. The aperture should be placed accurately below the patch and above the feed line as shown in Figure 1.6. Here, spurious radiation from the line is physically separated from that of the patch and can be completely avoided by enclosing the feed within a box. To avoid radiation towards the backside of the antenna, the slot must not resonate within the operating frequency band of the patch and should be placed far enough from the edge of the patch.

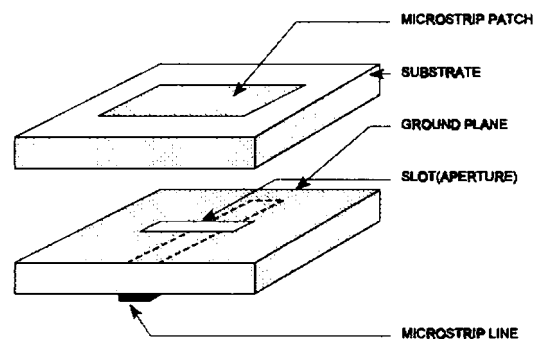


FIGURE 1.6 Slot (aperture) feeding arrangement

1.1.3 Broadband microstrip antennas

One major drawback of microstrip antennas, which limits its widespread application, is the narrow impedance bandwidth. There are different approaches for improving the impedance bandwidth of microstrip antennas. They include: using thicker substrates with low dielectric constant, addition of a parasitic patch on top of the original patch by using a separate dielectric substrate as support, using multiple patches in one plane and by means of proximity coupling of

feed line to the patch antenna.

The use of thicker substrates for bandwidth enhancement is limited by the excitation of surface waves. In the case of using parasitic patches, each element resonates at adjacent frequencies and as a result the impedance bandwidth improves. The parasitic loading will usually increase the overall surface area. In Appendix C, one new method for the enhancement of impedance bandwidth of microstrip antennas is described in detail. Appendix B demonstrates the enhancement in impedance bandwidth through proximity coupling.

1.1.4 Compact microstrip antennas

Depending upon the application, microstrip antennas having different geometrical shapes are used [7]. Commonly used geometries are rectangular and circular. However, recent developments in Personal Communication Systems (PCS), demand more and more compact microstrip antennas. This is clear from the review presented in the next chapter. The important approaches for reducing the size of microstrip antennas include: the use of new geometrical shapes, use of shorting posts, use of a high dielectric constant substrate, etc. A detailed review of the works towards the development of compact microstrip antennas is also included in Chapter 2.

1.1.5 Models/techniques used in the analysis of microstrip antennas

Different methods are available in literature for the analysis of microstrip antennas. For antennas having regular geometrical shapes (rectangular), analytical techniques like cavity model and transmission line model can be applied. For geometries which can be readily divided into few regular geometrical shapes, these analytical techniques could be applied along with segmentation technique. These techniques are unsuitable in the case of arbitrary shaped patches. Here numerical techniques like Finite Element Method (FEM), Finite Difference Time Domain

method (FDTD), etc., could be used. Some important techniques used for the analysis of Microstrip Antennas are described briefly in the following sessions.

1.1.5.1 Transmission line model

This model was proposed by Munson [23] and Demeryd [26]. Here the microstrip resonator is represented by two radiating slots (corresponding to the two radiating edges) separated and connected by an approximately half wavelength ideal transmission line. The input impedance is determined as a function of the distance from the edge of the patch to the feed point. The different radiation characteristics are determined by assuming that the fields vary along the length of the patch and remain constant across the width. The main shortcoming of this model is that, it is applicable only to rectangular (or square) patch geometries.

1.1.5.2 Cavity model

Here, the microstrip geometry is considered as a cavity bounded at its top and bottom by electric walls and on its sides by a magnetic wall. The magnetic current flowing on the cavity side walls radiate at the resonant frequencies of the cavity, which is assumed to be surrounded by free space. This model is suitable for geometries in which the Helmholtz equation possesses an analytical solution such as disks, rectangles, triangles, ellipses, etc.

1.1.5.3 Method of moments

In method of moments, the electric surface currents flowing over the patch metallisation and the ground planes are evaluated by using the Richmond's reaction method [13]. The reaction integral equation is solved using the boundary conditions and method of moments. Now using suitable expansion functions for electric surface currents, the integral equations are reduced to algebraic equations. These equations are then solved for the unknown coefficients using any of the known numerical techniques. This technique is analytically simple and versatile, but it requires large

amounts of computation. The limitation of this technique is usually the speed and storage capacity of the computer.

1.1.5.4 Finite element method (FEM)

The finite element method is a computer aided mathematical technique for obtaining approximate numerical solutions for the abstract equations of calculus that predict the response of physical systems subjected to external influences. In the case of microstrip antennas, the fields interior to the antenna cavity can be determined by this method. Here the region of interest is subdivided into small areas or volumes depending upon the dimensions of the region. Usually these small regions are polygons such as triangles and rectangles for two dimensional problems and tetrahedral elements for three dimensional problems. The interior electric field, satisfying the inhomogeneous wave equation along with an impedance boundary condition on the perimeter walls, is solved for each of the elements subdividing the region of interest. This method is applicable to arbitrary shaped patches also.

1.1.5.5 Finite Difference Time Domain (FDTD) method

This is a method which can be applied to all kinds of antennas for all types of feeds [82]. This method consists of a discretisation and a solution of the Maxwell's curl equations directly in the time domain. In FDTD, microstrip antennas are treated in the time domain for analysis. The frequency dependence of the different parameters are determined from the Fourier transform of the transient current. However, this method becomes computationally costly and requires large amounts of memory when the structure becomes complex.

1.1.5.6 Green's function method

This method can be employed when the shape of the microstrip radiating structure is simple, such

as rectangle, triangle or circle. The electric field inside the cavity is evaluated using Green's function and which in turn is used for the evaluation of the input impedance. This method is not suitable in the case of arbitrary geometrical shapes as the Green's functions are not available.

1.1.5.7 Segmentation technique

When the geometrical shape of the microstrip antenna is neither simple nor completely arbitrary, but is a composite of simple geometrical shapes for which the Green's functions are available, the segmentation method can be used. This method gives us the overall performance of the structure from a knowledge of the contributions from the segments constituting it. Here the effect of radiation loss from the periphery is incorporated through impedance loading of the patch at the periphery. The main disadvantage of this method is that radiation losses should be known in advance. This is very difficult to estimate in the case of arbitrary shaped antennas.

1.2 OUTLINE OF THE PRESENT WORK

The fast developments in the area of communication systems demand compact microstrip antennas suitable for use in MMIC's, satellite mobile communication system, personal communication systems, etc. In this thesis, the theoretical and experimental investigations towards the development of a new compact microstrip antenna is presented. The experimental investigations revealed that, the new antenna requires very less area compared to commonly used rectangular microstrip antennas. It also provides a method for reducing the resonant frequency without increasing the overall area of the patch. The investigations also revealed that the size reduction has been achieved without much sacrifice of the gain.

As the compact antenna does not have a regular geometrical shape (such as rectangular, circular, etc.), the analytical techniques like cavity model and transmission line model cannot be applied directly. But, popular numerical techniques like finite element method and finite

difference time domain method, etc., could be used. Here, the geometry is not completely arbitrary and can be readily divided into few regular geometrical shapes with very less effort, a combination of segmentation technique, cavity model and spatial Fourier transform technique are used for the analysis.

For the analysis, the new geometry is divided into four triangular and one rectangular segment (whose Green's functions are known). The continuous interconnection between different segments are now replaced by interconnection only at a number of discrete points. Each segment is now considered as a multiport planar network and the impedance matrix elements of them are computed. Through multiport interconnection method they are combined together to get the input reactance of the lossless (as the radiation, dielectric and surface wave losses are not accounted) cavity under the patch. From the input reactance variation, the resonant frequency is determined and the electric field variation along the periphery is computed to identify the mode of operation. These field variations are also used for the evaluation of the radiation patterns through spatial Fourier transform technique. The power radiated and the energy stored under the patch are determined to compute the cavity Q-factor. Now the different losses are incorporated as an effective loss tangent, which is nothing but the reciprocal of the Q-factor. This effective loss tangent modifies the dielectric constant to a complex value, which in turn is used for the evaluation of impedance matrix to get the actual input impedance of the antenna.

These experimental and theoretical investigations are presented in this thesis. The organisation of different chapters are given in the next section.

1.3 CHAPTER ORGANISATION

In chapter 2, a brief review of the important theoretical and experimental work done in the area of microstrip antennas is presented with an emphasis to compact microstrip antennas.

In chapter 3, the methodology adopted for the investigations is presented. The details of

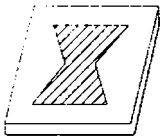
the procedure used for the fabrication of the microstrip antennas are presented. The techniques used for the measurement of different antenna characteristics like resonant frequency, return loss, radiation pattern, etc., are described. The theoretical approach used for the analysis is also briefly mentioned in this chapter.

The important observations and results of the experimental investigations carried out for the different antenna configurations are described in chapter 4.

Chapter 5 describes in detail the theoretical analysis of the antenna. The comparison between theoretical and experimental results are also included in this chapter.

The conclusions drawn from the experimental and theoretical investigations are presented in chapter 6. Some possible applications of the newly developed antenna along with scope for further work are also presented in this chapter.

The experimental work done by the author in related fields are incorporated as three appendices in this thesis. A single feed dual frequency microstrip antenna is presented in Appendix A. Appendix B describes a new broadband dual frequency microstrip antenna. The bandwidth enhancement effect of microstrip antennas through dielectric resonator loading is demonstrated in Appendix C.



EARLIER WORK IN THE FIELD- A BRIEF REVIEW

During the past few decades the researchers all over the world have studied the theoretical and experimental aspects of different types of microstrip antennas. Recently, development and analysis of compact microstrip antennas have become an interesting area in personnel communication systems due to the miniaturization of communication equipment. The relevant works in the field of microstrip antennas are reviewed with emphasis given to compact microstrip antennas.

2.1 MICROSTRIP ANTENNAS - BRIEF REVIEW

Microstrip Antennas are printed circuit antennas for the transmission and reception of

electromagnetic energy. In 1953, Deschamps [19] proposed the concept of microstrip antennas. Shortly thereafter, Gulton [20] developed a flat ariel for ultra-- high frequencies. The concept of microstrip antennas was not active until the early 1970's, when there was an immediate need for low profile antennas on the emerging new generation missiles. Revolution in electronic circuit miniaturisation brought by the developments in Large Scale Integration (LSI) made conventional antennas, bulky and costly part of the equipment. These two factors triggered the scientists for the design and development of compact and efficient Microstrip radiators.

Byron [21] in 1970, described a conducting strip radiator separated from a ground plane by a dielectric substrate. A strip radiator having length of several wavelengths and half wavelength width, was fed at periodic intervals along the radiating edges. This is the first reported Microstrip antenna array in the open literature. Howell [22] in 1972, presented useful data on basic rectangular and circular microstrip patches. Munson [23] in 1974, demonstrated a new class of microstrip wraparound antenna suitable for missiles using microstrip radiator and microstrip feed networks on the same substrate. This low profile microstrip array offered nearly 90% efficiency and nearly omnidirectional coverage. Sanford [24] presented the use of conformal microstrip array for L-band communication from KC-135 aircraft to the ATS-6 satellite. Weinschel [25] reported a practical pentagonal antenna in 1975. He demonstrated its use in a S-band cylindrical array producing circularly polarised patterns for a telemetry link from a sounding rocket.

Mathematical modelling of microstrip antennas was first carried out by the application of transmission line analogies to simple rectangular patches fed at the centre of a radiating wall. It was first proposed independently by Munson [23] and Demeryd [26,27]. The radiating edges were considered as slots that are approximately separated by a half wavelength and connected by an ideal transmission line. This model provides expressions for the radiated fields, radiation resistance, input impedance etc., and was applicable only for patches of rectangular shape.

The radiation mechanism of an open circuited microstrip termination was studied by James and Wilson [28]. They observed that the terminal plane region is the dominant radiating aperture. Theoretical and experimental pattern analysis of different radiating elements showed that they are similar to that of slot radiators.

Agarwal and Bailey [29] proposed the wire grid model for the evaluation of microstrip antenna characteristics. In this model, the microstrip radiating structure is modelled as a fine grid of wire segments and solved for the current on them using Richmond's reaction theorem. From these current values all the antenna characteristics of interest are obtained. This method is useful for the design of microstrip antennas of different geometries like circular disc, circular segment and triangular patches.

Lo *et al.* [30, 31, 32] suggested a new mathematical technique, called cavity model, for the analysis of microstrip antennas. In this model, the upper patch and the section of the ground plane located below it, is joined by a magnetic wall under the edge of the patch. The structure now behaves as a dielectric resonator. The antenna parameters of different patch geometries with arbitrary feed points can be calculated using this approach. The effects of radiation and other losses are introduced in terms of either an artificially increased substrate loss tangent [32] or by employing the impedance boundary conditions.

Newman *et al.* [33, 34] proposed the method of moments for the numerical analysis of microstrip antennas. They used the Richmond's reaction method in connection with method of moments for calculating the unknown surface currents flowing on the walls forming the microstrip patch, ground plane and magnetic walls. This method can be adopted for the calculation of input impedance of microstrip antennas of nonstandard patch shapes.

Hammer *et al.* [35] developed an aperture model for calculating the radiation fields of microstrip antennas. This model accounts radiation from all the edges of the patch and can give the radiation field and the radiation resistance of any mode in a microstrip resonator antenna.

Another numerical analysis based on finite element method is proposed by Carver *et al.* [36] for deciding the fields interior to the microstrip antenna cavity. This is a variational method that gives a solution closest to the true analytical solution. The problem can be solved via the eigen value problem. They analysed a pentagonal shaped patch using this method.

Many researchers have studied dual frequency operation of microstrip antennas at this time. Kerr *et al.* [37] suggested a dual frequency microstrip dish feed consisting of a microstrip element which resonates at one frequency imbedded within another element that resonates at a lower frequency. Schaubert *et al.* [38] suggested a piggy back antenna for dual frequency operation. They used two trapezoidal shaped patches stacked one over the other. McIlvenna *et al.* [39] achieved dual frequency operation from a circular patch antenna by etching two ears (bunny antenna) along with the patch at an angular separation of 60° .

Bartely *et al.* [40] developed a linear array consisting of 16 square elements each fed at two orthogonal points from an underlying stripline layer. This array produced two independent orthogonally polarised beams. Yee and Furlong [41] made a 2x16 element multilayered phased array operating at 970 MHz for remote piloted vehicle. The feed used was 16 way stripline power divider. Azimuth scanning of $\pm 60^\circ$ was provided by four bit diode phase shifter. The designs of a 7.5 GHz receive array for satellite communication was given by Cipolla [42]. In this array radiating elements are placed on one board and feedline, phase shifter and bias line are all placed on a second board. Murphy [43] suggested a special purpose array used for ocean and land surveillance in a space borne radar imaging system. They were the 10.7 x 2.2 m SEASAT array at 1275 MHz and 9.4 x 2.2 m SIR-A array at 1278 MHz. The peak power handled by these antennas are 3000 and 1800 W respectively. Weiss [44] demonstrated a 32x32 element array for 38.4 GHz. Here the *E*- and *H*-plane sidelobes were minimised by proper amplitude tapering.

Wood [45] proposed a new technique for the production of circular polarisation from a compact microstrip antenna based on radiation from curved microstrip transmission lines

supporting a single travelling wave. He has given the theoretical and experimental radiation patterns of circular sector antenna and a spiral antenna. Using these antennas he has achieved an impedance bandwidth of 40% at 10 GHz.

Mink [46] developed a circular ring microstrip antenna, which operates at a substantially low frequency compared to a circular patch antenna of the same size.

R. Chadha *et al.* [47] reported Green's functions for triangular segments in microwave planar circuits. This work enabled the analysis of certain triangular shaped antenna using Green's function method.

A single feed circularly polarised elliptical antenna of small eccentricity is analysed by Shen *et. al.* [48]. Long *et al.* [49] experimentally verified this result.

R. Chadha and K.C. Gupta [50] developed Green's functions of circular sector, annular ring and annular sector shaped segments in microwave planar circuits and microstrip antennas. This also helped the analysis of microstrip antennas using Green's function method or segmentation/desegmentation method.

R. Chadha *et al.* [51] put forward a computationally efficient segmentation technique for the analysis of microwave planar circuits. Another method called the desegmentation method is discussed by P.C. Sharma and K.C. Gupta [52] for the analysis of two dimensional planar circuits. This technique is applicable to configurations, which can be converted to regular shapes (for which Green's functions are available) by adding one or more regular shaped segments to them.

Newman *et al.* [53] used moment method for the analysis of microstrip patch antennas of different shapes. The patch is modelled by surface currents and the dielectric by polarisation current. This method is accurate, but requires precise computation.

A comprehensive review of the of the microstrip antenna technology till 1981 is provided by K.R. Carver *et al.* [54]. Certain numerical and analytical techniques for the analysis of

microstrip antennas are briefed in the paper. The substrates available are also discussed. Design procedures for the most popular geometries (rectangular and circular) are given and the need for further research is also discussed.

A full wave method for the analysis of open printed circuit structures is presented by T. Itoh *et al.* [55]. From the spectral domain equivalent circuits the spectral domain immittance matrix is derived and it forms the basis of this method. Finally numerical results are compared with experimental results. This method is also applicable to coplanar and slotline printed structures, structures involving stratified substrates, several radiating elements and conductor elements at different interfaces of stratified substrates.

K.C. Gupta *et al.* [56] presented a review of two-dimensional analysis approach applicable to circuits, resonators and antennas. Methods like Green's function approach, segmentation method, desegmentation, numerical methods for arbitrary shaped structures etc., are discussed.

Some of the researchers worldwide, started working towards overcoming the inherent disadvantage of narrow impedance bandwidth and came out with interesting results.

A method for doubling the bandwidth of rectangular patch antennas was proposed by Wood [57]. He used two $\lambda/4$ short circuited parasitic elements placed parallel to the radiating edges. The antenna characteristics are explained in terms of antiphase mode of a pair of coupled resonators. He also noted that the bandwidth improvement is independent of the coupling capacitance.

M.D. Deshpande *et al.* [58] derived an expression for the input impedance of microstrip patch antennas. Both the microstrip and coaxial type feeding can be considered. This method considers the effects of dielectric constant, dielectric losses, substrate thickness, surface waves and dielectric cover. The input impedance of rectangular microstrip antenna is computed and compared with experimental results to check the validity of the method. This technique can be

extended to other microstrip antenna geometries like circular, triangular, elliptical etc.

D.R. Poddar *et al.* [59] presented microstrip antennas fabricated on stepped and wedge-shaped dielectric substrates. They observed significant improvement in antenna impedance bandwidth compared to that of an equivalent rectangular microstrip antenna.

Das *et al.* [60] modified the ordinary circular patch antenna configuration by slightly depressing the patch conically into the substrate. This antenna gives a much larger bandwidth compared to ordinary antenna.

Lee *et al.* [61] reported the design of a quasi-log-periodic microstrip antenna for enhanced bandwidth.

The rectangular microstrip antenna has been extensively analysed by E. Lier *et al.* [62] for both finite and infinite ground plane dimensions. For the case of infinite ground plane, existing formulas have been improved. In the finite ground plane case, contribution from ground plane edge diffraction is also accounted in the analysis. The accuracy of the method is tested through comparison with experimental results.

P.C. Sharma *et al.* [63] presented the analysis and designs of three types of circularly polarised microstrip antennas. The antenna configurations were analysed by using the Green's function approach and desegmentation technique. The axial ratio bandwidths, VSWR bandwidths and radiation patterns are evaluated and verified experimentally.

Analysis of an arbitrary shaped microstrip antenna with multiterminals is presented by Y. Suzuki and T. Chiba [64]. An approach based on variational method and modal-expansion technique uses Rayleigh-Ritz method for the determination of eigen values and eigen functions. The input impedance and other antenna parameters are computed at non resonance and the theoretical results are compared with experimental results for a pentagonal patch. This method can be applied to microstrip antennas with arbitrary shaped boundaries and multiterminals.

Theoretical and experimental investigations on annular, annular sector and circular sector

Theoretical and experimental investigations on annular, annular sector and circular sector microstrip antennas were presented by W.F. Richards *et al.* [65]. They analysed the structures after the full expansion of resonant modes within the cavity formed by the radiating patch and the ground plane. For comparison experimental results were also presented.

H. Pues *et al.* [66] presented a more accurate and efficient method for the analysis of rectangular microstrip antennas. They modified transmission line model by incorporating the mutual coupling between the equivalent slots and by considering the influence of the side slots on the radiation conductance. For a rectangular microstrip antenna fed with a single microstrip feed line, the method shows very good agreement with available experimental and theoretical results.

V. Palanisamy and R. Garg [67] presented two new geometries, which could be used as substitutes for rectangular microstrip antennas. They presented the theoretical and experimental results of rectangular ring and *H*-shaped antennas. Finally a comparison with the characteristics of ordinary rectangular patch antenna is also presented.

Bhatnagar *et al.* [68] proposed a broadband microstrip antenna configuration for wideband operation. The configuration consists of one triangular patch placed parasitically over a driven patch.

A wide-band coaxial fed microstrip antenna element on electrically thick multilayer substrate was presented by Fong *et al.* [69]. A technique for feeding thick substrate is also presented in his paper.

Prior *et al.* [70] showed that the placement of short circuited annular ring near a disc antenna enhances the bandwidth of the disc. Nearly two times enhancement in bandwidth is achieved with slight reduction in gain.

The effect of placing a parasitic element parallel to the non radiating edge of a rectangular microstrip patch was studied by Mosig and Gardiol [71]. They used the integral equation

G. Kumar *et al.* [72, 73] studied the bandwidth enhancement using parasitic elements. They observed significant improvement in impedance bandwidth when the driven patch and the parasitic elements are resonating at adjacent frequencies.

V. Palanisamy and R. Garg [74] developed a new technique based on segmentation technique and cavity model for the analysis of arbitrarily shaped microstrip patch antennas. The analysis could predict accurately the resonant frequency, input impedance and radiation patterns of the rectangular ring antenna which had been proposed by them. According to them this method is more efficient compared to other methods available for arbitrary shapes.

V. Palanisamy *et al.* [75] performed the analysis of circularly polarised square ring and crossed strip microstrip patch antennas based on segmentation technique and cavity model. They have validated the predicted results with experimental results and observed good agreement.

C.K.Aanandan and K.G. Nair [76] presented the development of a compact and broadband microstrip antenna configuration. They used a number of parasitic elements, gap-coupled to a driven patch to get improvement in bandwidth.

Operation of microstrip antennas over multioctave bandwidth has been shown to be possible by using electromagnetically coupled patches in a log-periodic series fed array by P.S. Hall [77]. The measured results show that the array bandwidth is greater than two octaves.

A two-port rectangular patch antenna providing an accurate control of the radiated power is reported by A. Benalla and K.C. Gupta [78]. They analysed the patch with the input and output ports on the non radiating edges by using transmission line model.

D.M. Pozar and B. Kaufman [79] presented a broadband proximity coupled microstrip antenna configuration. The antenna consists of a microstrip patch coupled to a microstrip feed line below the patch. The antenna offered a bandwidth of 13%.

D.M. Pozar *et al.* [80] presented a rigorous solution for a rectangular microstrip antenna fed by a microstripline. The currents on the feedline and the patch are expanded in a suitable set

of modes and a moment method solution is formulated in the spectral domain. Here, the analysis is performed on patches fed at the radiating edge, nonradiating edge. He also analysed proximity coupled patches. He observed that the results are not good if the feeding is at the nonradiating edge.

H.Y. Yang and N.G. Alexopoulos [81] demonstrated the use of multiple superstrates for gain enhancement. They observed that through the proper selection of the thickness of substrate and superstrate, high directive gain can be obtained in any desired scan angle. The reciprocity theorem and transmission line method are used for the analysis of such antenna configurations. Finite Difference Time Domain (FDTD) method has been used for the analysis of microstrip antennas by A. Reineix and B. Jecko [82]. The method is so versatile that almost all types of antennas and all types of feeding can be treated by this method. Here the antenna is treated directly in the time domain. The frequency dependence of the relevant parameters can be determined by taking the Fourier transform of the transient currents after assuming a proper excitation.

The multiport network approach has been extended to incorporate the mutual coupling between the two edges of a rectangular patch antenna by A. Benalla and K.C. Gupta [83]. An admittance matrix is used to model the mutual coupling among the edges. This method is compatible with the segmentation technique. The obtained results are compared with the data available in the literature and found good agreement.

J.L. Drewniak and P.E. Mayes [84] proposed a simple, low-profile, broadband antenna with circularly polarised radiation pattern. Both senses of circular polarisation can be transmitted or received from the same structure. The antenna is proposed to have 30% impedance bandwidth. J.J.H. Wang and V.K. Tripp [85] demonstrated a spiral- mode microstrip antenna with a bandwidth of 6:1 for patterns and wider for VSWR. This new antenna does not require a cavity loaded with absorbing materials and hence is not bulky and lossy. The gain of the antenna is also

found to be greater for a 5:1 band compared to a loaded cavity spiral.

A.J. Svitak *et al.* [86] demonstrated a new technique for feeding a microstrip antenna through RF modulated light wave signals via an optical fibre. A module containing a photodiode, RF circuitry and a microstrip antenna element performs the lightwave-to-RF conversion. They have designed and tested three transmitting antenna configurations each containing an aperture coupled microstrip patch as the radiating element. Here the connections to the antenna modules are through an optical fibre.

A.A. Kishk [87] presented the analysis of a spherical annular microstrip antenna. The input impedance of the patch is computed using the generalised transmission line model. Method of moments has been used for the computation of the radiation patterns. He observed that the sphere radius has significant influence on the input impedance and the resonant frequency.

T. Kashiwa *et al.* [88] demonstrated the analysis of rectangular microstrip antennas mounted on the curved surface using the curvilinear FDTD method. The numerical results agreed well with almost all the experimental results and this confirms the validity of the technique.

Results of an iterative procedure for the determination of the effective loss tangent is presented by K.F. Lee *et al.* [89]. They observed that the final value of δ_{eff} depends on the value of the initially taken substrate loss tangent ($\tan \delta$).

H. An *et al.* [90] introduced a new approach for the design of broadband active antennas by using the simplified real frequency technique. They presented a sequential design procedure for the optimal design of transmitting and receiving antennas with multiple active stages, taking into account of input and output matching, the gain vs. frequency curve and the noise performance.

The near fields of single layer microstrip patch antennas computed through an iterative method is presented by S.A. Bokhari *et al.* [91]. A combination of mixed potential integral equation method, the FFT algorithm and the biconjugate gradient resulted in an efficient

numerical solution. The computed results are compared with measured results.

X.H. Shen *et al.* [92] used method of moments to determine the radiation and impedance properties of microstrip patch antennas in multilayered configurations. The resonance condition of the structure which allows high gain are studied. The gain, impedance, beamwidth and bandwidth of the are also discussed. They observed two conditions for the high gain operation according $\epsilon_r \gg 1$ or $\mu_r \gg 1$. A practical microstrip antenna geometry with superstrates are established and observed that both the impedance and gain bandwidths are inversely proportional to the gain.

A proximity coupled rectangular microstrip antenna giving circular polarisation is demonstrated by H.Iwasaki [93]. The feeding arrangement consists of a microstrip line placed offset from the centre of a rectangular microstrip antenna. A practical antenna suitable for applications in phased arrays with an axial ratio of less than 0.3dB is realised.

D.M. Pozar and S.M. Duffy [94] presented the design and test results of an aperture coupled circularly polarised antenna for GPS. The antenna operates both in the L_1 and L_2 frequencies of 1575 and 1227 MHz required for differential GPS to provide maximum positioning accuracy. It offers a relatively narrow beamwidth (10 dB) of the order of 120 to 140°.

C.R. Rowell and R.D. Murch [95] showed that the addition of a capacitive load can significantly reduce the size of a PIFA for a given resonant frequency. The antenna requires a resonant length of $\lambda/8$ only. A design with a bandwidth of 178 MHz centred at 1.8 GHz is demonstrated and analysed through FDTD. This antenna is suitable for application in PCS.

An annular ring microstrip antenna suitable for vehicle antennas in mobile satellite communication is developed by H. Ohmine *et al.* [96]. The antenna is fed by a branch line hybrid coupler and is circularly polarised. Impedance matching as well as broadband operation is achieved through placing a parasitic element over the patch. The antenna works in the TM_{21} mode and produced a conical pattern, with high gain in low-elevation angle for mobile satellite communications. The antennas suitability for mobile communication has been established by performing experiments in the L-band.

2.2. COMPACT MICROSTRIP ANTENNAS

Recently, due to the developments in the present communication area, researchers all over the world are interested in the design and development of compact microstrip antennas suitable for communication applications. A review of compact microstrip antennas is presented in this section.

V. Palanisamy and R. Garg [97] reported *H*-shaped and rectangular ring microstrip antennas as substitute to commonly used rectangular patch antennas. They found that the *H*-shaped patch antenna requires very less area compared to the rectangular patch antenna. Because of size reduction the *H*-shaped patch looks attractive for UHF applications.

C. K. Aanandan and K. G. Nair [98] developed a compact broadband microstrip antenna configuration. The system uses a number of parasitic elements which are gap coupled to a driven patch. They achieved a bandwidth of 6% without deteriorating the radiation pattern.

G. Kossiavas *et al.*[99] presented *C*-shaped microstrip radiating element operating in the UHF and L-bands. Its dimensions are found to be smaller than those of conventional square or circular elements. Like other microstrip geometries, the bandwidth of this antenna is also narrow. However, the antenna offers good matching and omnidirectional radiation pattern with a coaxial feed.

J. L. Volakis and J. M. Jin [100] proposed simple schemes for lowering the resonant frequency of the rectangular patch antenna without changing the size. Resonant frequency reduction is obtained by placing a perturbation below the patch. They obtained as much as 30 percent decrease in resonant frequency. He has given the design curves for cavity backed and aperture backed patch configurations.

The frequency reduction obtained through loading the patch antenna with a dielectric resonator is demonstrated by E. K. N. Yung *et al.* [101]. They observed that the resonant frequency of a circular microstrip antenna decreases with the position of the DR on the antenna.

Supriyo Dey *et al.* [102] modified the geometry of an ordinary microstrip circular patch antenna by putting two sectoral slots shunted by conducting strips to get reduced resonant frequency. They observed wide variation in input impedance along the circumference of the modified structure and hence can be matched directly with a microstrip line. They were able to achieve 19% reduction in resonant frequency by this method.

By using a very small number of thin shorting posts (say 3), instead of a complete short circuit, M. Sanad [103] showed that the size of a quarter wavelength antenna could be reduced considerably with out any degradation in the gain of the antenna. The gain of many antenna configurations have been measured with a complete short circuit and with 3 shorting posts and no significant difference in the results were observed.

Y. Hwang [104] demonstrated a planar inverted F antenna loaded with a high permittivity material suitable for mobile communication handsets.

Y. Zhang [105] studied the feasibility of miniaturisation of the antennas used for microcellular and personal communications by using barium titanate as superstrate in microstrip antennas designed on 900 MHz and 1800 MHz bands. The resonant frequencies, input impedances and VSWR of these type of antennas have been studied by him.

S. Dey *et al.* [106] proposed the design of a compact, low-cost wide band circularly polarised antenna suitable for personal communication applications. The configuration consists of four shorted rectangular patches. Two of them are fed directly and the others are fed parasitically. The antenna shows good polarisation characteristics over a wide frequency band and also has a large angular coverage in both the principal planes.

M. G. Douglas and R. H. Johnston [107] demonstrated the *U* patch antenna. This antenna may be used as an alternative to the half wave square patch antenna, but it requires only one third to one quarter of the surface area of the square half wave antenna. Though, the bandwidth is smaller, the pattern is more omnidirectional. The isolation between the elemental antennas is about 20 dB.

Mohamed Sanad [108] experimentally investigated double C-patch antennas having different aperture shapes. He achieved size reduction through shorting the zero potential plane of the antenna as well as through varying the length and width of the apertures. The effect of different design parameters on the performance of the antenna is also presented.

Jacob George *et al.* [109] proposed a broad band low profile microstrip circular patch antenna. Four sectoral slots are cut on the circular patch antenna with a uniform intersectoral angle 90° and a slot angle 8° . The antenna requires about 59.8% lesser area compared to an ordinary circular patch antenna resonating at the same frequency.

R. Waterhouse [110] presented a probe fed circular microstrip antenna which incorporates a single shorting pin. The presence of the shorting pin significantly reduced the overall size of the antenna. Experimental and theoretical impedance behaviour and radiation characteristics of the modified patch are given. Very good agreement between experiment and theory are achieved.

R. B. Waterhouse [111] compared the probe-fed circular patch incorporating a single shorting post, with patches designed on the same substrate having larger area and circular patches of the same size (the dielectric constant of the substrate for the conventional patches was significantly increased to reduce the overall size) as the shorted patch. This latter comparison is the most appropriate for applications where size is of primary concern.

M. Sanad [112] developed a compact microstrip antenna suitable for application in cellular phones. It consists of a driven element and five small parasitic patches distributed in two stacked layers. The two layers have similar geometries and their dimensions are almost equal. This antenna operates at two separate frequency with broad bandwidths. This antenna helps to eliminate the expensive duplexer or at least making it cheaper and easier to design.

I. Park and R. Mittra [113] demonstrated a quarter-wave aperture-coupled microstrip antenna with a shorting pin. This antenna requires less than half the size of conventional microstrip antennas and hence is suitable for applications where only a limited area is available for the installation of the antenna.

M. Sanad [114] experimentally studied non-planar shorted and partially shorted double C-patch antennas with and without parasitic elements.

S. Dey and R. Mitra [115] presented the design and development of a compact microstrip patch antenna. The length of the antenna is only one eighth of the effective wavelength at resonance. They used method of moments for the analysis of the current distribution on the patch surface.

T. K. Lo *et al.* [116] used a high permittivity substrate for the design of a miniature microstrip antenna. The aperture-coupling is used for feeding power and the gain of the antenna has been increased by adding superstrates of appropriate thickness. Experimental data for the return loss, radiation pattern and measured antenna gain are presented for a 1.66 GHz antenna. Here size reduction is obtained without much alterations in the electrical performance of the antenna compared to an ordinary antenna fabricated on a low dielectric constant substrate. The antenna gain is 5.3 dB, and the patch size is greatly reduced to one fifth of that of the conventional microstrip antenna.

K. L. Wong and S. C. Pan [117] loaded a triangular microstrip antenna with a shorting pin and observed significant reduction in antenna size at a given operating frequency. Experimental results on the variation of resonant frequency with shorting pin positions are given and finally a comparison with the characteristics of ordinary triangular microstrip antennas was also given.

Experimental details of a single feed dual frequency compact microstrip antenna is presented by K. L. Wong and W. S. Chen [118]. This new rectangular microstrip antenna provides very large frequency ratio of >3.0 between the two operating frequencies.

Compact broad band microstrip antennas are experimentally demonstrated by K. L. Wong and Y. F. Lin [119] through chip-resistor-loading. The impedance matching can be achieved by adjusting the coupling-slot size or by the position or size of the slot. The chip resistor loading

shows a lower resonant frequency, large bandwidth as compared with the shorting pin loading.

C. L. Tang *et al.* [120] demonstrated a dual frequency compact microstrip circular patch antenna. The antenna configuration utilises a single probe feed and a single shorting pin. The frequency ratio of the two operating frequencies is tunable in the range of 2.55 - 3.83.

D. Singh *et al.* [121] presented the design of a quarter wavelength H-shaped microstrip antenna suitable for application in MMIC's. This new design requires only one tenth of the area of ordinary half wavelength patch antenna. The variation of resonant frequency, bandwidth and gain of the antenna with the central width is also presented.

R. B. Waterhouse [122] demonstrated broadband operation of shorted circular patches by coupling an annular ring to it. The size of the antenna is compatible with typical mobile communications hand set terminals and impedance bandwidth satisfies the requirements of such systems.

By cutting slits on the patch surface, K. L. Wong and J. Y. Wu [123] produced circular polarisation from a shorted square patch antenna. The design has the advantage of reduced size achieved through the presence of the shorting pin.

R. B. Waterhouse [124] demonstrated a shorted patch configuration in which significant reduction in the cross-polarised fields. The cross-polarised fields have been measured at more than 20 dB below the co-polar levels. The new shorted patch is approximately a quarter wavelength in size and has a bandwidth comparable to a conventional microstrip patch antenna.

K. L. Wong and K. P. Yang [125] demonstrated a new design of single-feed, reduced-size, dual-frequency rectangular microstrip antenna with a cross slot of equal length. Here the two frequencies are orthogonally polarised and the ratio between them depends on the aspect ratio of the patch.

D. M. Kokotoff *et al.* [126] analysed, fabricated and measured the characteristics of an annular ring loaded probe fed circular microstrip antenna incorporating a shorting pin. They have

used a rigorous full wave analysis for predicting the characteristics and observed enhanced impedance bandwidth with the presence of the parasitically coupled ring. This configuration also gets the added advantage of compactness through the use of the shorting pin.

K. L. Wong *et al.* [127] reported the design of a compact meandered circular microstrip antenna with a shorting pin. Here they applied meandering along with shorting and could reduce the patch size to less than 10% of a conventional circular patch antenna operating at the same resonant frequency.

Owing to the miniaturisation of communication equipment, designs for reducing the size of the microstrip antenna have received much attention and in this scenario, H.T. Chen [128] experimentally studied the characteristics of compact microstrip antennas and compared them with those of conventional microstrip antennas. Compactness achieved through the placement of shorting pin and through meandering are studied.

R.B. Waterhouse *et al.* [129] have investigated techniques to improve the overall performance of shorted microstrip patch antennas. Problems with mechanical tolerances and high H-plane cross-polarized fields have been addressed and solutions are proposed to overcome them.

J. H. Lu *et al.* [130] have put forward the design of compact slot coupled triangular microstrip antennas with a shorting pin or chip resistor loading. They achieved the desired matching for TM_{10} mode by adjusting the coupling slot size.. The chip resistor loaded antenna provided compactness along with enhanced impedance bandwidth.

K. L. Wong and K. P. Yang [131] implemented a modified planar inverted F antenna operating in the 800 MHz band with reduced size and enhanced impedance bandwidth suitable for applications in hand-held communication equipment. They achieved compactness through meandering the patch and bandwidth enhancement through the placement of a chip resistor.

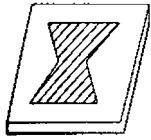
S. K. Satpathy *et al.* [132] presented shorted versions of semi-circular and 90° sectoral

microstrip antennas. The shorted 90° sectoral microstrip antenna provided a size reduction of four times without any significant change in performance.

The implementation of a compact and broadband rectangular microstrip antenna having enhanced gain is described by C. Y. Huang *et al.* [133]. They used chip resistor loading for bandwidth enhancement and placement of superstrates for gain enhancement. Without much deterioration in antenna gain, they could reduce the size of the antenna to 6% and the bandwidth to 6 times that of a conventional patch antenna.

A. S. Vaello and D. S. Hernandez [134] presented a bow-tie antenna similar to the drum-shaped antenna for dual frequency operation. The antenna requires very lesser size compared to conventional patch antennas and have similar radiation characteristics.

From the above review, it is clear that design and development of compact microstrip antenna is an emerging field. Compact nature of a microstrip antenna can be achieved by suitable geometrical shape. With this idea in mind, the author of this thesis designed a new geometry for size reduction. The present thesis is the outcome of the experimental and theoretical investigations carried out on a new compact drum-shaped microstrip antenna.



METHODOLOGY - EXPERIMENTAL SETUP, MEASUREMENT TECHNIQUES AND THEORETICAL APPROACH

This chapter describes the fabrication techniques employed for the microstrip antennas. A brief description of the experimental setup and measurement techniques used for the study of various antenna characteristics are also given in this chapter. This chapter concludes with description of the theoretical approach employed to predict different antenna characteristics.

3.1 FABRICATION OF MICROSTRIP ANTENNA

For the fabrication of the microstrip antennas, two different techniques are employed depending upon the dimensional tolerance.

3.1.1 Photolithographic Technique

Most commonly used method for the fabrication of microstrip antenna is photolithographic technique [7, 10]. A step-by-step procedure of this technique is shown in Figure 3.1. As the figure is self explanatory and the technique is most popular, it is not elaborated here.

This technique is employed for the fabrication of L-band antennas where fabrication tolerance is more critical.



FIGURE 3.1 Step-by-step procedure of photolithographic technique

3.1.2 Fast fabrication process

For fast and reasonably accurate fabrication of microstrip antennas, an alternate method is used. The different steps in this process are shown in Figure 3.2. Here, the copper clad substrate is cleaned thoroughly (1) and a drawing of the antenna is made on one side (2). The entire top and bottom metallisation regions are covered with transparent cellophane tape (3). The tape is then selectively removed from the top metallisation layer (4) by means of a sharp diamond tipped

cutting tool in such a manner that tape over the antenna geometry is unaltered. The exposed metallisation regions(5) are etched out. After the etching process, tape is removed from both the surfaces and cleaned (6) once again to get the antenna ready to test. This simpler and faster technique is used for the fabrication of UHF antennas, since, at higher wavelengths this technique yields fabrication tolerance within acceptable limits.

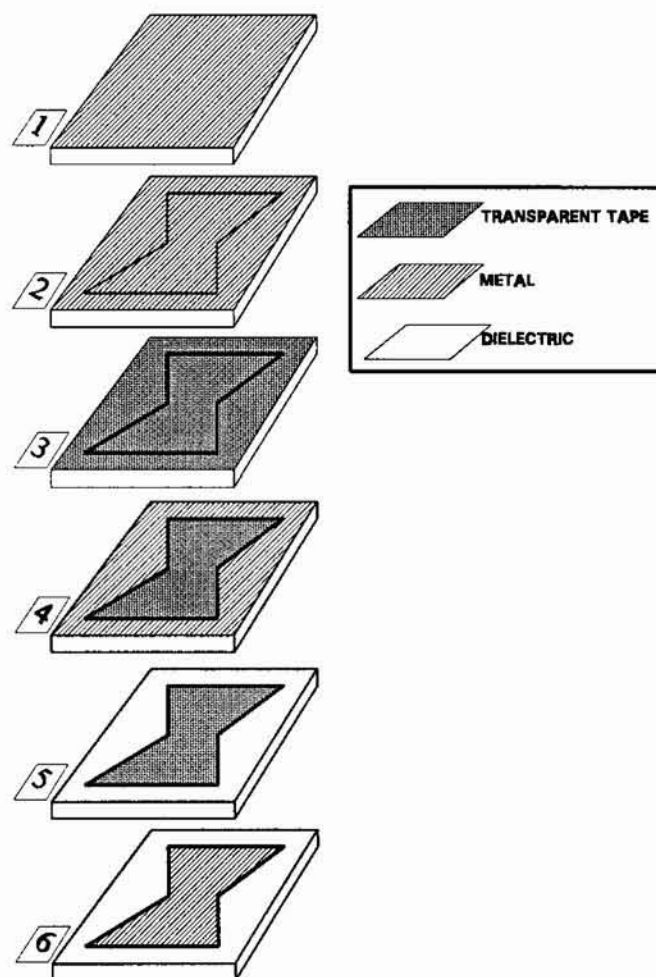


FIGURE 3.2 Different steps in the fast fabrication process

This method is very fast and simple compared to the photolithographic technique mentioned earlier. The validity of this technique has been established by fabricating conventional

rectangular patch antennas. In the case of the drum-shaped antenna, periphery is constituted by few line segments and can be easily fabricated by this method with fabrication tolerances in acceptable limits.

3.2 EXCITATION TECHNIQUES

Two types of feeding mechanisms are used for the excitation of the present microstrip antenna.

They are

- a. microstrip feed
- b. coaxial feed

The general nature of these feeding mechanisms are already discussed in section 1.1.2 (Chapter 1). As in the case of a rectangular microstrip antenna, the input impedance of the drum-shaped antenna varies from zero to a maximum value as we move from the centre towards the edges (see section 4.2) and thereby provides a simple means for matching of 50Ω feed line. In this thesis, coaxial type feed is employed in most of the cases.

3.3 MEASUREMENT OF RETURN LOSS, RESONANT FREQUENCY AND BANDWIDTH

The HP8510B Network Analyzer is used for the measurement of return loss, resonant frequency and bandwidth. The block diagram of the experimental setup for the automatic measurement controlled by an IBM PC interfaced to the Network Analyzer is shown in Figure 3.3.

Network Analyzer is calibrated for one full port (PORT 1) and the test antenna is connected to PORT 1 of the S-parameter test set. The measured S_{11} LOGMAG data in the Network Analyzer is acquired and stored in ASCII format in the computer using *MERL Soft* (A software indigenously developed by the microwave group of the Department for antenna studies)

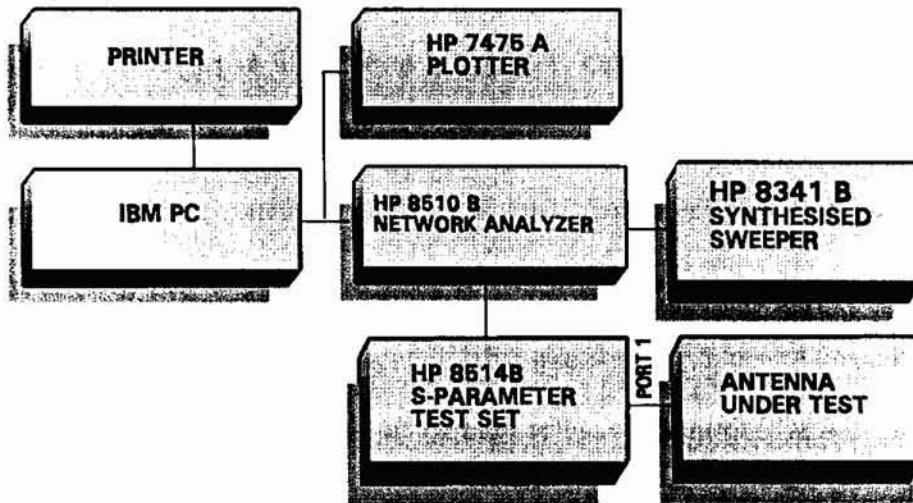


FIGURE 3.3. Experimental set up for the measurement of return loss and resonant frequency

The resonant frequency of the antenna for a particular mode is determined from dip of the return loss curve for that mode. The bandwidth can be directly obtained from the return loss data by noting the range of frequencies (Δf_r) over which the return loss is $\leq -10\text{dB}$. Now percentage bandwidth is given by, $\frac{\Delta f_r}{f_r} 100 \%$, where f_r is the centre frequency of the operating

band. The stored return loss data in ASCII format is analysed for bandwidth and resonant frequency using *MERL Soft*.

3.4 MEASUREMENT OF RADIATION PATTERN

The principal *E*- and *H*-plane radiation patterns (both co-polar and cross-polar) of the test antenna are measured by keeping the test antenna inside an anechoic chamber in the receiving mode. The experimental arrangement for the measurement is shown in Figure. 3.4. A standard wideband (1-18GHz) ridged horn is used as the transmitter.

HP 8510B Network Analyzer, interfaced to an IBM PC, is used for the pattern measurement. The PC is also attached to a STIC 310C positioner controller. The test antenna is mounted on the antenna positioner kept inside the chamber. The test and the standard transmitting antennas are connected to PORT 2 and PORT 1 respectively of the Network Analyzer.

The radiation pattern of the antenna at multiple frequency points can be measured in a single rotation of the test antenna positioner by using *MERL Soft*. The positioner will stop at each step angle and will take S_{21} measurements till it reaches the stop angle. The entire measured data are stored in ASCII format and can be used for further processing like analysis and plotting. The different pattern characteristics like half power beamwidth, cross-polar level, etc., are obtained after analysis of the stored patterns.

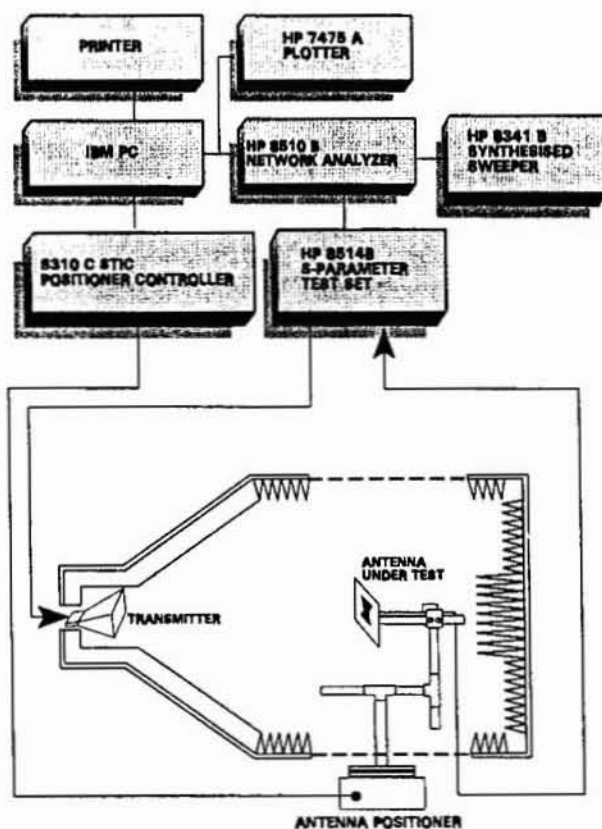


FIGURE 3.4 Set up for measuring the radiation pattern of the antenna

3.5 MEASUREMENT OF GAIN

The set up for the measurement of gain is same as that used for pattern measurement. A comparative measurement of gain of the new antenna is made with standard rectangular patch antenna operating at the same frequency and fabricated on the same substrate.

The standard rectangular antenna is kept inside the chamber and connected to PORT 2 of the Network Analyzer. PORT 1 is connected to the transmitting antenna. The antenna is bore-sighted and a THRU RESPONSE calibration is performed in the Network Analyzer and stored in the CAL SET. This will act as the reference gain response. The standard antenna is now replaced by the corresponding drum-shaped antenna and the plot displayed on the Network Analyzer will directly give the relative gain of the new antenna.

3.6 MEASUREMENT OF ELECTRIC FIELD INTENSITY

The probe assembly used for sampling the field intensity over the patch is shown in Figure 3.5. The probe is fabricated by removing the outer conductor and the dielectric from a 2 mm section at the end of a long semirigid cable as given in [135]. The probe assembly is now mounted on a precision XY positioner, which can position the probe at any point over the patch surface with an accuracy of 1 mm. The length of the probe P_L is 2 mm and the height of the probe above the patch surface s is 2.5 mm. The dimensions of the probe plate are 5 cm x 5 cm.

For the measurement of electric field variation, the probe is connected to PORT 2 and the test antenna to PORT 1 of the Network Analyzer. The probe is moved over the entire patch area with a resolution of 1 mm and the entire S_{21} data at the resonant frequency is stored. The stored data are normalised and plotted to get the variation of electric field magnitude.

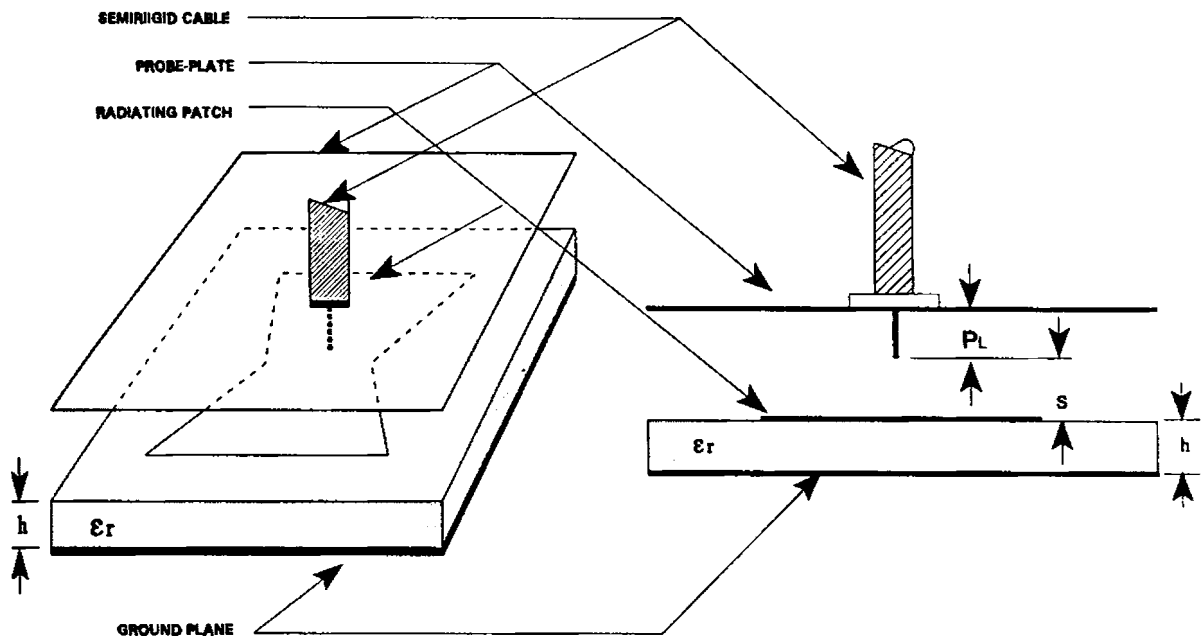


FIGURE 3.5 Set up for measuring the electric field variation over the patch

3.7 THEORETICAL ANALYSIS OF THE ANTENNA

Experimental results are verified theoretically using segmentation technique along with cavity model and spatial Fourier Transform technique. This method is selected because of the fact that, it is computationally more efficient compared to Finite Element Method (FEM) and Finite Difference Time Domain (FDTD) methods for geometries which can be readily divided into few regular geometrical shapes whose Green's functions are known.

The complicated geometry of the drum-shaped antenna is divided into triangular and rectangular segments as shown in Figure 3.6. Now the continuous interconnection between the segments are replaced by interconnection at discrete points. The impedance matrix elements of the different segments are computed and combined together to get the input reactance of the

lossless cavity (as we have not incorporated the radiation, dielectric and surface wave losses). A large value of this reactance shows the resonance. Now the electric field variation along the periphery of the antenna is computed and the mode is identified. This field variation along the periphery is used in the aperture model to get the radiation pattern, power radiated, stored energy, etc. Finally the radiation loss is incorporated in the Q-factor and this in turn modifies the dielectric constant to a complex value. This modified dielectric constant is used in the impedance matrix evaluation to get the actual input impedance of the antenna. The elaborate steps followed for the theoretical analysis are described in chapter 5.

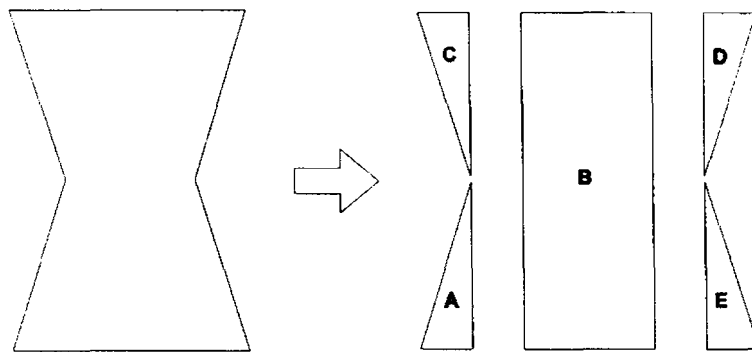
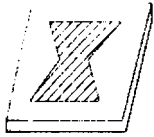


FIGURE 3.6 Segmentation of the drum-shaped antenna into four triangular and one rectangular segment

For the theoretical analysis of the antenna, the programmes are written in *MATHEMATICA* 3.0 [11]. From the geometrical dimensions and substrate parameters, the programme will compute the resonant frequency, electric field variation along the periphery, radiation pattern, input impedance, etc.



EXPERIMENTAL RESULTS AND OBSERVATIONS

This chapter deals with the outcome of the exhaustive experimental investigations performed on the new drum-shaped compact microstrip antenna. The aim of the work is to develop a compact microstrip antenna suitable for communication systems. As compact microstrip antennas are more suitable for mobile satellite communication systems, Personal Communication System (PCS), Global Positioning System (GPS), Phased Arrays, etc., the experiments were conducted in the UHF and L-bands.

The geometry of the new compact microstrip antenna is shown in Figure 4.1. The geometrical shape of the antenna is same as the projection of a *Japanese drum* on a plane parallel to the axis of the drum and hence it is named as drum-shaped antenna. The antennas are fabricated on a low loss substrate of dielectric constant ϵ_r , and thickness h . L is the length of the

antenna, B , the width of the radiating edge, W is the width of central region and s is the distance of the feed point. The antennas are etched on the substrate and proper feeding as explained earlier is used to couple microwave energy to the antenna.

In each frequency band, three possible drum-shaped antenna configurations are studied in detail. They are;

1. $L/B > 1$
2. $L/B = 1$
3. $L/B < 1$

For each configuration, the following antenna characteristics were studied in detail.

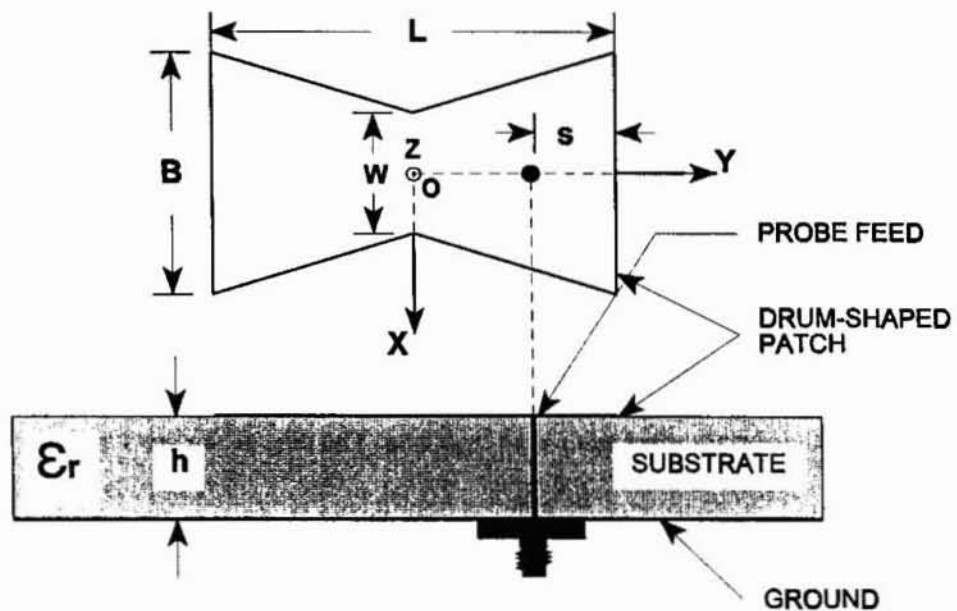


FIGURE 4.1 Geometry of the compact drum-shaped antenna showing probe feed

1. Characteristics of TM_{01} mode resonant frequency
 - a. Variation of resonant frequency with central width (W) and L/B ratios
 - b. Study of different antenna radiation characteristics like 2:1 VSWR impedance

- bandwidth, radiation pattern, gain, beamwidth, etc., with central width (W)
 - c. Mode identification by means of near field probing
2. Characteristics of TM_{10} mode resonant frequency
- a. Typical variation of resonant frequency with central width (W)
 - b. Typical 2:1 VSWR impedance bandwidth behaviour
 - c. Typical radiation patterns and their characteristics

The above study enabled the development of a design criterion of the drum-shaped antenna whose performance is better compared to rectangular patch antenna elements operating at the same frequency.

Before going into the experimental details, the basic resonant modes of importance and the excitation techniques adopted in each case are explained in the next section.

4.1 RESONANT MODES AND EXCITATION TECHNIQUES

4.1.1 Resonant modes

The resonant frequency of the antenna is one of the important characteristics to be studied initially. It is found that the resonant frequency depends on the length, L of the antenna. This length could be termed as the resonating length as in the case of a rectangular microstrip antenna. Here the resonating length is modified due to the geometrical shape and the effective value of it would be greater than the physical length, L . It is observed that the effective resonating length increases i.e., the resonant frequency decreases with decrease of W , the central width. The unmodified edges of length B could be termed as the radiating edges, as in the case of a rectangular patch antenna. The radiation occurs mainly (the other edges also contribute to the total radiated power) from these pair of edges. This is the case of TM_{01} mode. Whereas in the case of TM_{10} mode, the effective resonating length is determined by the edges of length B and

the central width W . The effective resonating length is observed to be less than B and its value decreases, i.e., the resonant frequency increases with decrease in W . In this case the two modified sides act as the radiating edges.

4.1.2 Excitation techniques

Like other microstrip antennas, here also, the feed point can be located on the edges or within the patch. By suitably selecting the feed point we can excite the desired mode. The input impedance also varies with the location of the feed point. The feed can be microstrip or coaxial type. For the TM_{01} mode (half wave variation of electric field along the length of the patch), a variation of input impedance from a minimum value to a maximum value is observed, when the feed is moved from the centre towards the edges. Figure 4.2 shows the impedance loci of three typical antenna configurations with a coaxial feed along the centre line (OY) of the antenna. A similar variation is observed when the feed point is moved from the centre towards the edges along the non-radiating edges and are shown in Figure 4.3. Here, in the former case the mode due to field variation along the width is eliminated and in the later case there is a possibility for the excitation of both the modes simultaneously depending upon the location of the feed point. In all the cases it is observed that when the feed point is at the centre, the impedance is very low. When we move from the centre to the edges the impedance is gradually increasing. This shows that by the proper selection of the feed point, the antenna can be properly matched to 50Ω transmission line.

Figure 4.4. shows the TM_{10} mode impedance loci of the drum-shaped antenna for different parameters. Here the feed point is moved from the centre towards the modified edge along the non radiating edge. The feed point is not selected inside the patch along the central region of width W as it will be very small in some cases. As in the previous case, here also impedance at resonance varies from a minimum to a maximum value as we move from the centre towards the edges.

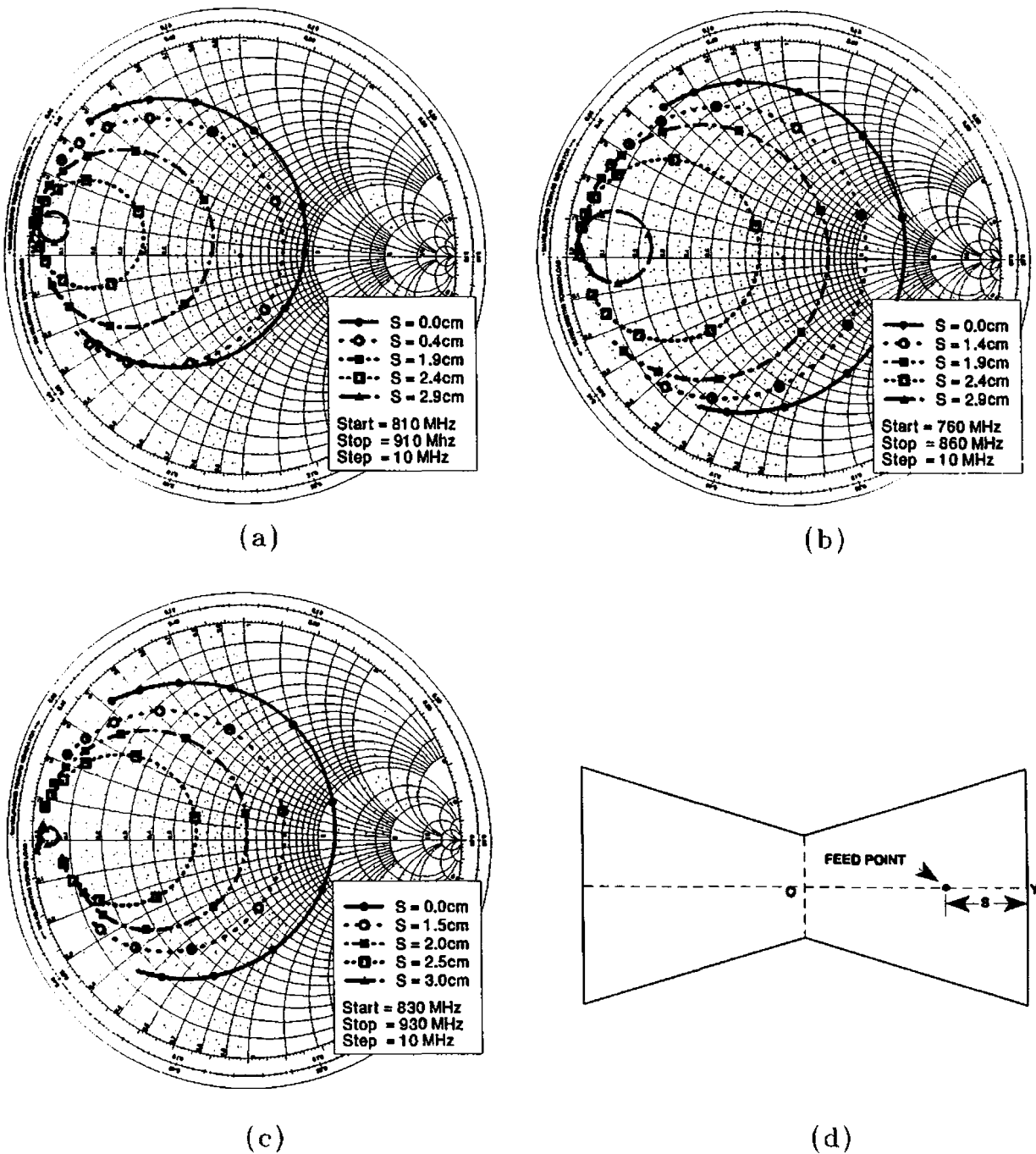


FIGURE 4.2 Variation of Input impedance with feed location for TM_{01} mode (central feeding)

- (a) $L/B < 1$, $L = 6.93$ cm, $B = 8.93$ cm, $W/B = 0.5$, $\epsilon_r = 4.5$, $h = 0.16$ cm (increasing frequency is clockwise direction)
- (b) $L/B > 1$, $L = 6.93$ cm, $B = 6.0$ cm, $W/B = 0.33$, $\epsilon_r = 4.5$, $h = 0.16$ cm (increasing frequency is clockwise direction)
- (c) $L/B = 1$, $L = 7.0$ cm, $B = 7.0$ cm, $W/B = 0.5$, $\epsilon_r = 4.5$, $h = 0.16$ cm (increasing frequency is clockwise direction)
- (d) Diagram of the drum-shaped antenna indicating the location of the feed point

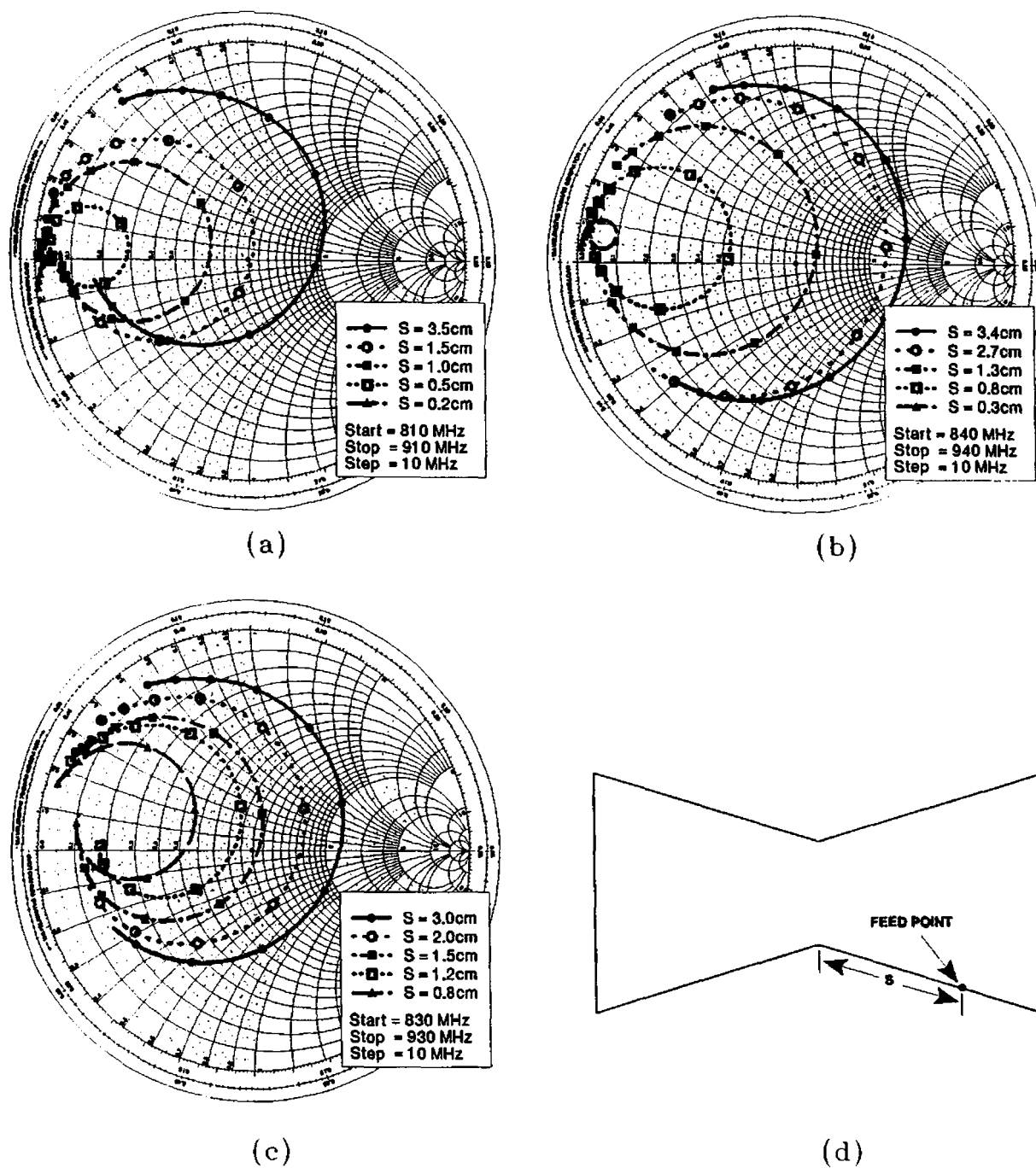


FIGURE 4.3 Variation of Input impedance with feed location for TM_{01} mode (edge feeding)

- (a) $L/B < 1$, $L = 6.93\text{ cm}$, $B = 8.93\text{ cm}$, $W/B = 0.5$, $\epsilon_r = 4.5$, $h = 0.16\text{ cm}$ (increasing frequency is clockwise direction)
- (b) $L/B > 1$, $L = 6.93\text{ cm}$, $B = 6.0\text{ cm}$, $W/B = 0.5$, $\epsilon_r = 4.5$, $h = 0.16\text{ cm}$ (increasing frequency is clockwise direction)
- (c) $L/B = 1$, $L = 7.00\text{ cm}$, $B = 7.0\text{ cm}$, $W/B = 0.5$, $\epsilon_r = 4.5$, $h = 0.16\text{ cm}$ (increasing frequency is clockwise direction)
- (d) Diagram of the drum-shaped antenna indicating the location of the feed point

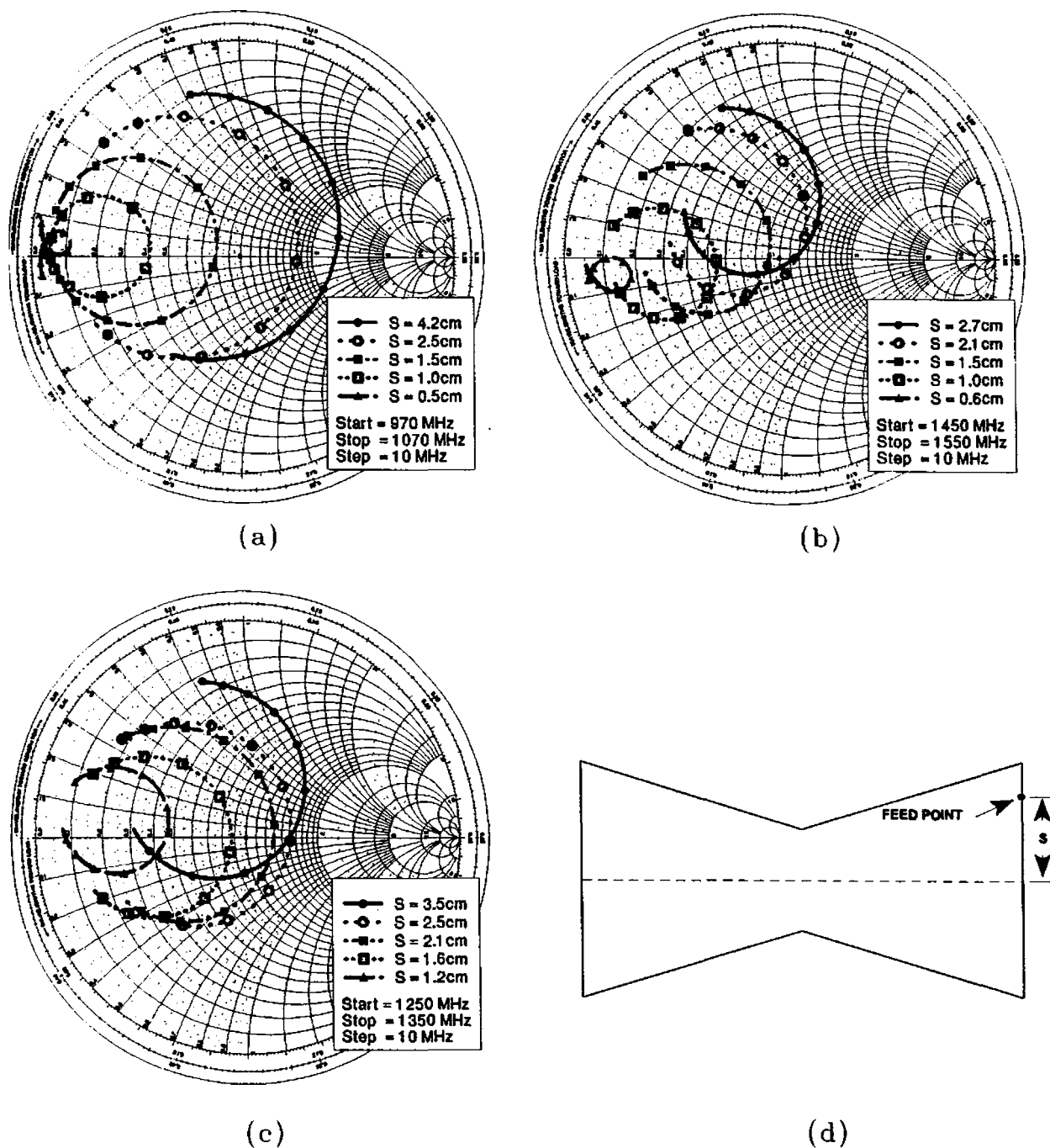


FIGURE 4.4 Variation of Input impedance with feed location for TM_{10} mode (edge feeding)

- (a) $L/B < 1$, $L = 6.93$ cm, $B = 8.93$ cm, $W/B = 0.5$, $\epsilon_r = 4.5$, $h = 0.16$ cm (increasing frequency is clockwise direction)
- (b) $L/B > 1$, $L = 6.93$ cm, $B = 6.0$ cm, $W/B = 0.5$, $\epsilon_r = 4.5$, $h = 0.16$ cm (increasing frequency is clockwise direction)
- (c) $L/B = 1$, $L = 7.0$ cm, $B = 7.0$ cm, $W/B = 0.5$, $\epsilon_r = 4.5$, $h = 0.16$ cm (increasing frequency is clockwise direction)
- (d) Diagram of the drum-shaped antenna indicating the location of the feed point

From these experimental observations it is established that by the suitable selection of feed point, matching and excitation of mode as desired could be obtained.

4.2 CHARACTERISTICS OF THE TM_{01} MODE

As described in the previous section, by moving the feed point along the centre line, a change in input impedance is observed. A feed point which provides good matching to the 50Ω feed line is selected and a coaxial probe is used for feeding energy to the selected point. The radius of the feed probe is 0.25 mm. Selection of the feed point along the centre line (OY) eliminates the excitation of the TM_{10} mode. The radiated fields of this mode are linearly polarised along YZ plane. The dimensions of different drum-shaped antenna configurations used in the study are given in Table 4.1. Here the antennas are fabricated on a low loss substrate of dielectric constant $\epsilon_r = 4.5$ and thickness $h = 0.16\text{cm}$. The experiments were also conducted using substrates of dielectric constants $\epsilon_r = 6$ and $\epsilon_r = 2.21$ of thickness 0.065 and 0.055 cms.

4.2.1 Resonant frequency variation with respect to central width (W)

The resonant frequency of the antenna is affected by the central width, W . When we reduce the central width, the effective resonating length increases and as a result the resonant frequency is found to be decreasing. This effect has been studied in detail and the return loss variation with respect to W for the UHF- and L-band antennas are given in Figure 4.5.

It can be seen from Figure 4.5(i).(a) that, when $L/B = 0.7$, the resonant frequency decreases by $\approx 42\%$ for $W/B = 0.1$. In the case of L-band antennas when $L/B = 0.5$, the resonant frequency decreases by $\approx 45\%$ for $W/B = 0.1$.

TABLE 4.1(i) Dimensions, TM_{01} mode resonant frequency (f_{01}) and feed location (s) of various UHF-band drum-shaped antenna configurations used in the study ($\epsilon_r = 4.5$ and thickness $h = 0.16\text{cm}$)

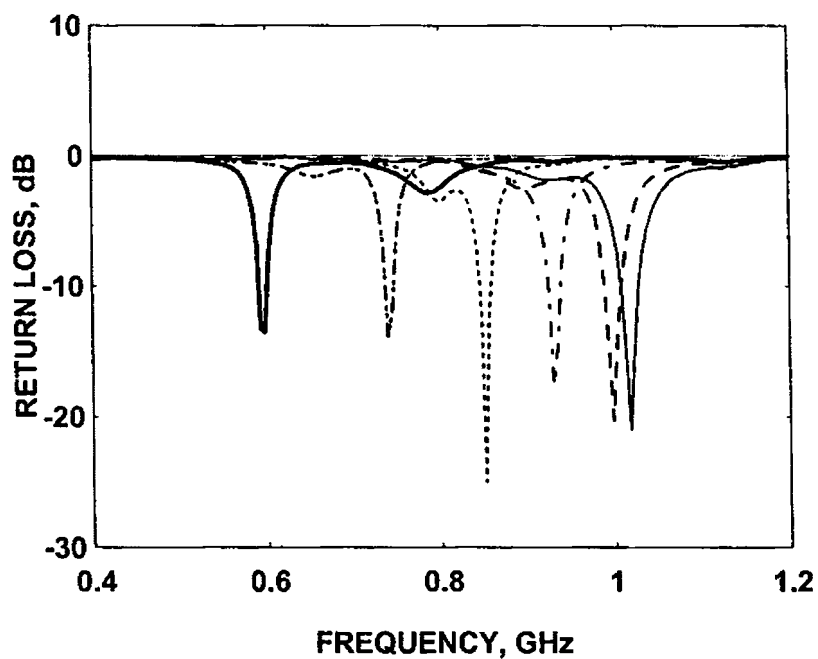
s : Feed location distance from the centre of the edge (Y) as shown in Figure 4.2(d)

L cm	B cm	L/B	W/B	s cm	f_{01} MHz
7.00	10.00	0.70	1.0	0.5	1017.0
			0.9	0.5	998.00
			0.7	1.5	929.00
			0.5	2.0	851.00
			0.3	2.0	739.00
			0.1	2.5	592.00
6.93	8.93	0.776	1.0	1.5	1022.0
			0.9	1.5	998.00
			0.7	1.5	939.00
			0.5	2.0	866.00
			0.3	2.0	758.00
			0.224	2.0	709.00
7.00	7.00	1.00	1.0	0.5	1032.0
			0.9	1.0	1011.0
			0.7	2.0	958.00
			0.5	2.5	881.00
			0.3	3.0	787.00
			0.1	3.5	651.00
6.93	6.00	1.155	1.0	2.0	1040.0
			0.9	2.0	1013.0
			0.7	2.0	963.00
			0.5	2.0	890.00
			0.333	2.0	812.00
			0.1	3.0	665.00
10.50	7.00	1.50	1.0	2.5	695.00
			0.9	2.0	680.00
			0.7	2.5	646.00
			0.5	3.0	597.00
			0.3	3.0	543.00
			0.1	4.0	455.00
10.50	5.25	2.00	1.0	3.5	695.00
			0.9	3.0	685.00
			0.7	3.0	651.00
			0.5	3.5	611.00
			0.3	3.5	553.00
			0.1	3.5	465.00

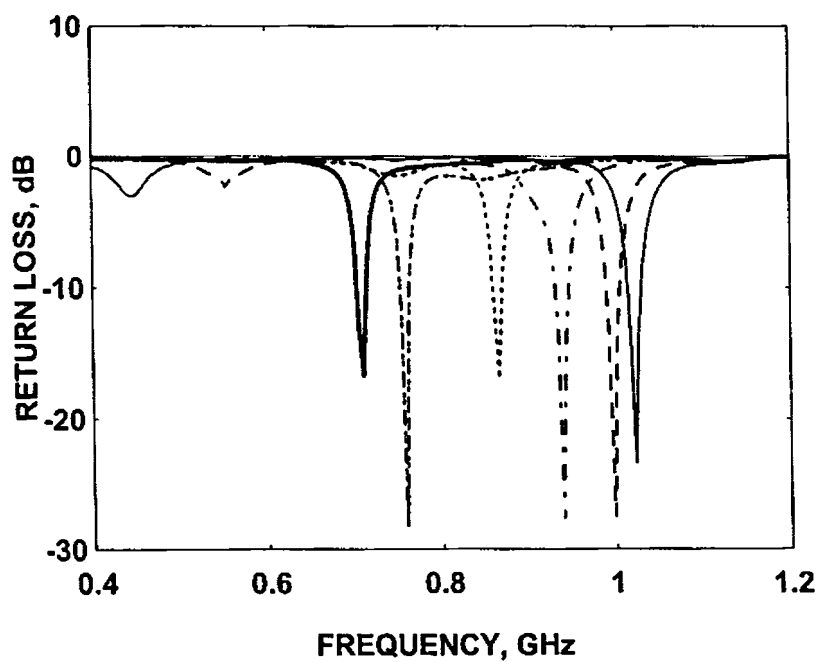
TABLE 4.1(ii) Dimensions, TM_{01} mode resonant frequency (f_{01}) and feed location (s) of various L-band drum-shaped antenna configurations used in the study ($\epsilon_r = 4.5$ and thickness $h = 0.16\text{cm}$)

s : Feed location distance from the centre of the edge (Y) as shown in Figure 4.2(d)

L cm	B cm	L/B	W/B	s cm	f_{01} MHz
3.50	7.00	0.50	1.0	0.4	2015
			0.9	0.6	1971
			0.7	0.6	1837
			0.5	0.4	1631
			0.3	0.4	1478
			0.1	1.0	1110
3.80	4.80	0.792	1.0	0.8	1877
			0.9	1.0	1833
			0.7	1.0	1751
			0.5	1.4	1581
			0.2083	1.6	1308
			0.1	1.4	1168
3.50	3.50	1.00	1.0	1.0	2059
			0.9	1.0	2021
			0.7	1.2	1922
			0.5	1.2	1784
			0.3	1.2	1628
			0.1	1.4	1381
3.811	3.20	1.191	1.0	1.0	1899
			0.9	1.0	1862
			0.7	1.2	1778
			0.5	1.2	1648
			0.3125	1.2	1515
			0.1	1.4	1278
3.80	2.53	1.50	1.0	1.2	1931
			0.9	1.2	1918
			0.7	1.4	1831
			0.5	1.4	1708
			0.3	1.6	1562
			0.1	1.6	1353
4.00	2.00	2.00	1.0	1.4	1860
			0.9	1.4	1818
			0.7	1.6	1758
			0.5	1.6	1665
			0.3	1.6	1528
			0.1	1.8	1340



(a)



(b)

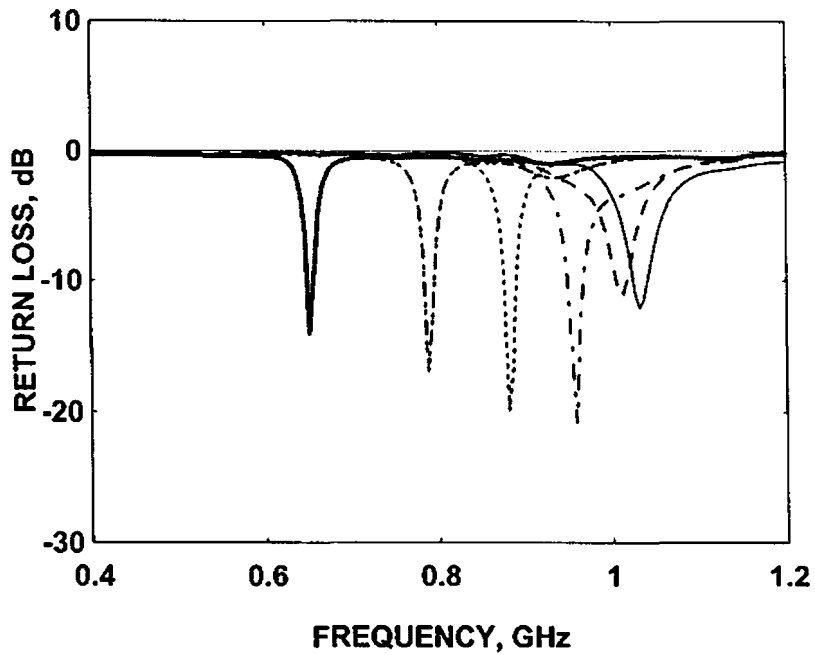
FIGURE 4.5(i) Variation of return loss with frequency for UHF antennas

(a) $L = 7$ cm, $B = 10$ cm

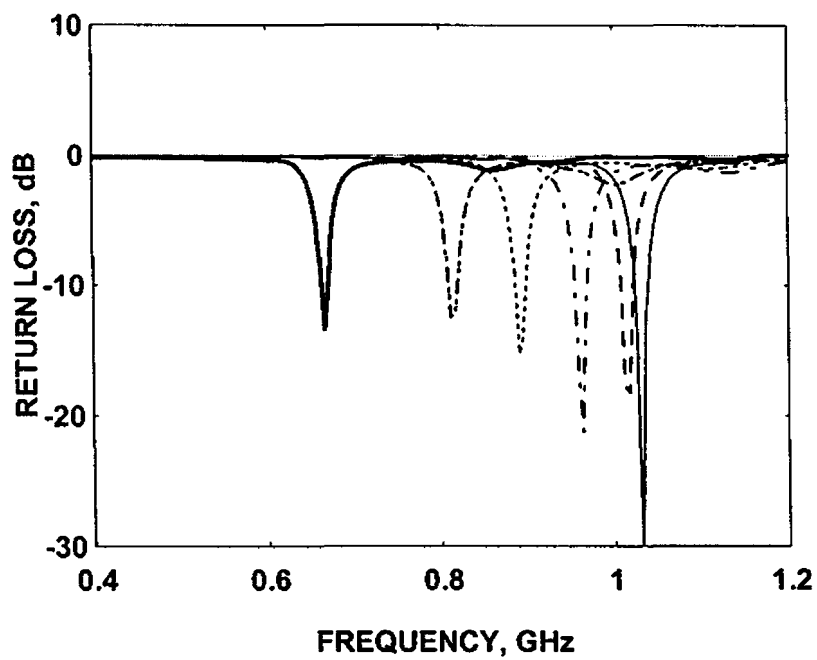
—————	$W/B = 1.0$	-----	$W/B = 0.9$	- · - · -	$W/B = 0.7$
.....	$W/B = 0.5$	- · - · -	$W/B = 0.3$	—————	$W/B = 0.1$

(b) $L = 6.93$ cm, $B = 8.93$ cm

—————	$W/B = 1.0$	-----	$W/B = 0.9$	- · - · -	$W/B = 0.7$
.....	$W/B = 0.5$	- · - · -	$W/B = 0.3$	—————	$W/B = 0.224$



(a)



(b)

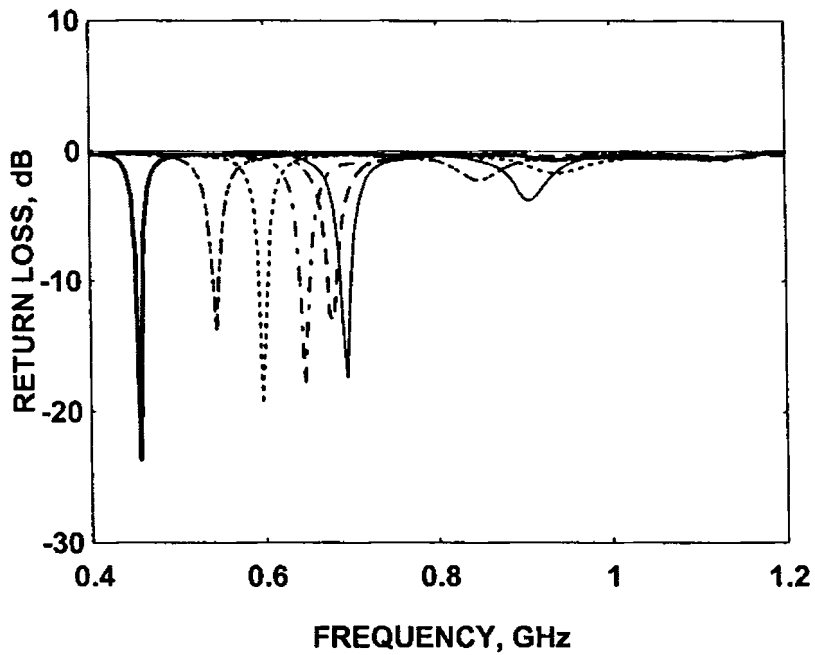
FIGURE 4.5(ii) Variation of return loss with frequency for UHF antennas

(a) $L = 7$ cm, $B = 7$ cm

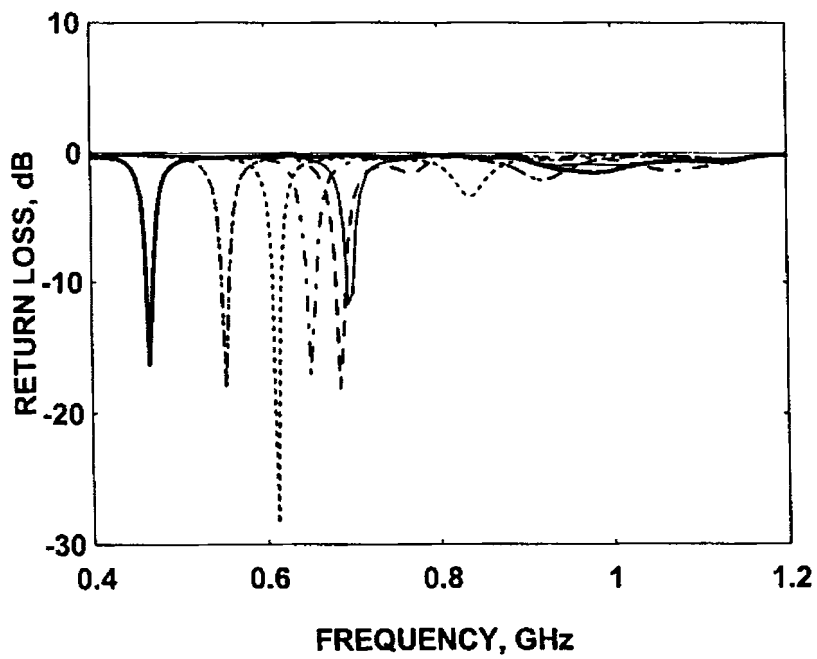
—————	$W/B = 1.0$	-----	$W/B = 0.9$	- . - . - .	$W/B = 0.7$
.....	$W/B = 0.5$	- . - . - .	$W/B = 0.3$	—————	$W/B = 0.1$

(b) $L = 6.93$ cm, $B = 6$ cm

—————	$W/B = 1.0$	-----	$W/B = 0.9$	- . - . - .	$W/B = 0.7$
.....	$W/B = 0.5$	- . - . - .	$W/B = 0.333$	—————	$W/B = 0.1$



(a)



(b)

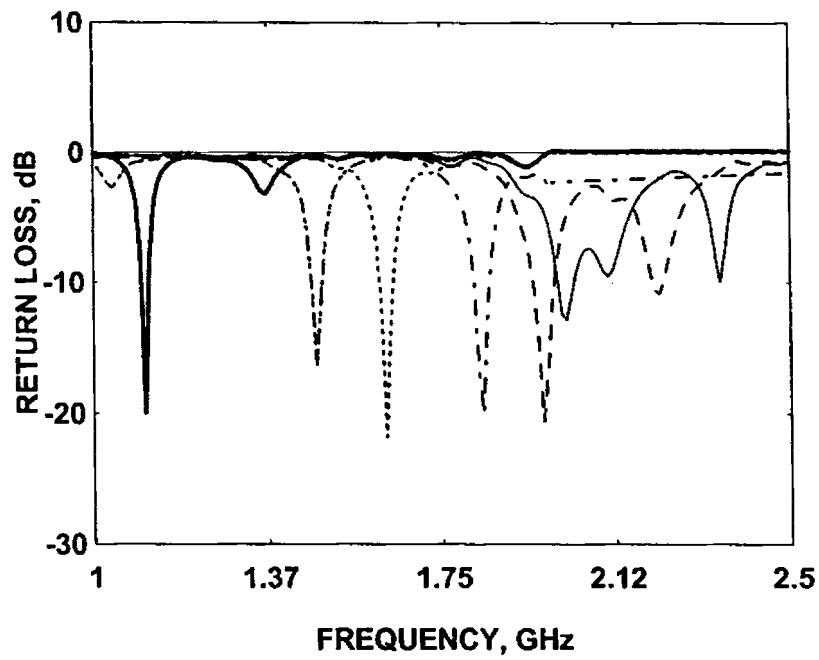
FIGURE 4.5(iii) Variation of return loss with frequency for UHF antennas

(a) $L = 10.5$ cm, $B = 7$ cm

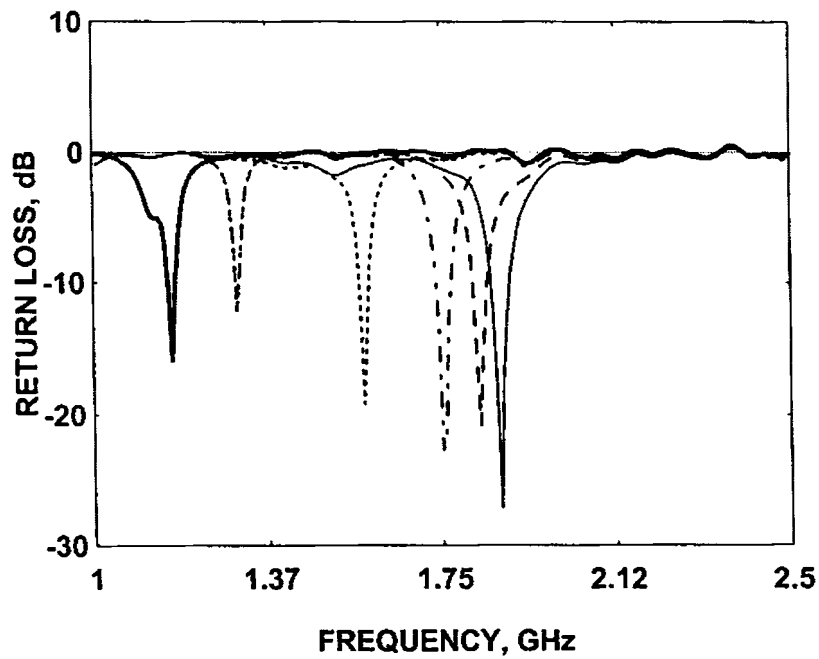
—————	$W/B = 1.0$	- - - - -	$W/B = 0.9$	- . - . -	$W/B = 0.7$
.....	$W/B = 0.5$	—————	$W/B = 0.3$	—————	$W/B = 0.1$

(b) $L = 10.5$ cm, $B = 5.25$ cm

—————	$W/B = 1.0$	- - - - -	$W/B = 0.9$	- . - . -	$W/B = 0.7$
.....	$W/B = 0.5$	—————	$W/B = 0.3$	—————	$W/B = 0.1$



(a)



(b)

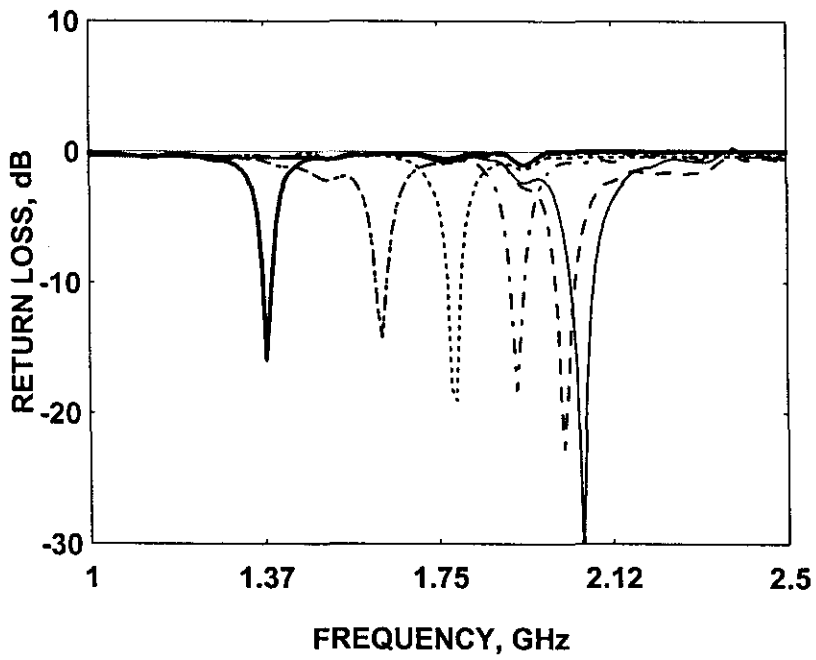
FIGURE 4.5(iv) Variation of return loss with frequency for L-band antennas

(a) $L = 3.5$ cm, $B = 7$ cm

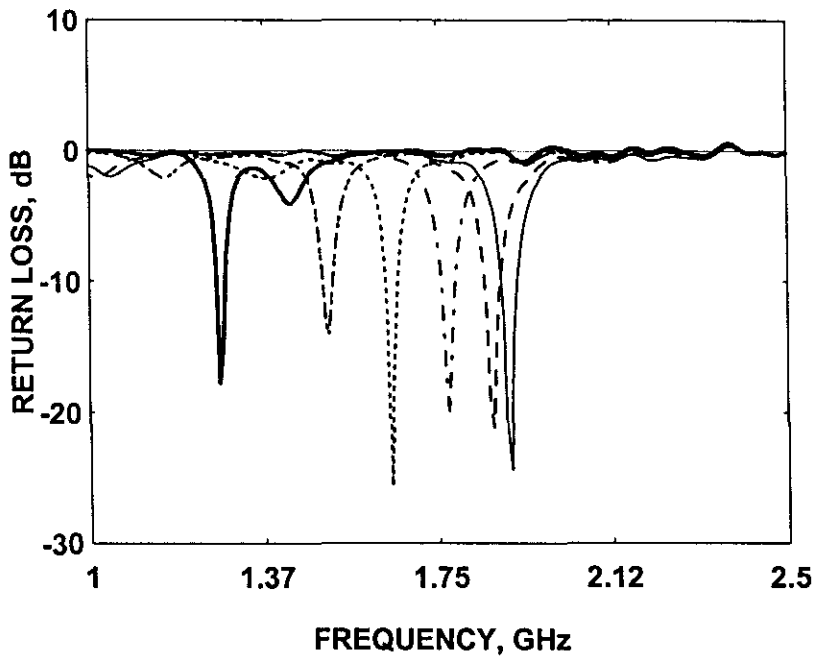
—————	$W/B = 1.0$	-----	$W/B = 0.9$	- . - . - .	$W/B = 0.7$
.....	$W/B = 0.5$	- . - . - .	$W/B = 0.3$	—————	$W/B = 0.1$

(b) $L = 3.8$ cm, $B = 4.8$ cm

—————	$W/B = 1.0$	-----	$W/B = 0.9$	- . - . - .	$W/B = 0.7$
.....	$W/B = 0.5$	- . - . - .	$W/B = 0.2083$	—————	$W/B = 0.1$



(a)



(b)

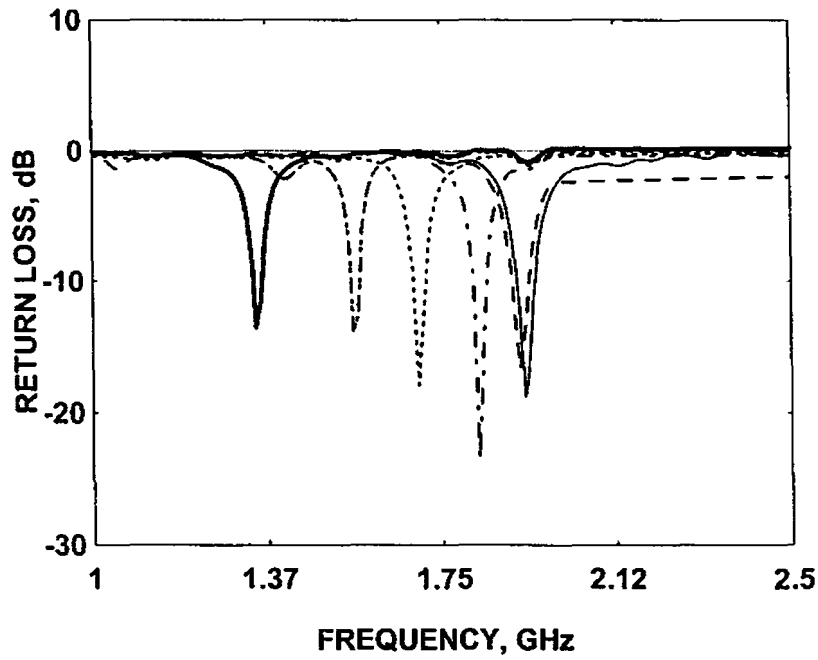
FIGURE 4.5(v) Variation of return loss with frequency for L-band antennas

(a) $L = 3.5$ cm, $B = 3.5$ cm

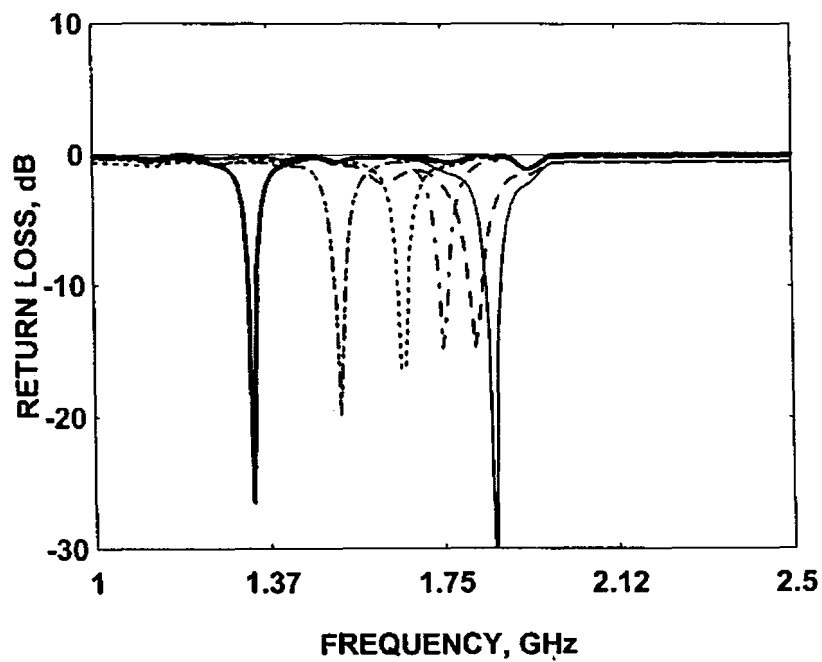
—————	$W/B = 1.0$	-----	$W/B = 0.9$	- . - . - .	$W/B = 0.7$
.....	$W/B = 0.5$	- . - . - .	$W/B = 0.3$	—————	$W/B = 0.1$

(b) $L = 3.811$ cm, $B = 3.2$ cm

—————	$W/B = 1.0$	-----	$W/B = 0.9$	- . - . - .	$W/B = 0.7$
.....	$W/B = 0.5$	- . - . - .	$W/B = 0.3125$	—————	$W/B = 0.1$



(a)



(b)

FIGURE 4.5(vi) Variation of return loss with frequency for L-band antennas

(a) $L = 3.8$ cm, $B = 2.53$ cm

—————	$W/B = 1.0$	-----	$W/B = 0.9$	- . - . - .	$W/B = 0.7$
.....	$W/B = 0.5$	$W/B = 0.3$	—————	$W/B = 0.1$

(b) $L = 4$ cm, $B = 2$ cm

—————	$W/B = 1.0$	-----	$W/B = 0.9$	- . - . - .	$W/B = 0.7$
.....	$W/B = 0.5$	$W/B = 0.3$	—————	$W/B = 0.1$

For clarity, the resonant frequency and its % reduction, physical area of the drum-shaped antenna (A_d) and equivalent rectangular patch antenna (A_r), etc., are given in Table 4.2. The % reduction in resonant frequency is calculated using the formula $(F_r - f_d)/F_r$, where F_r is the resonant frequency of the rectangular antenna having same L and B as those of the corresponding drum-shaped antenna resonating at f_d . From the Table it can be seen that the metallisation area of the new antenna decreases as the resonant frequency decreases, whereas in the case of the rectangular antennas the metallisation area increases with decrease of resonant frequency. In the UHF case, when $L/B = 0.7$ and $W/B = 0.1$, the area requirement of a rectangular patch antenna (203.0 cm^2) operating at the same frequency and having the same L/B ratio is 5.27 times that of the new drum-shaped antenna (38.5 cm^2). In a similar manner, in the L-band, when $L/B = 0.5$ and $W/B = 0.1$, the area required for an equivalent rectangular patch antenna is 5.93 times that of the drum-shaped antenna. This establishes the compact nature of the antenna.

Another important property of the new antenna, which is very clear from Table 4.2 is the ability to tune the resonant frequency without increasing the overall size. i.e., frequency tuning through reduction of resonant frequency can be achieved by slightly reducing the central width (no need to fabricate a new antenna) whereas in the case of a rectangular patch antenna, resonant frequency reduction requires the extension of the resonant length and this in turn requires the fabrication of a new antenna. Frequency tuning through the increase of resonant frequency can be achieved by reducing the length in both the cases.

It can also be seen from Table 4.2 that, in almost all the cases, for the same W/B ratio, the percentage reduction in resonant frequency increases with decrease in L/B ratio. For the same percentage reduction in central width, the range of variation of resonant frequency is larger when L/B is less and it decreases as L/B increases. In the UHF-band the range of resonant frequency variation corresponding to a change of central width from maximum to 10% of maximum value is 425 MHz when $L/B = 0.7$ and 230 MHz when $L/B = 2.0$. In the L-band, the range of variations are 905 MHz and 520 MHz when $L/B = 0.5$ and 2.0 respectively.

TABLE 4.2(i) Resonant Frequency (f_{01}), % reduction in resonant frequency, % bandwidth, metallisation area of drum-shaped antenna (A_d) and metallisation area of equivalent rectangular patch having the same L/B ratio (A_r) of different UHF-band drum-shaped antennas.

L/B	W/B	f_{01} MHz	% reduction in resonant frequency	% bandwidth	A_d cm ²	A_r cm ²
0.70	1.0	1017.0	0.00	1.97	70.00	70.00
	0.9	998.00	1.87	1.87	66.50	71.24
	0.7	929.00	8.65	1.36	59.50	82.09
	0.5	851.00	16.32	1.41	52.50	97.95
	0.3	739.00	27.34	1.22	45.50	130.03
	0.1	592.00	41.79	1.46	38.50	203.00
0.776	1.0	1022.0	0.00	1.43	61.88	61.88
	0.9	998.00	2.35	1.54	58.79	64.41
	0.7	939.00	8.12	1.42	52.60	72.70
	0.5	866.00	15.26	0.93	46.41	85.58
	0.3	758.00	25.83	1.19	40.23	111.72
	0.224	709.00	30.63	1.50	34.04	127.89
1.00	1.0	1032.0	0.00	1.49	49.00	49.00
	0.9	1011.0	2.03	1.02	46.55	49.14
	0.7	958.00	7.17	1.67	41.65	54.61
	0.5	881.00	14.63	1.44	36.75	64.64
	0.3	787.00	23.74	1.27	31.85	81.00
	0.1	651.00	36.92	1.02	26.95	118.37
1.155	1.0	1040.0	0.00	1.49	41.58	41.58
	0.9	1013.0	2.60	1.25	39.50	42.55
	0.7	963.00	7.40	1.31	35.34	47.02
	0.5	890.00	14.42	1.12	31.19	56.56
	0.333	812.00	21.92	1.31	27.03	66.16
	0.1	665.00	36.06	0.90	22.87	98.59
1.50	1.0	695.00	0.00	1.63	73.50	73.50
	0.9	680.00	2.16	1.37	69.83	73.08
	0.7	646.00	7.05	1.55	62.48	81.00
	0.5	597.00	14.10	1.45	55.13	94.76
	0.3	543.00	21.87	0.86	47.78	114.36
	0.1	455.00	34.53	1.43	40.43	162.60
2.00	1.0	695.00	0.00	1.05	55.13	55.13
	0.9	685.00	1.44	1.46	52.37	54.50
	0.7	651.00	6.33	1.23	46.86	60.28
	0.5	611.00	12.09	1.47	41.34	68.39
	0.3	553.00	20.43	1.21	35.83	83.21
	0.1	465.00	33.09	1.29	30.32	117.58

TABLE 4.2(ii) Resonant Frequency (f_{01}), % reduction in resonant frequency, % bandwidth, metallisation area of drum-shaped antenna (A_d) and metallisation area of equivalent rectangular patch having the same L/B ratio (A_r) of different L-band drum-shaped antennas.

L/B	W/B	f_{01} MHz	% reduction in f_{01}	% bandwidth	A_d cm ²	A_r cm ²	
0.50	1.0	2015	0.00	1.50	24.50	24.50	0.0000
	0.9	1971	2.18	2.18	23.28	24.78	0.01181
	0.7	1837	8.83	1.72	20.83	28.58	0.01134
	0.5	1631	19.06	1.77	18.38	36.64	0.01127
	0.3	1478	26.65	1.48	15.93	44.75	0.0078
	0.1	1110	44.91	1.30	13.48	79.88	0.01214
0.792	1.0	1877	0.00	2.13	18.24	18.24	0.00972
	0.9	1833	2.34	1.69	17.33	18.54	0.00915
	0.7	1751	6.71	1.50	15.50	20.33	0.00955
	0.5	1581	15.77	1.20	13.68	25.01	0.00865
	0.2083	1308	30.31	0.61	11.86	36.58	0.00807
	0.1	1168	37.77	1.35	10.03	45.95	0.00850
1.00	1.0	2059	0.00	2.43	12.25	12.25	0.00595
	0.9	2021	1.85	2.03	11.64	12.25	0.00576
	0.7	1922	6.65	1.61	10.41	13.54	0.00532
	0.5	1784	13.36	1.51	9.19	15.76	0.00515
	0.3	1628	20.93	1.29	7.95	18.92	0.00488
	0.1	1381	32.93	1.16	6.74	26.32	0.00488
1.191	1.0	1899	0.00	1.66	12.19	12.19	0.00619
	0.9	1862	1.95	1.62	11.58	12.26	0.00622
	0.7	1778	6.37	1.52	10.36	13.44	0.00583
	0.5	1648	13.22	1.37	9.14	15.60	0.00555
	0.3125	1515	20.22	1.35	7.92	18.48	0.00523
	0.1	1278	32.70	1.33	6.71	26.07	0.00525
1.50	1.0	1931	0.00	1.76	9.61	9.61	0.00498
	0.9	1918	0.67	1.62	9.13	9.29	0.00476
	0.7	1831	5.18	1.56	8.17	10.14	0.00416
	0.5	1708	11.55	1.58	7.21	11.66	0.00392
	0.3	1562	19.11	1.03	6.25	13.94	0.00407
	0.1	1353	29.93	1.41	5.29	18.50	0.00397
2.00	1.0	1860	0.00	1.70	8.00	8.00	0.00410
	0.9	1818	2.26	1.54	7.60	7.90	0.00418
	0.7	1758	5.48	0.91	6.80	8.38	0.00396
	0.5	1665	10.48	1.34	6.00	9.40	0.00380
	0.3	1528	17.85	1.37	5.20	11.12	0.00370
	0.1	1340	27.96	1.37	4.40	14.36	0.00375

The system resonates at the minimum frequency when W/B is a minimum. The variation of resonant frequency for the different antenna structures defined in Table 4.1 are shown in Figure 4.6. It is found that the resonant frequency gradually increases with W/B .

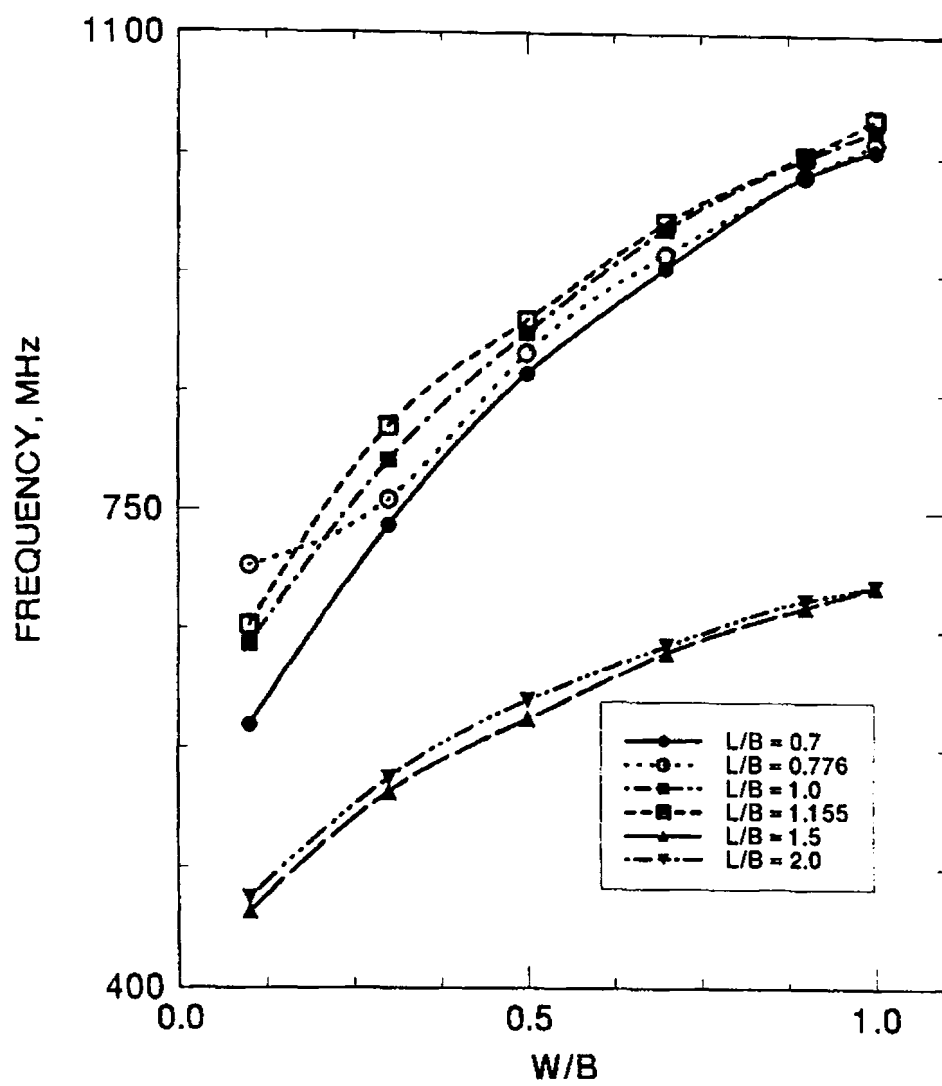


FIGURE 4.6(i) Variation of TM_{01} mode resonance frequency with central width (W) for different aspect ratios (L/B) of UHF antennas

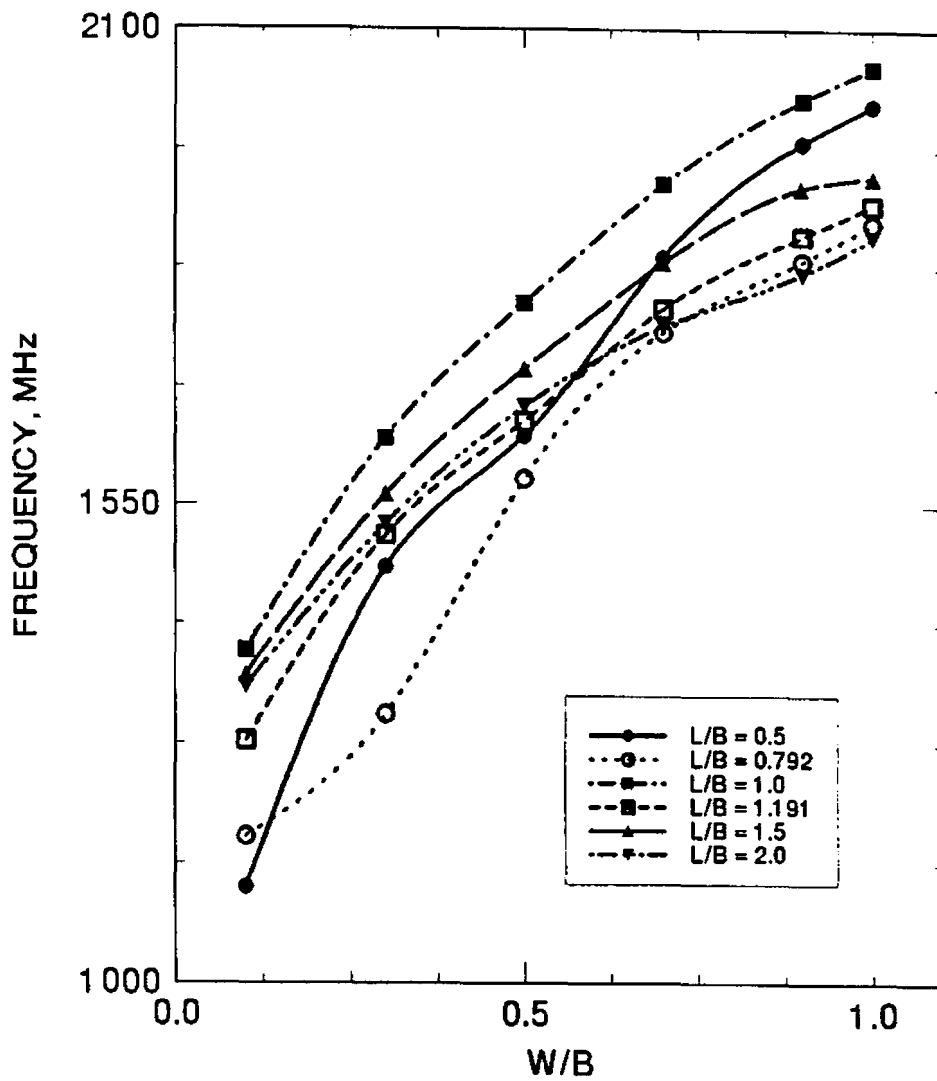


FIGURE 4.6(ii) Variation of TM_{01} mode resonance frequency with central width (W) for different aspect ratios (L/B) of L-band antennas

4.2.2 Impedance bandwidth

The bandwidth of a microstrip antenna is the range of frequencies over which the return loss is less than -10 dB. Like other microstrip antennas these antennas are also narrow banded and hence the bandwidth can be conveniently expressed as a percentage of the frequency difference over the centre frequency of the band. The percentage bandwidths for the different antenna configurations studied are also given in Table 4.2.

It is observed that there is not much variation in impedance bandwidth with L/B and W/B . From Table 4.2 we can see that in almost all cases for both the bands the value of bandwidth lies between 1 and 2. This is typical for microstrip antennas and hence we can say that frequency reduction is achieved without disturbing the bandwidth. In the UHF-band when $L/B = 0.7$, the percentage bandwidth varies from 1.97% to 1.22% only, as the central width reduces to 10% of the maximum value. In the L-band, when $L/B = 0.5$, the percentage bandwidth varies from 2.18% to 1.30% only, as the central width reduces from maximum value to 10% of the maximum value. This shows that the compact nature of the antenna is achieved without sacrificing the bandwidth considerably.

4.2.3 Radiation Pattern

Being a new type of compact microstrip antenna, its radiation pattern characteristics have been studied in detail. The co-polar and cross-polar radiation patterns of different antenna configurations in the principal planes are taken at 11 frequency points in the operating frequency band of each antenna. The measured co-polar and cross-polar radiation patterns at the corresponding central frequencies of different configurations are shown in Figure 4.7. The E - and H -plane 3 dB beamwidths and peak cross-polar levels are given in Table. 4.3.

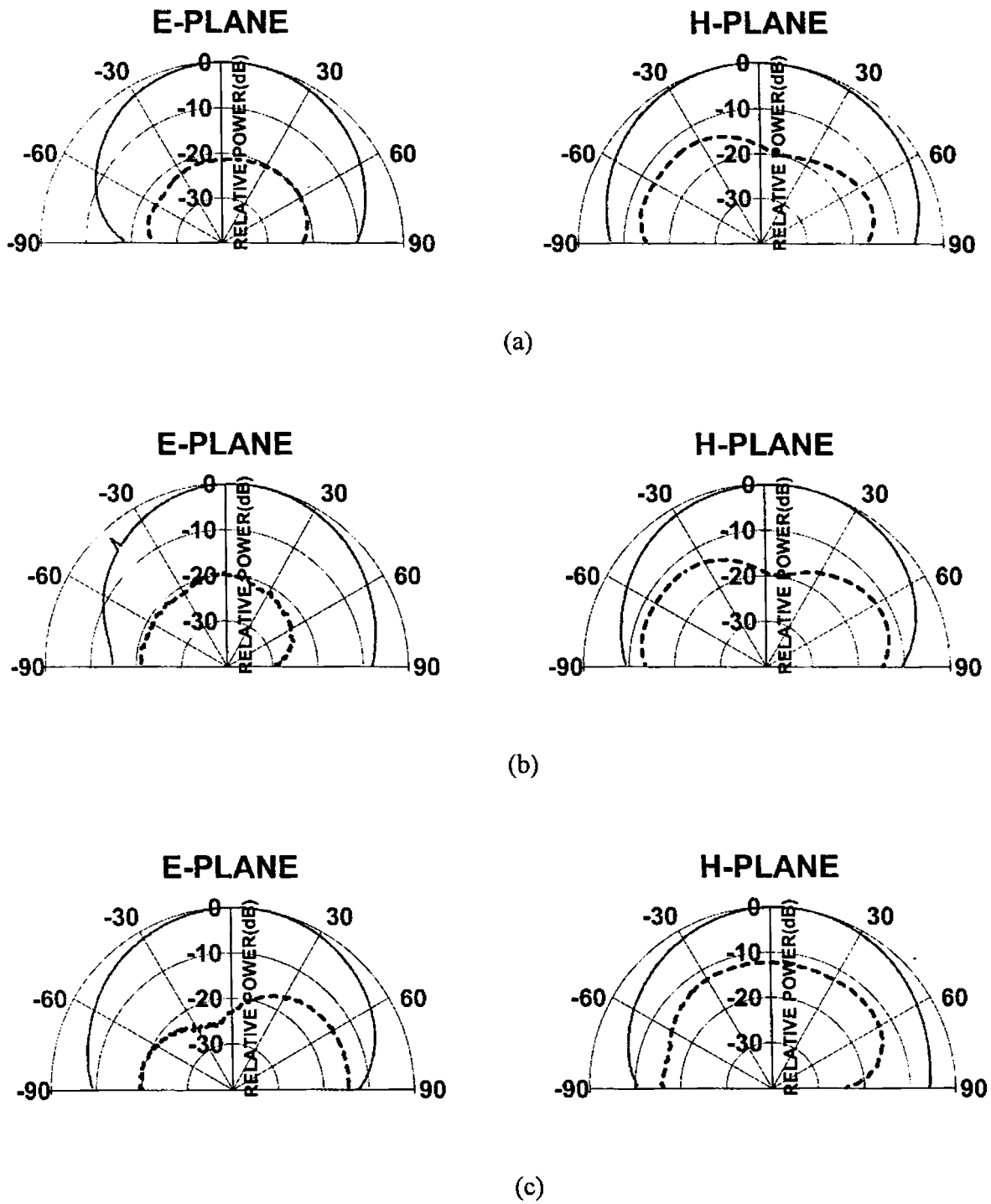


FIGURE 4.7(i) E- and H-plane co and cross polar radiation patterns of different UHF-band antennas

————— co polar - - - - - cross polar

- (a) $L = 10.5$ cm, $B = 7$ cm, $W/B = 1.0$
- (b) $L = 10.5$ cm, $B = 7$ cm, $W/B = 0.9$
- (c) $L = 10.5$ cm, $B = 7$ cm, $W/B = 0.7$

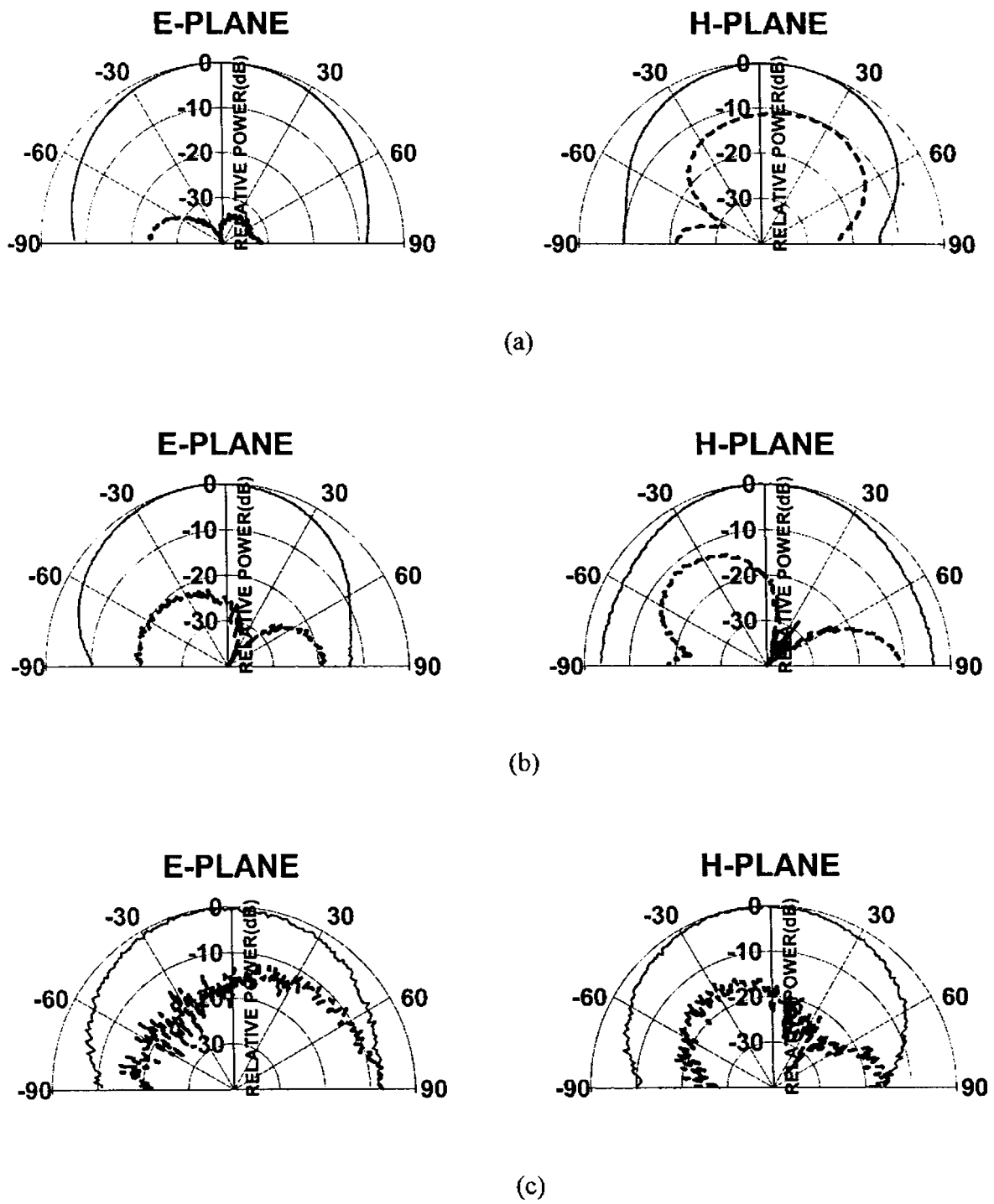


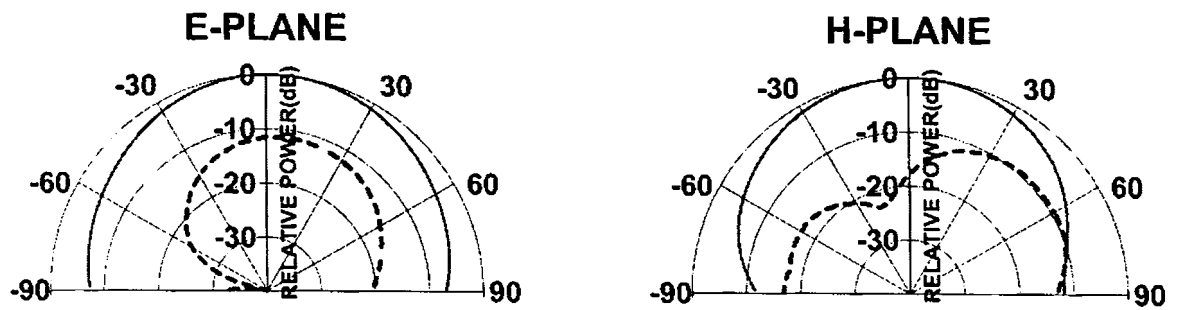
FIGURE 4.7(ii) *E*- and *H*-plane co and cross polar radiation patterns of different UHF-band antennas

————— co polar - - - - - cross polar

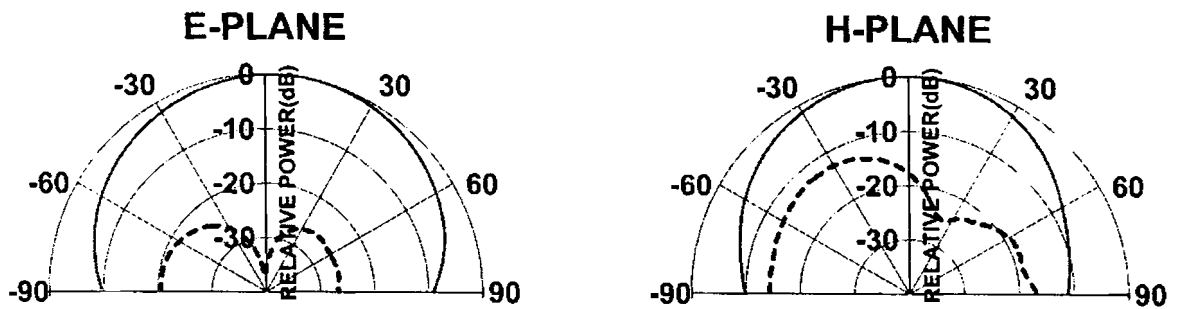
(a) $L = 10.5$ cm, $B = 7$ cm, $W/B = 0.5$

(b) $L = 10.5$ cm, $B = 7$ cm, $W/B = 0.3$

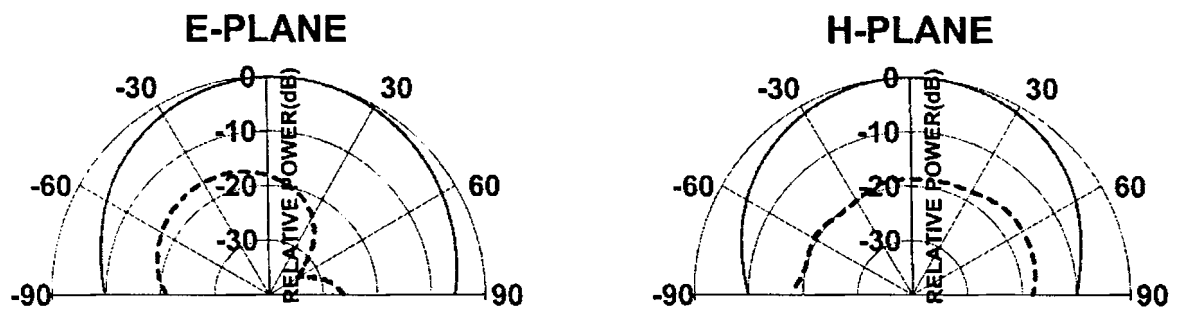
(c) $L = 10.5$ cm, $B = 7$ cm, $W/B = 0.1$



(a)



(b)



(c)

FIGURE 4.7(iii) E- and H-plane co and cross polar radiation patterns of different UHF-band antennas

————— co polar - - - - - cross polar

(a) $L = 7$ cm, $B = 7$ cm, $W/B = 1.0$

(b) $L = 7$ cm, $B = 7$ cm, $W/B = 0.9$

(c) $L = 7$ cm, $B = 7$ cm, $W/B = 0.7$

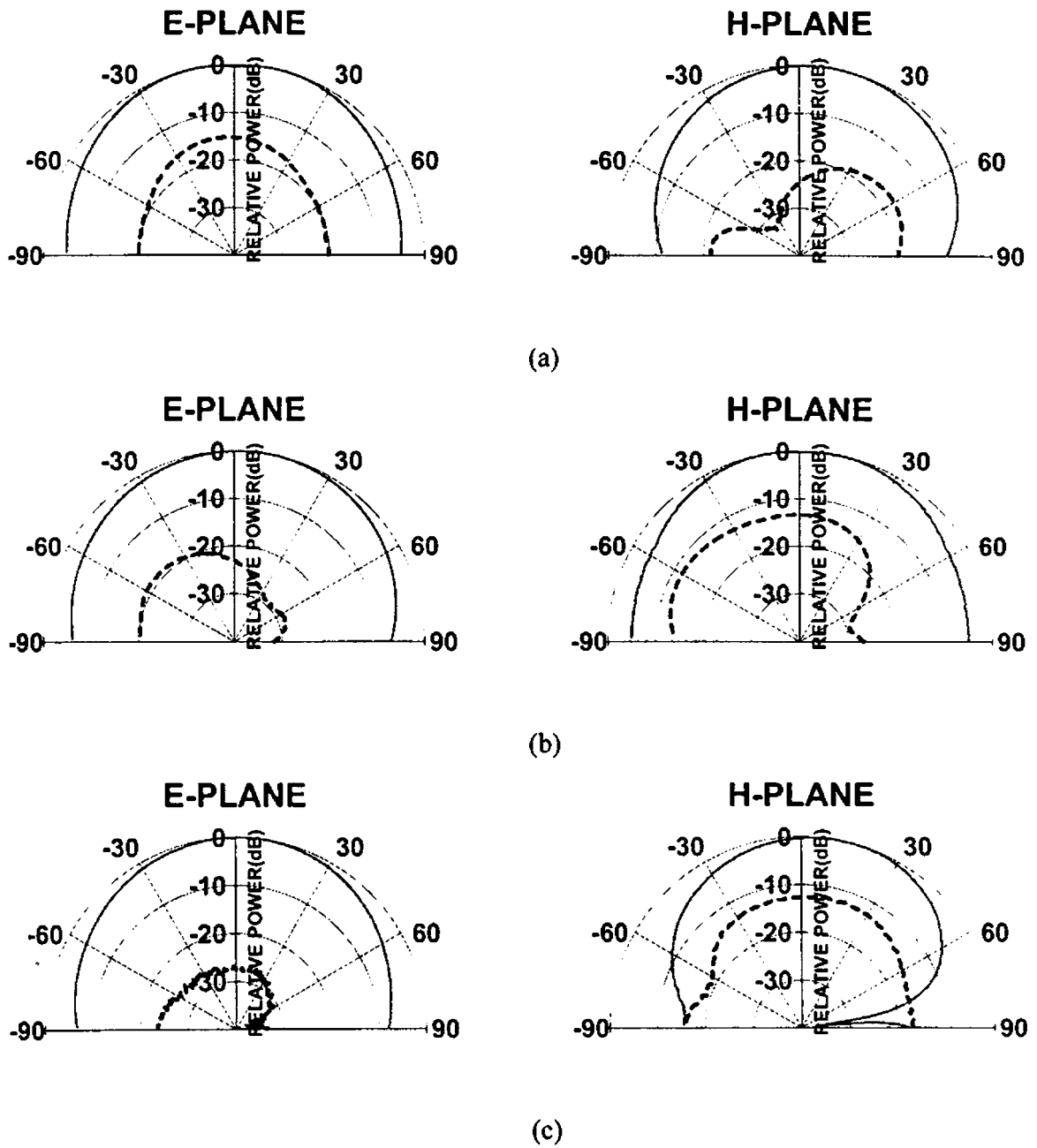


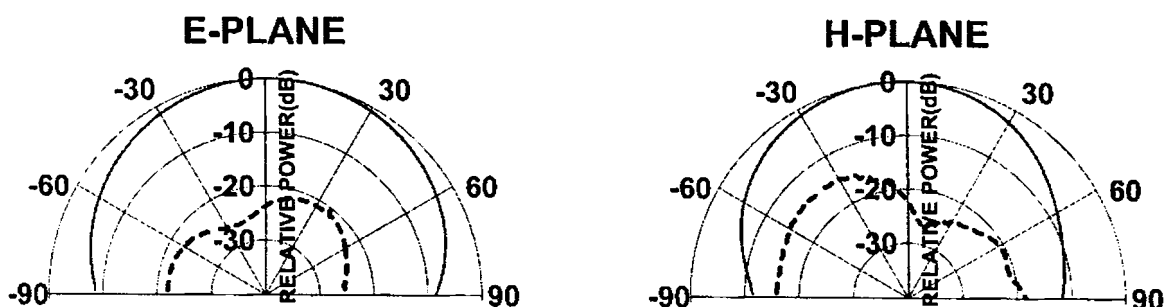
FIGURE 4.7(iv) E- and H-plane co and cross polar radiation patterns of different UHF-band antennas

————— co polar - - - - - cross polar

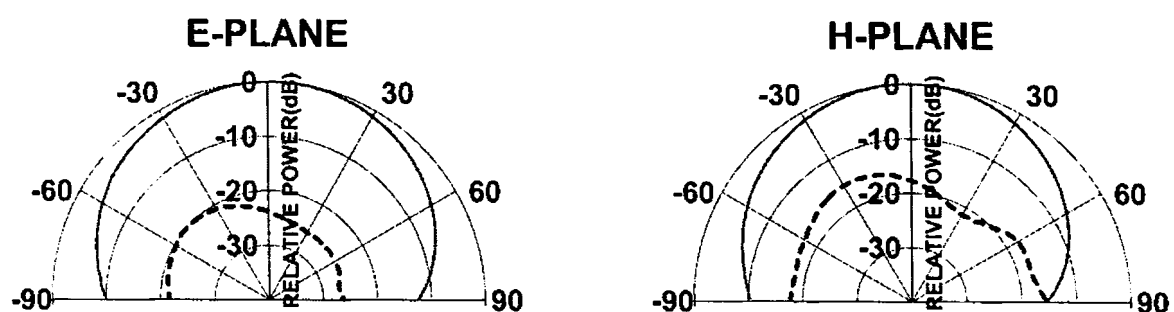
(a) $L = 7$ cm, $B = 7$ cm, $W/B = 0.5$

(b) $L = 7$ cm, $B = 7$ cm, $W/B = 0.3$

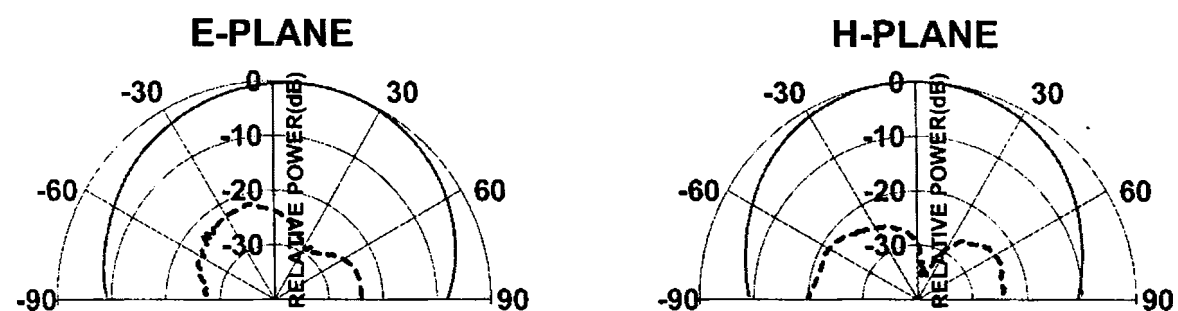
(c) $L = 7$ cm, $B = 7$ cm, $W/B = 0.1$



(a)



(b)



(c)

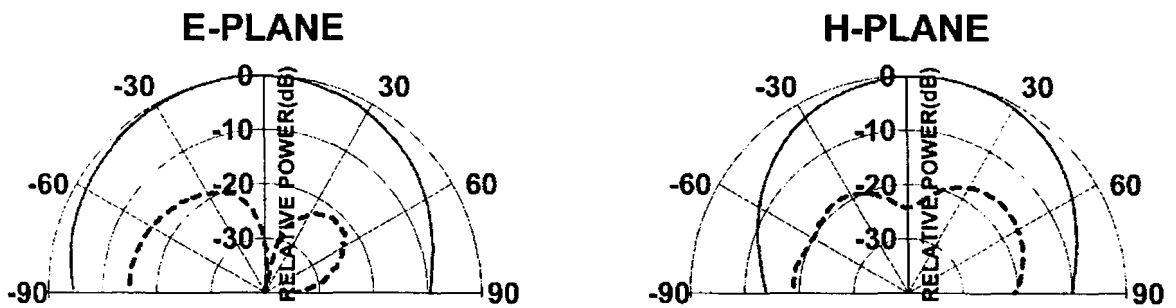
FIGURE 4.7(v) E- and H-plane co and cross polar radiation patterns of different UHF-band antennas

————— co polar - - - - - cross polar

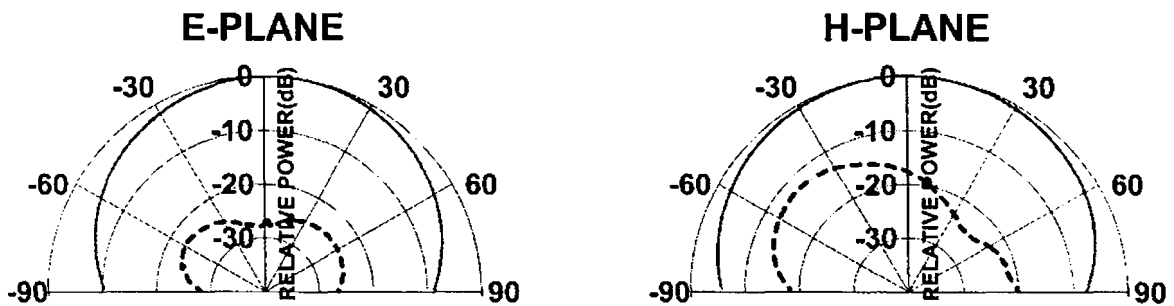
(a) $L = 7$ cm, $B = 10$ cm, $W/B = 1.0$

(b) $L = 7$ cm, $B = 10$ cm, $W/B = 0.9$

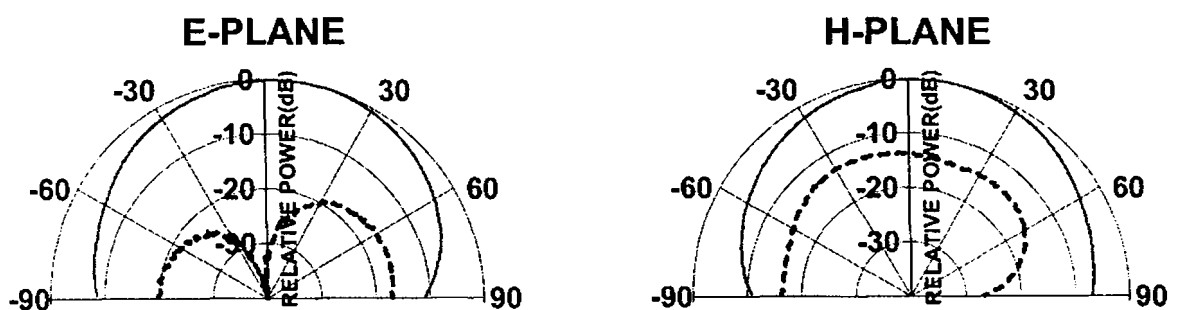
(c) $L = 7$ cm, $B = 10$ cm, $W/B = 0.7$



(a)



(b)



(c)

FIGURE 4.7(vi) *E*- and *H*-plane co and cross polar radiation patterns of different UHF-band antennas

————— co polar - - - - - cross polar

(a) $L = 7$ cm, $B = 10$ cm, $W/B = 0.5$

(b) $L = 7$ cm, $B = 10$ cm, $W/B = 0.3$

(c) $L = 7$ cm, $B = 10$ cm, $W/B = 0.1$

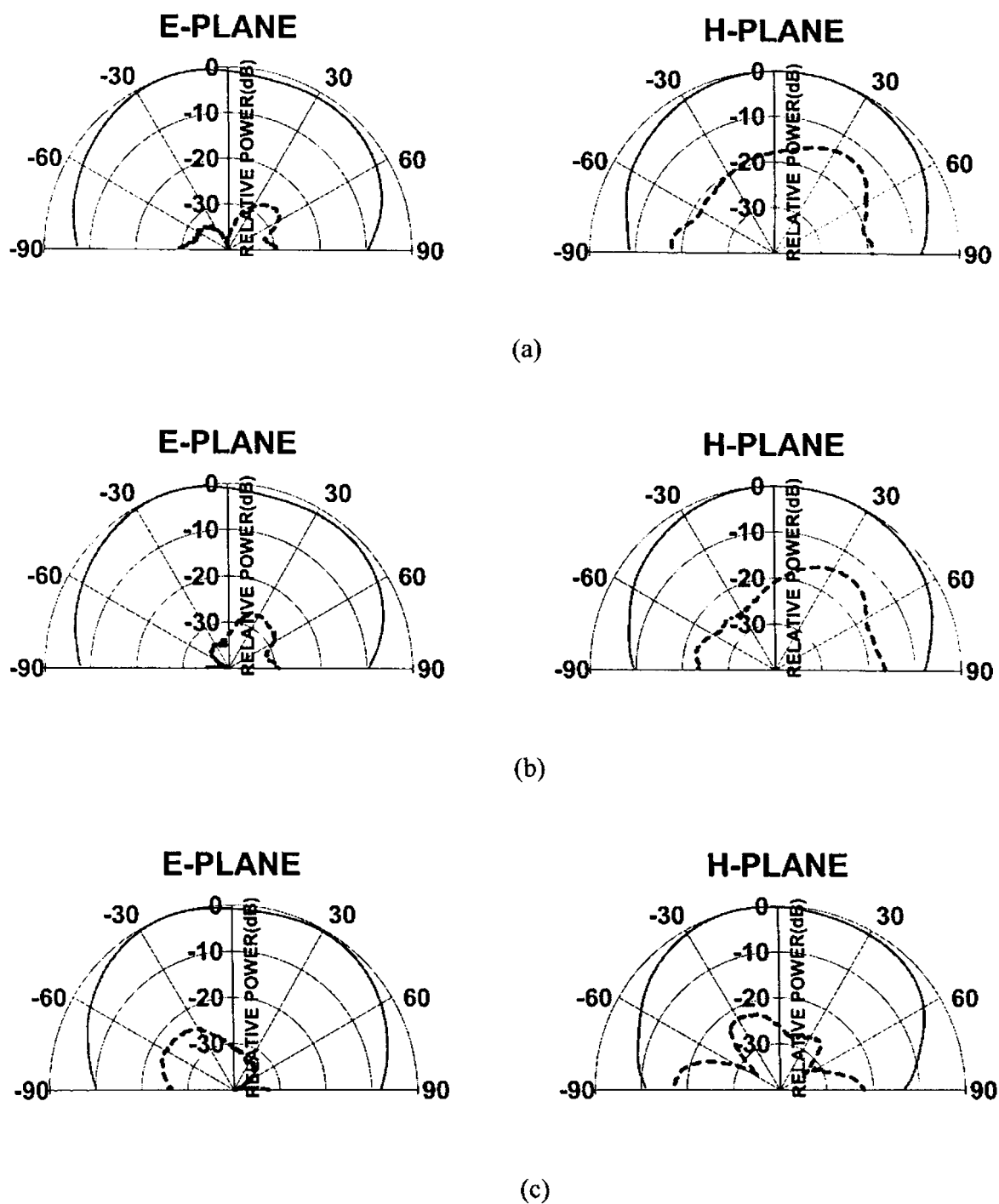


FIGURE 4.7(vii) *E*- and *H*-plane co and cross polar radiation patterns of different L-band antennas

————— co polar - - - - - cross polar

(a) $L = 3.8$ cm, $B = 2.53$ cm, $W/B = 1.0$

(b) $L = 3.8$ cm, $B = 2.53$ cm, $W/B = 0.9$

(c) $L = 3.8$ cm, $B = 2.53$ cm, $W/B = 0.7$

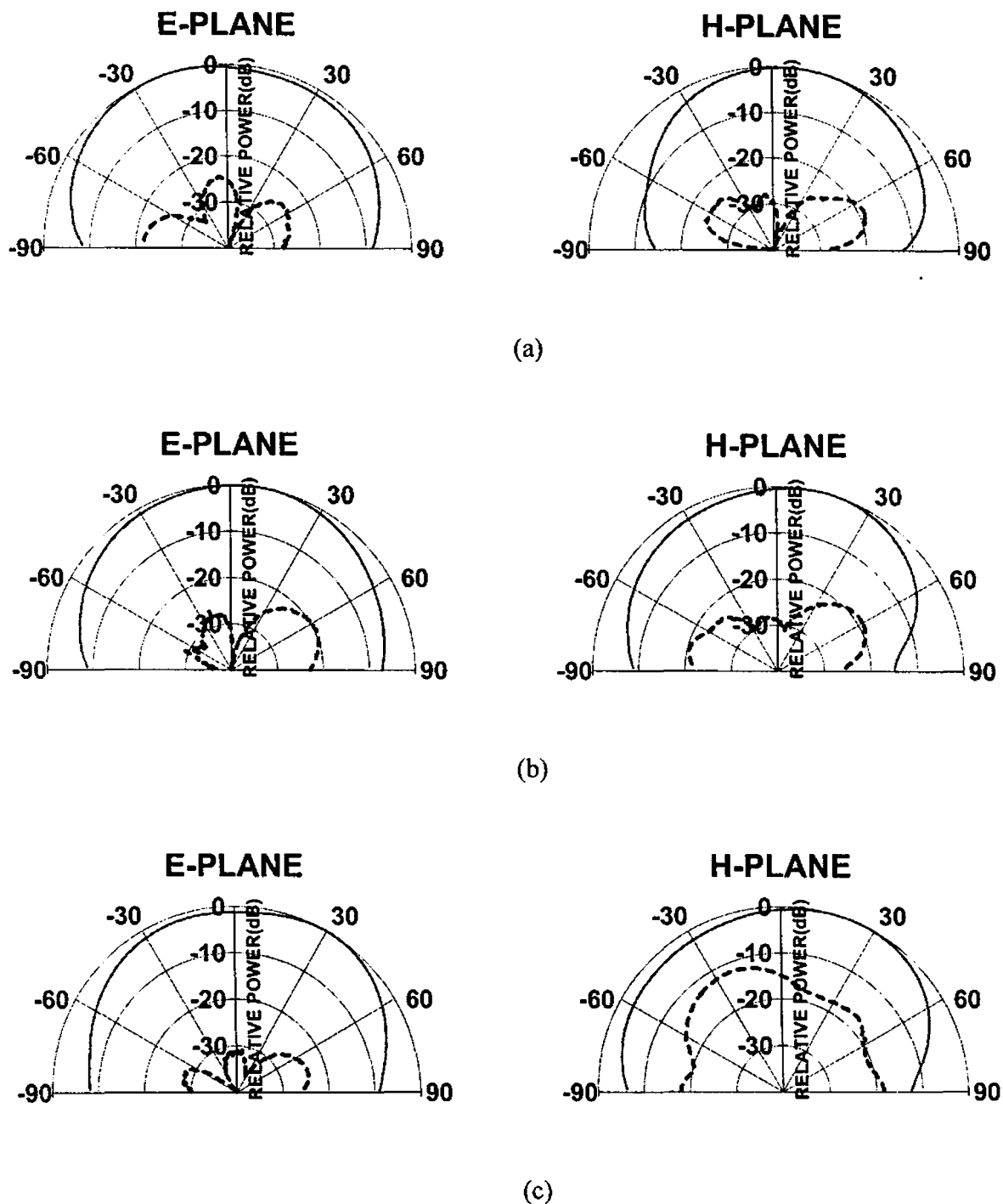


FIGURE 4.7(viii) *E*- and *H*-plane co and cross polar radiation patterns of different L-band antennas

—— co polar - - - - - cross polar

(a) $L = 3.8$ cm, $B = 2.53$ cm, $W/B = 0.5$

(b) $L = 3.8$ cm, $B = 2.53$ cm, $W/B = 0.3$

(c) $L = 3.8$ cm, $B = 2.53$ cm, $W/B = 0.1$

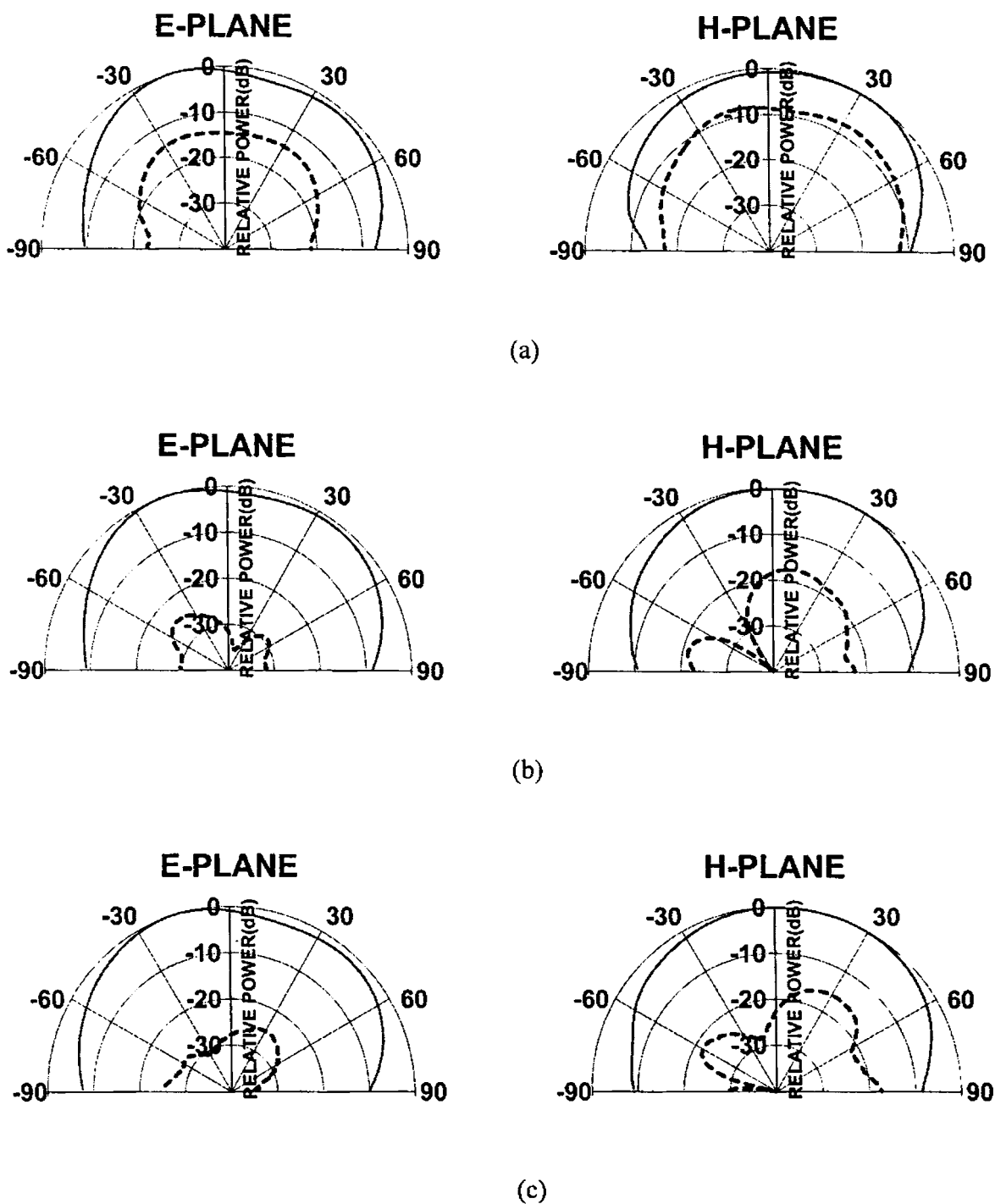


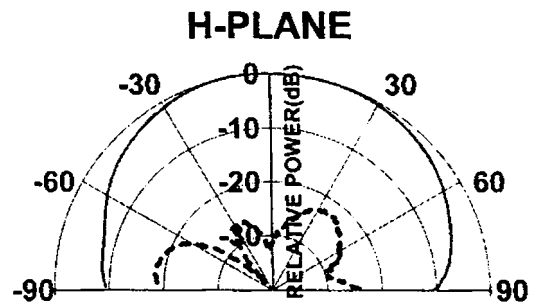
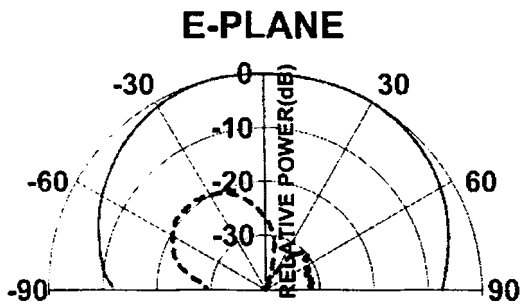
FIGURE 4.7(ix) E- and H-plane co and cross polar radiation patterns of different L-band antennas

—— co polar - - - - - cross polar

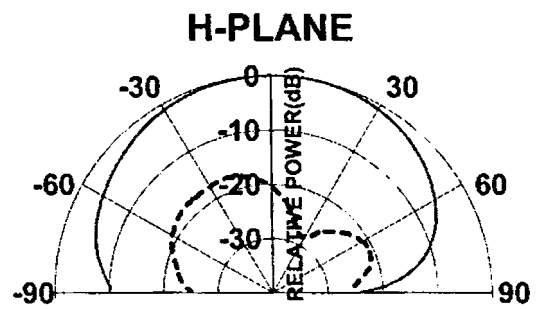
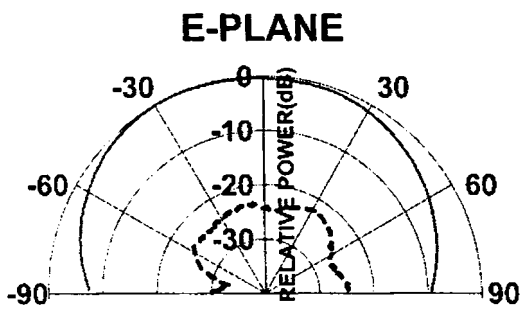
(a) $L = 3.5$ cm, $B = 3.5$ cm, $W/B = 1.0$

(b) $L = 3.5$ cm, $B = 3.5$ cm, $W/B = 0.9$

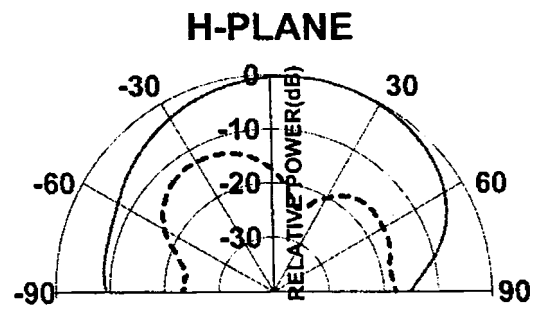
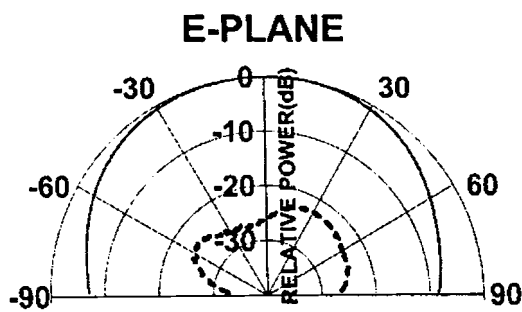
(c) $L = 3.5$ cm, $B = 3.5$ cm, $W/B = 0.7$



(a)



(b)



(c)

FIGURE 4.7(x) E- and H-plane co and cross polar radiation patterns of different L-band antennas

————— co polar - - - - - cross polar

(a) $L = 3.5$ cm, $B = 3.5$ cm, $W/B = 0.5$

(b) $L = 3.5$ cm, $B = 3.5$ cm, $W/B = 0.3$

(c) $L = 3.5$ cm, $B = 3.5$ cm, $W/B = 0.1$

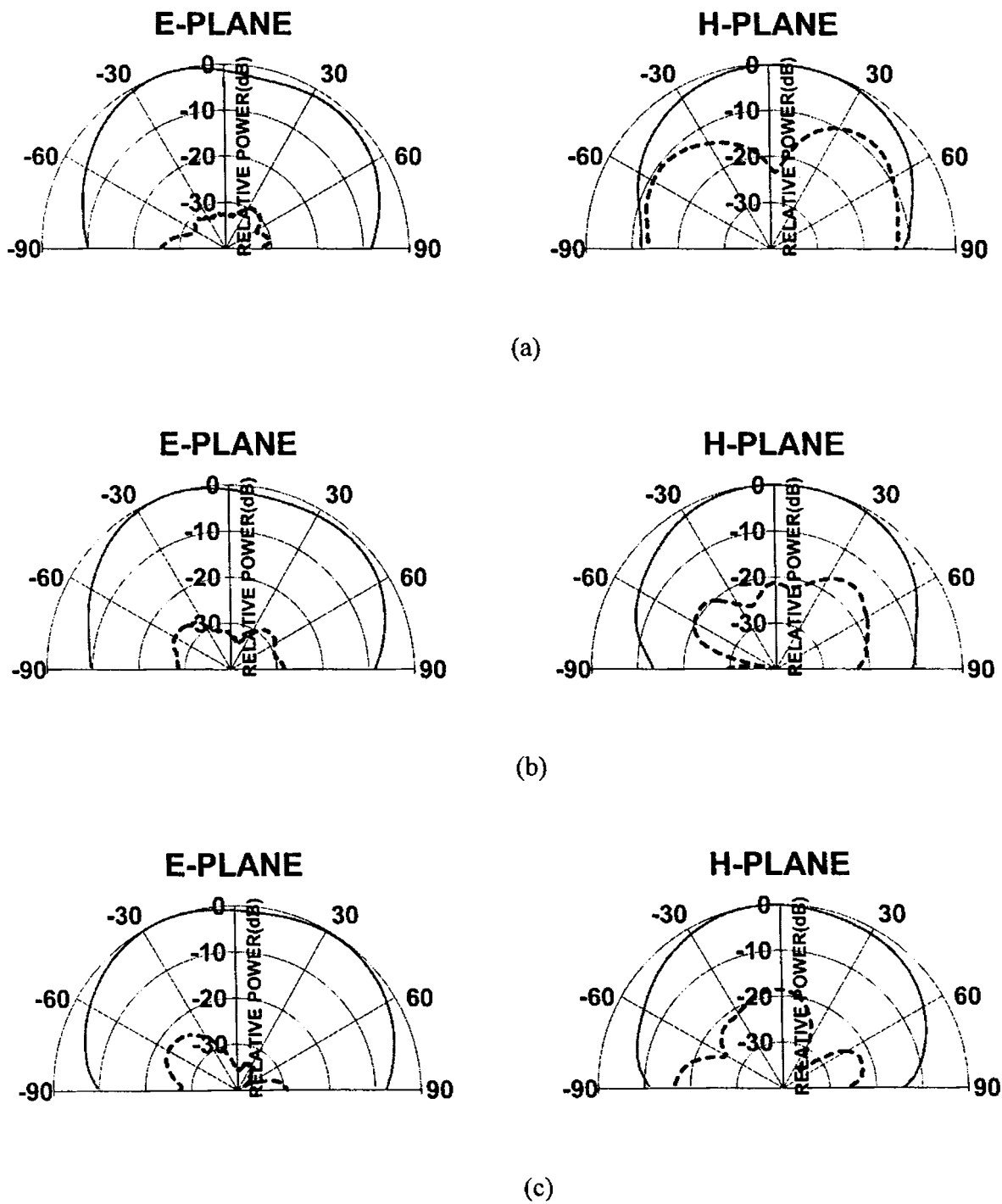
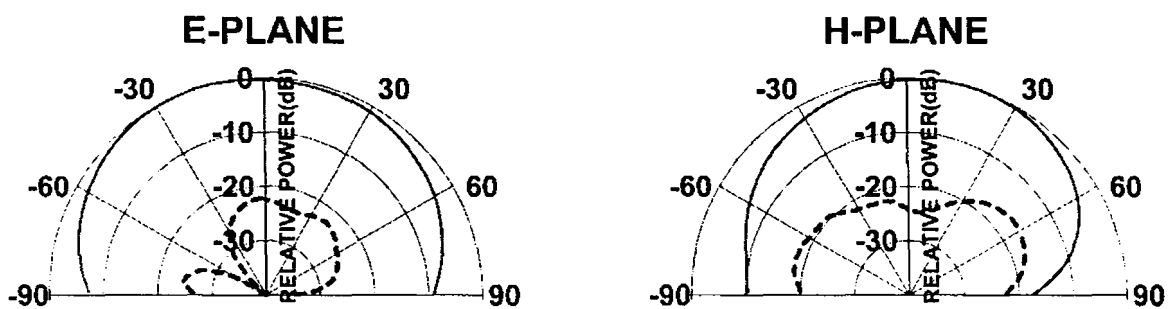


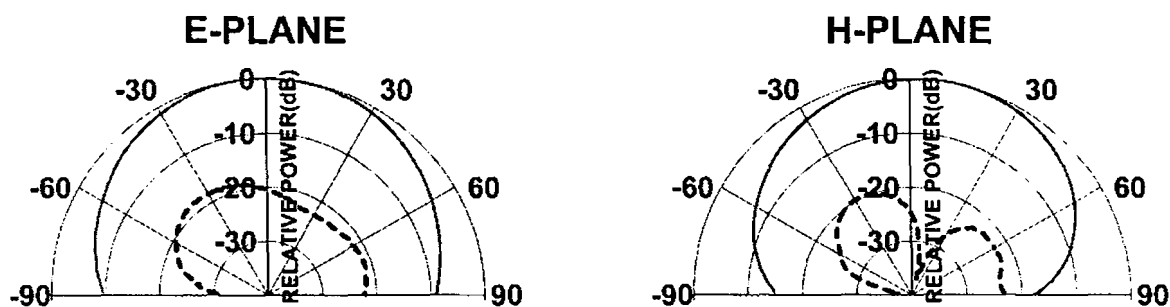
FIGURE 4.7(xi) *E*- and *H*-plane co and cross polar radiation patterns of different L-band antennas

————— co polar - - - - - cross polar

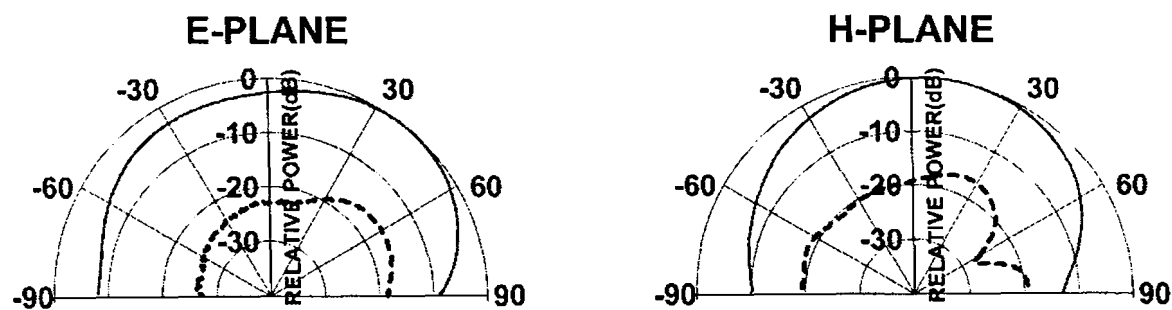
- (a) $L = 3.5$ cm, $B = 7.0$ cm, $W/B = 1.0$
 (b) $L = 3.5$ cm, $B = 7.0$ cm, $W/B = 0.9$
 (c) $L = 3.5$ cm, $B = 7.0$ cm, $W/B = 0.7$



(a)



(b)



(c)

FIGURE 4.7(xii) *E*- and *H*-plane co and cross polar radiation patterns of different L-band antennas

————— co polar - - - - - cross polar

(a) $L = 3.5$ cm, $B = 7.0$ cm, $W/B = 0.5$

(b) $L = 3.5$ cm, $B = 7.0$ cm, $W/B = 0.3$

(c) $L = 3.5$ cm, $B = 7.0$ cm, $W/B = 0.1$

TABLE 4.3(i) Characteristics of radiation patterns of the UHF-band antennas given in Figure 4.7.

<i>L/B</i>	<i>W/B</i>	3 dB beamwidth (deg.)		Peak cross-polar level (dB)	
		<i>E</i> -plane	<i>H</i> -plane	<i>E</i> -plane	<i>H</i> -plane
1.5	1.0	85	122	-19.83	-12.9
	0.9	82	101	-19.37	-12.08
	0.7	93	96	-14.1	-12.17
	0.5	97	85	-23.62	-10.27
	0.3	90	91	-18.36	-10.42
	0.1	86	89	-7.04	-13.76
1.0	1.0	92	88	-11.42	-9.39
	0.9	98	80	-20.57	-12.55
	0.7	102	90	-16.31	-16.59
	0.5	115	93	-15.09	-17.36
	0.3	111	99	-18.83	-11.82
	0.1	98	77	-23.52	-12.39
0.7	1.0	102	79	-20.48	-14.57
	0.9	93	81	-19.97	-15.41
	0.7	92	87	-21.85	-19.98
	0.5	116	79	-14.8	-16.36
	0.3	96	128	-23.05	-12.4
	0.1	92	89	-16.27	-12.97

TABLE 4.3(ii) Characteristics of radiation patterns of the L-band antennas given in Figure 4.7

<i>L/B</i>	<i>W/B</i>	3 dB beamwidth (deg.)		Peak cross-polar level (dB)	
		<i>E</i> -plane	<i>H</i> -plane	<i>E</i> -plane	<i>H</i> -plane
1.5	1.0	118	107	-26.31	-13.57
	0.9	121	111	-26.77	-14.27
	0.7	115	103	-23.01	-16.76
	0.5	122	85	-21.37	-18.83
	0.3	104	94	-19.48	-18.83
	0.1	105	116	-23.94	-11.92
1.0	1.0	110	102	-14.04	-7.62
	0.9	112	99	-24.65	-17.35
	0.7	115	110	-24.87	-15.83
	0.5	111	106	-19.05	-18.17
	0.3	110	95	-22.17	-17.3
	0.1	105	86	-22.53	-12.47
0.5	1.0	111	86	-26.08	-8.1
	0.9	113	90	-26.04	-15.45
	0.7	125	94	-22.8	-16.49
	0.5	120	90	-22.19	-16.49
	0.3	94	82	-18.28	-19.7
	0.1	79	86	-16.1	-16.55

From Table 4.3 it is clear that in almost all the cases for both the bands, the 3 dB beamwidth of the present antenna is comparable with that of a rectangular patch antenna. The cross-polar levels are also found to be better than 12 dB in most of the cases.

Another observation is the betterment in the cross-polar levels when $L/B = 1$. From Table 4.3 we can see that when $W/B = 1.0$ (this is the case of a square patch antenna), the cross-polar levels are higher in both the bands. As the central width becomes less than B , the cross-polar level improves to 15 dB or more in almost all cases.

4.2.4 Gain

Gain transfer method has been utilised for measuring the relative gain of the antennas. Few typical antenna configurations have been selected from both the bands for gain studies. Rectangular microstrip antennas resonating at the same frequency as that of the selected antennas have been fabricated on the same substrate.

By using a standard wideband ridged horn as the transmitter, an S_{21} THRU calibration is performed by keeping the rectangular patch as the receiver. This antenna is then replaced by the drum-shaped test antenna and the S_{21} is measured. The measured S_{21} will give the relative gain of the test antenna with respect to the standard rectangular patch antenna. Typical relative gain plots are shown in Figure 4.8 for both the bands.

The gain of the antenna is not much deteriorated when $W/B > 0.5$. However, the gain of the antenna becomes less than that of the corresponding rectangular patch antenna as the centre width becomes less than $0.5 B$. This loss in gain may be compensated by integrating suitable amplifier circuits [121] or loading with proper superstrates.

4.2.5 Mode identification through near field probing

The mode structure supported by planar microstrip antennas could be analysed through near field probe measurements. Since antennas are open structures, field probing could be performed very easily. The electric field intensity just above and perpendicular to the top conductor is measured as given in [7, 135]. These field values are seen to be a good indication of the fields that are expected to lie on the lower side of the patch.

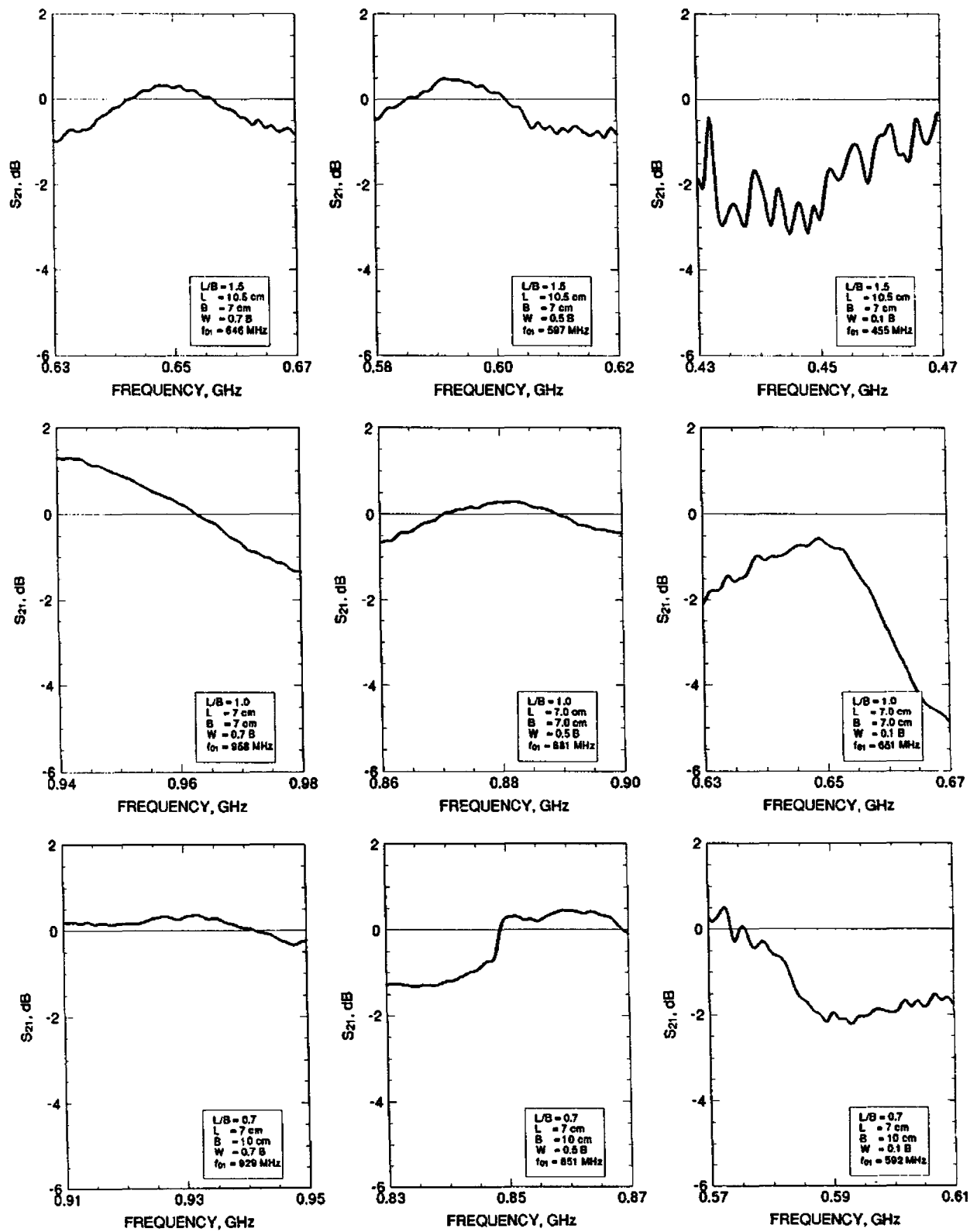


FIGURE 4.8(i) S_{21} plots of UHF-band drum-shaped antenna configurations for different central widths (W) and aspect ratios (L/B) with respect to standard rectangular microstrip patch antennas fabricated on the same substrate and resonating at the same frequency

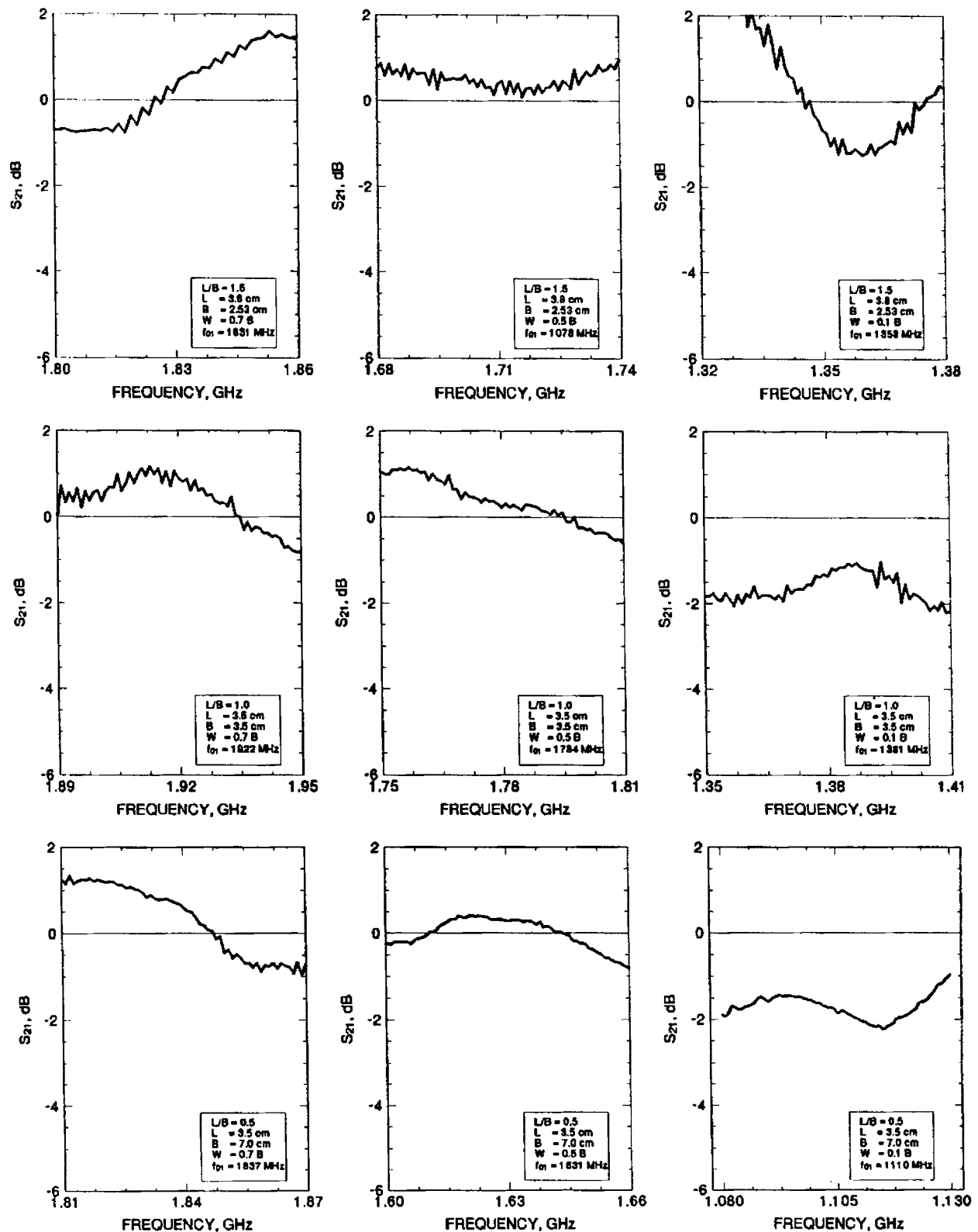


FIGURE 4.8(ii) S_{21} plots of L-band drum-shaped antenna configurations for different central widths (W) and aspect ratios (L/B) with respect to standard rectangular microstrip patch antennas fabricated on the same substrate and resonating at the same frequency

Figure 4.9 shows the measured Z-directed electric field distribution for a typical drum-shaped antenna configuration at the corresponding resonant frequency. From the figure, it is clear that, for the TM_{01} mode, the field amplitude varies from a maximum value at the radiating edges to a minimum value at the centre.

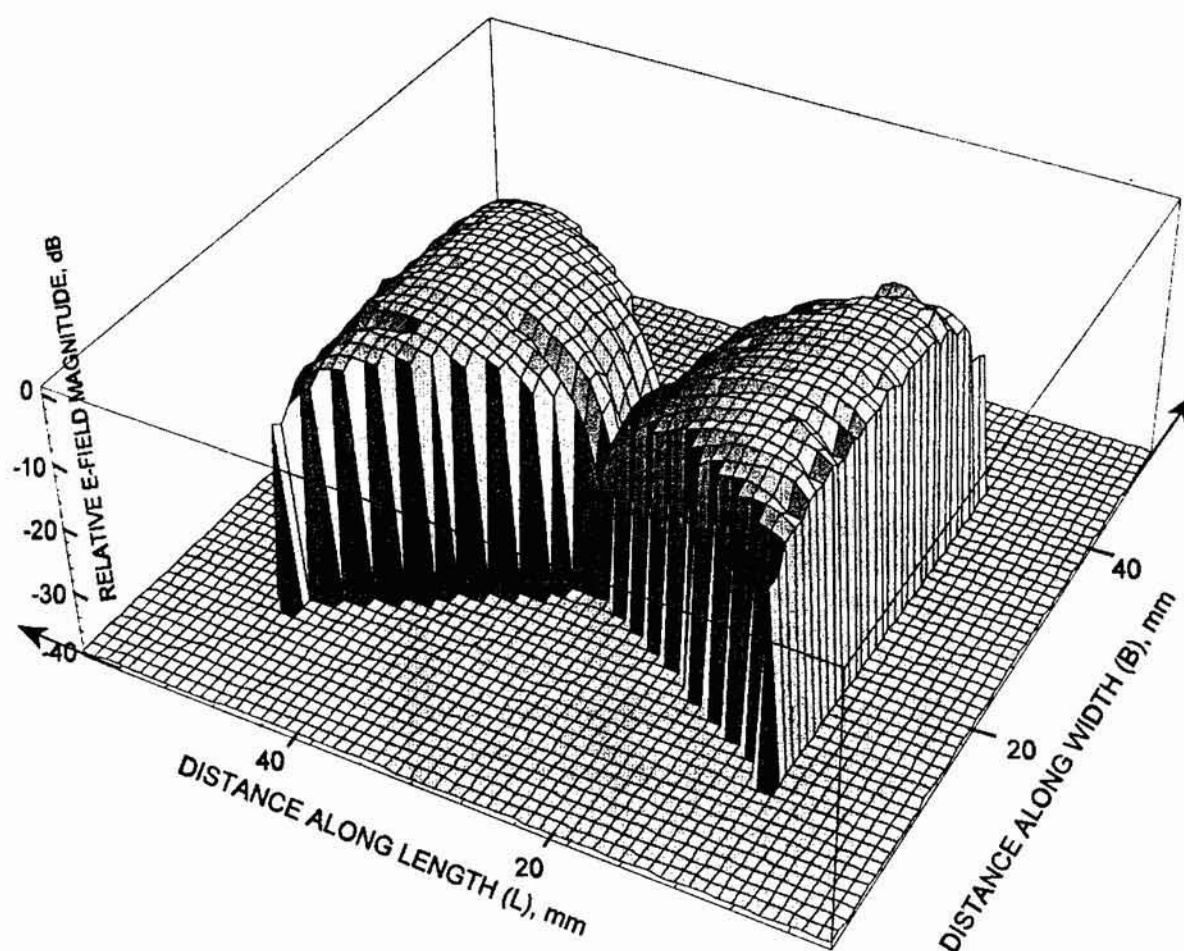


FIGURE 4.9 Measured magnitude of Z-directed electric field of a typical drum-shaped microstrip antenna at resonance

Length, L	=	3.811 cm
Width, B	=	3.200 cm
W/B	=	0.3125
Resonant frequency = 1515 MHz		

4.3 CHARACTERISTICS OF TM_{10} MODE

This mode is excited by selecting a feed point along the unmodified side. The variation of input impedance with feed point has already been shown in Figure 4.4. The radiated fields of this mode are also linearly polarised, but in the XZ plane.

4.3.1 Resonant Frequency

The resonant frequency of this mode is also affected by the central width, W . It is found to be increasing with the decrease of W . As we are interested in the reduction of resonant frequency, this mode is not of much interest in this study. The resonant frequency becomes maximum, when W is a minimum. The dimensions and location of feed point along the edge of the studied drum-shaped antennas are given in Table 4.4. The variation of resonant frequency with W are shown in the Figure 4.10. From figure it is clear that in both the operating bands (UHF and L) for all the L/B values, the TM_{10} mode resonant frequency decreases with central width. From Table 4.4 we can see that in the UHF band when $L/B = 0.7$, the resonant frequency increases from 724 MHz to 1032 MHz when the central width decreases from its maximum value to 10% of the maximum value. In the L-band, when $L/B = 0.5$, the resonant frequency increases from 1058 MHz to 1525 MHz corresponding to the same variation in central width.

From the Table it is also clear that the percentage increase in resonant frequency decreases when the L/B ratio is greater than 1. In the UHF band when $L/B = 2$ and $W/B = 0.1$, the percentage increase in frequency is 28.25% and in the L-band it is 7.39%. These values are very less compared to the corresponding values (40.02% in the UHF and 39.39% in the L-band) when $L/B = 1.0$.

TABLE 4.4(i) Dimensions, feed location (s), TM_{10} mode resonant frequency (f_{10}), % increase in resonant frequency and % bandwidth of various UHF-band drum-shaped antenna configurations used in the study

s : Feed location distance from the centre of the edge (Y) as shown in Figure 4.4(d)

L cm	B cm	L/B	W/B	s cm	f_{10} MHz	% increase in resonant frequency	% bandwidth
7.00	10.00	0.70	1.0	4.5	724	0.00	1.38
			0.9	3.0	758	4.70	1.19
			0.7	3.0	837	15.61	1.79
			0.5	1.5	919	26.93	2.19
			0.3	1.5	998	37.85	2.00
			0.1	1.5	1032	42.54	2.81
7.00	7.00	1.00	1.0	1.0	1037	0.00	1.36
			0.9	1.5	1076	3.76	1.86
			0.7	1.5	1188	14.56	1.60
			0.5	2.0	1301	25.46	1.92
			0.3	1.5	1398	34.81	3.13
			0.1	1.0	1452	40.02	1.66
10.50	7.00	1.50	1.0	3.5	1027	0.00	1.85
			0.9	3.5	1076	4.77	1.86
			0.7	3.5	1188	15.68	2.12
			0.5	2.5	1271	23.76	1.18
			0.3	1.0	1345	30.96	2.23
			0.1	1.0	1384	34.76	2.09
10.50	5.25	2.00	1.0	2.5	1363	0.00	1.02
			0.9	2.5	1433	5.14	3.43
			0.7	2.5	1555	14.09	1.92
			0.5	2.0	1667	22.30	2.64
			0.3	2.0	1721	26.67	2.27
			0.1	1.5	1748	28.25	2.23

TABLE 4.4(ii) Dimensions, feed location (s), TM_{10} mode resonant frequency (f_{10}), % increase in resonant frequency and % bandwidth of various L-band drum-shaped antenna configurations used in the study

s : Feed location distance from the centre of the edge (Y) as shown in Figure 4.4(d)

L cm	B cm	L/B	W/B	s cm	f_{10} MHz	% increase in resonant frequency	% bandwidth
3.50	7.00	0.50	1.0	1.4	1058	0.00	0.95
			0.9	1.4	1110	4.91	1.80
			0.7	1.2	1210	14.37	1.65
			0.5	1.0	1334	26.09	1.50
			0.3	1.0	1398	32.14	2.15
			0.1	0.8	1525	43.19	1.98
3.50	3.50	1.00	1.0	0.2	2087	0.00	1.44
			0.9	1.0	2134	2.25	4.47
			0.7	0.8	2368	13.46	2.95
			0.5	0.8	2590	24.10	2.70
			0.3	0.8	2787	33.54	2.16
			0.1	0.4	2909	39.39	2.07
3.80	2.53	1.50	1.0	0.8	2834	0.00	3.17
			0.9	1.2	2955	4.27	3.05
			0.7	1.0	3280	15.74	1.82
			0.5	1.0	3780	33.38	2.12
			0.3	0.4	3800	34.09	2.62
			0.1	0.4	3940	39.03	5.05
4.00	2.00	2.00	1.0	0.4	3760	0.00	2.13
			0.9	0.8	3760	0.00	2.67
			0.7	0.6	3800	1.06	2.62
			0.5	0.8	3880	3.19	1.54
			0.3	0.8	3820	1.60	1.57
			0.1	0.8	4038	7.39	0.99

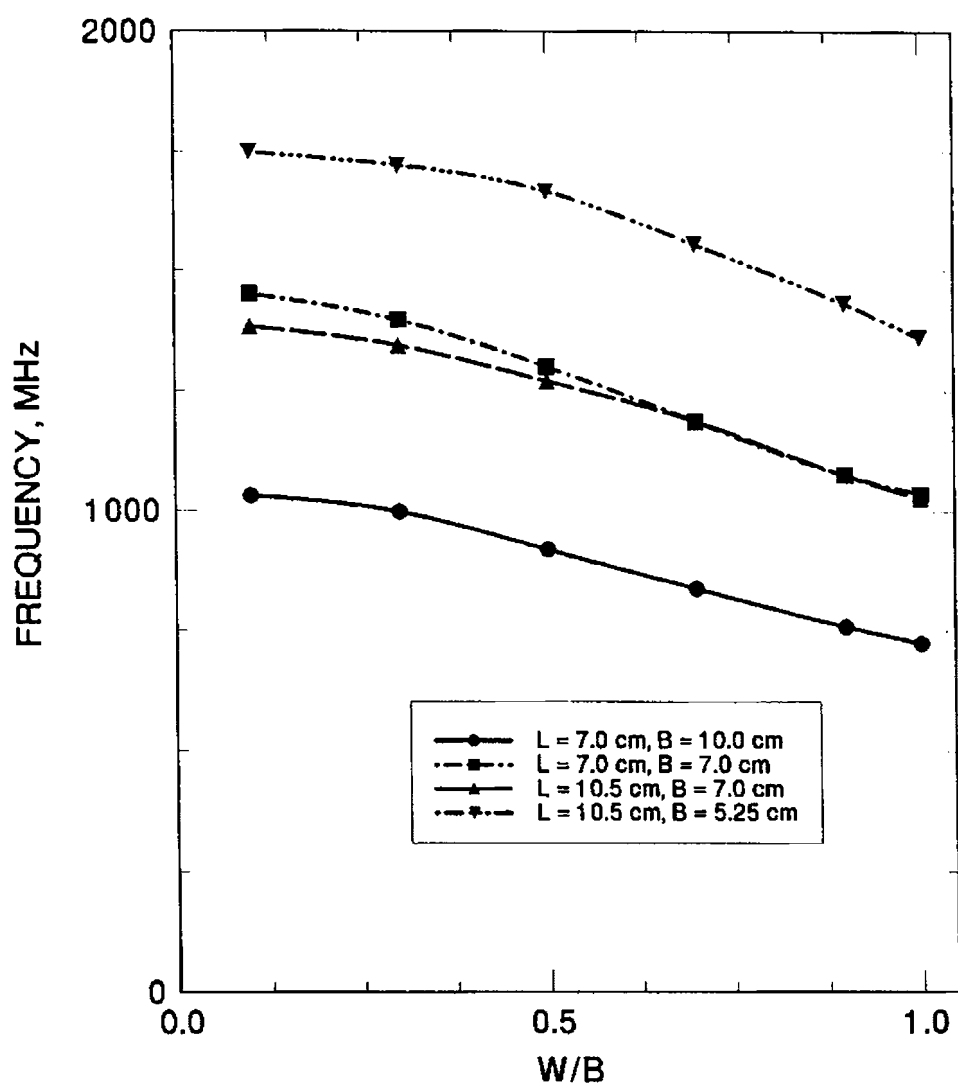


FIGURE 4.10(i) Variation of TM_{10} mode resonance frequency with respect to the central width (W) for different UHF-band antennas

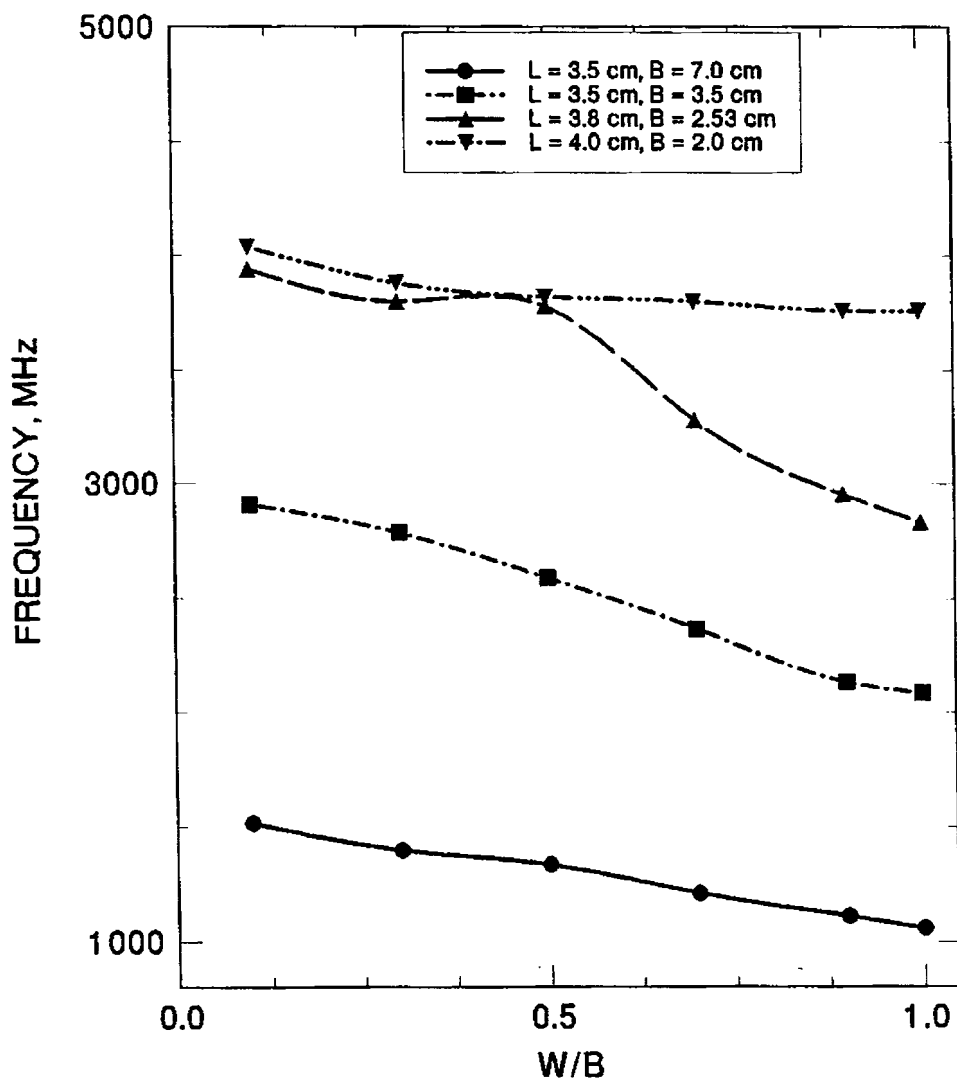


FIGURE 4.10(ii) Variation of TM_{10} mode resonance frequency with respect to the central width (W) for different L-band antennas

The variation of frequency ratio with W is shown in Figure 4.11. The frequency ratio between TM_{10} and TM_{01} modes (f_{10}/f_{01}) decreases with W . The frequency ratio between these two modes could be tuned to any value between a maximum and a minimum by suitably adjusting the central width. Both the modes could be excited separately or together by suitably selecting the feed point. This dual frequency operation with wide frequency ratio tunability without increasing the overall antenna size would be of use in typical dual frequency applications like SAR, GPS, PCS, etc.

4.3.2 Impedance Bandwidth

The 10 dB return loss impedance bandwidth of the different antennas are given in Table 4.4. From the Table we can see that the percentage bandwidth in almost all cases is found to be less than 3%. This is typical for microstrip antennas and hence it is clear that the geometrical modification does not have significant effect on the impedance bandwidth of this mode also.

4.3.3 Radiation pattern

Principal plane co-and cross-polar radiation patterns of few representative antenna configurations are shown in Figure 4.12. For these antennas the different pattern characteristics like E - and H -plane 3 dB beamwidths, peak cross-polar level, etc., are given in Table 4.5.

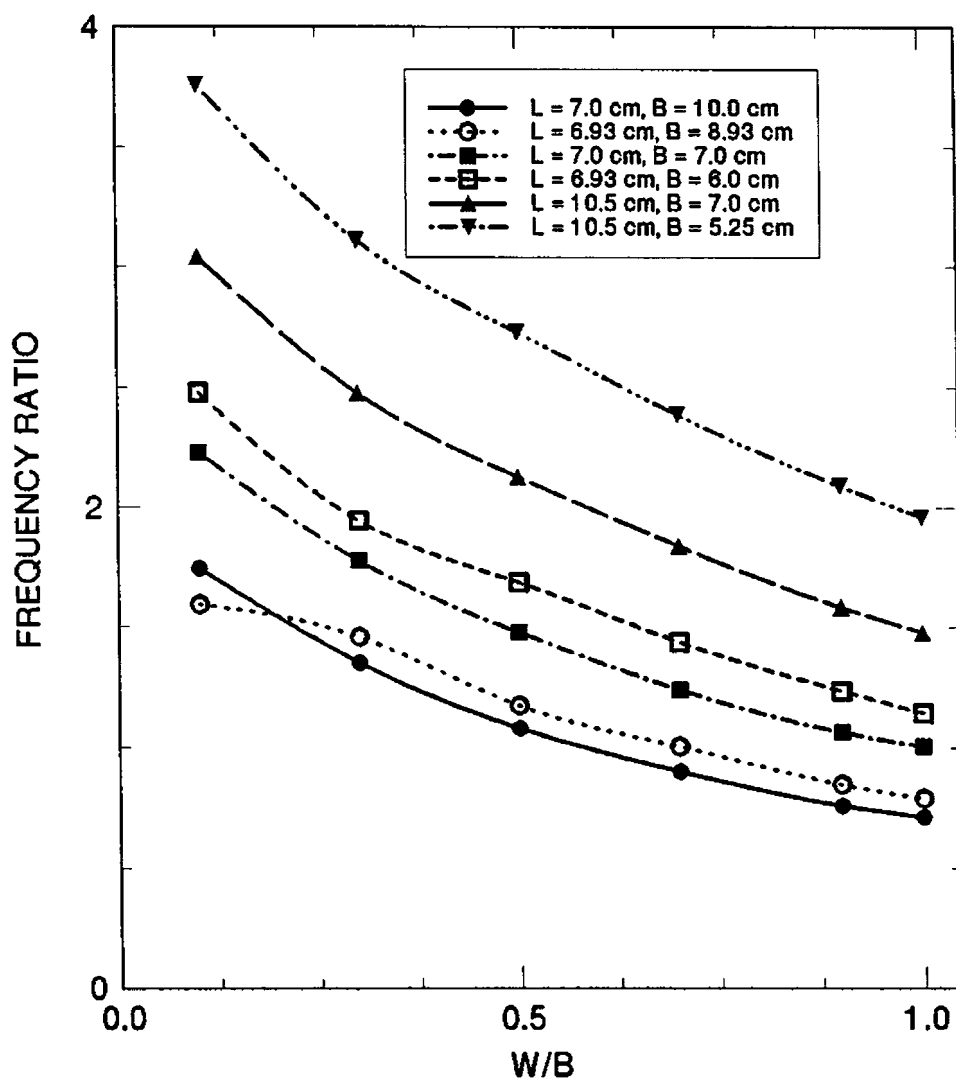


FIGURE 4.11(i) Variation of frequency ratio with central width (W) for different UHF-band antennas

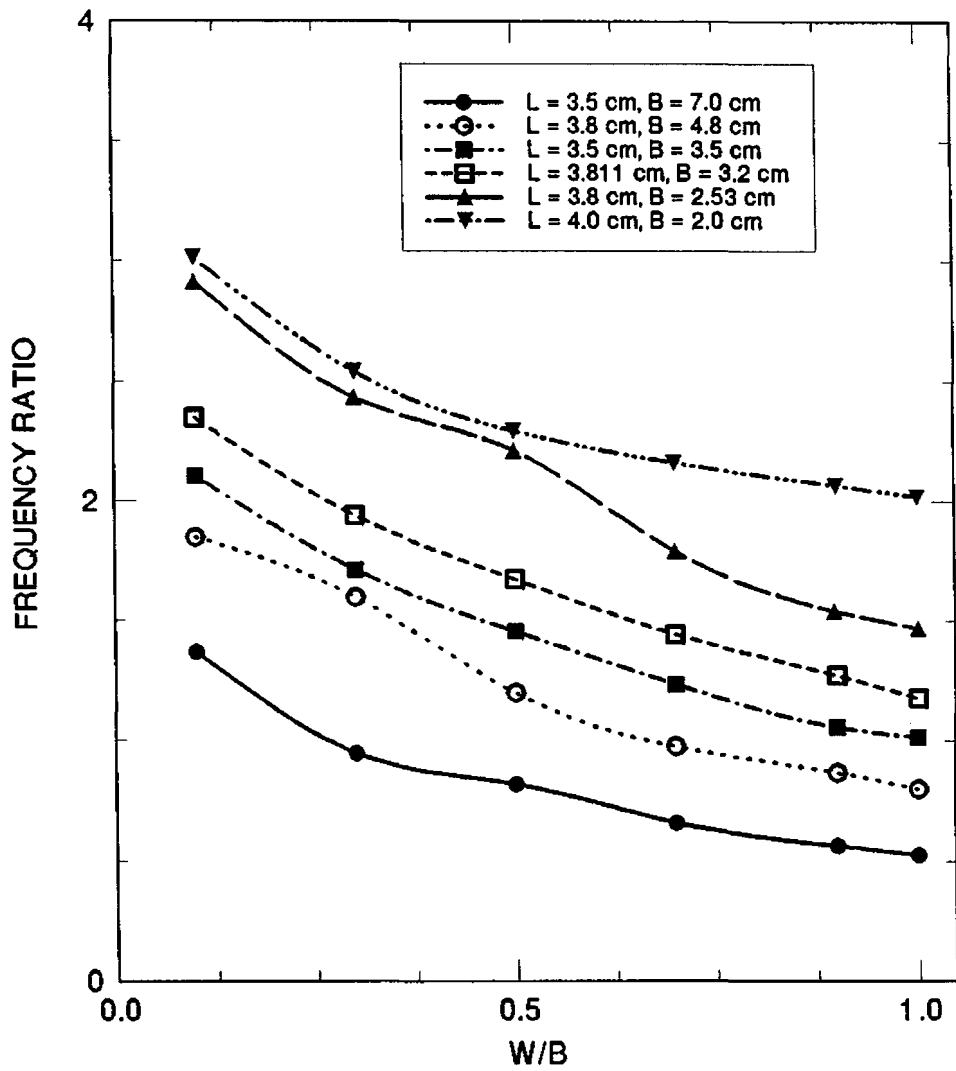


FIGURE 4.11(ii) Variation of frequency ratio with central width (W) for different L-band antennas

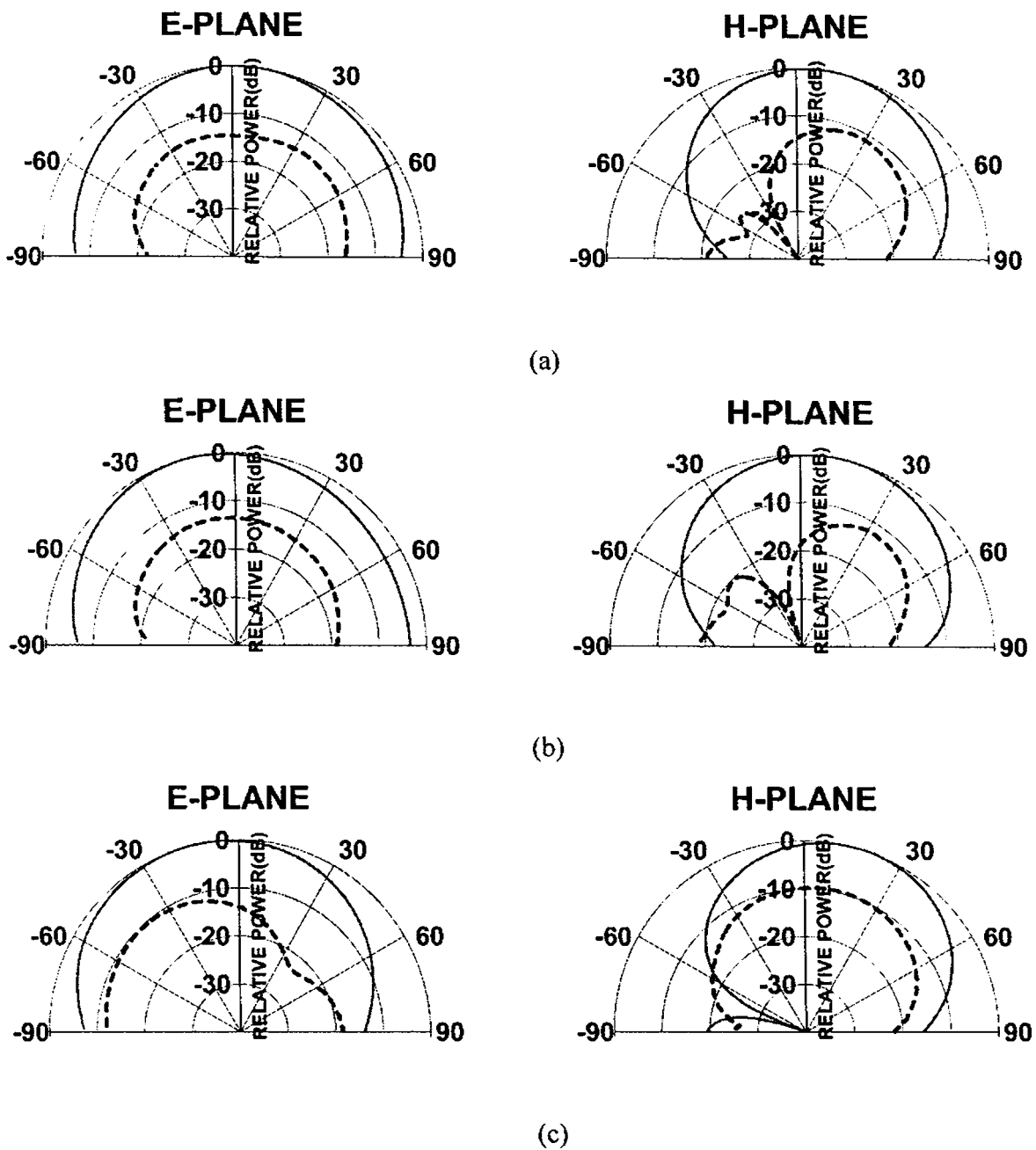


FIGURE 4.12(i) TM_{10} mode *E*- and *H*-plane co and cross polar radiation patterns of different UHF-band antennas

———— co polar - - - - - cross polar

(a) $L = 10.5$ cm, $B = 7$ cm, $W/B = 0.7$

(b) $L = 7$ cm, $B = 7$ cm, $W/B = 0.7$

(c) $L = 7$ cm, $B = 10$ cm, $W/B = 0.7$

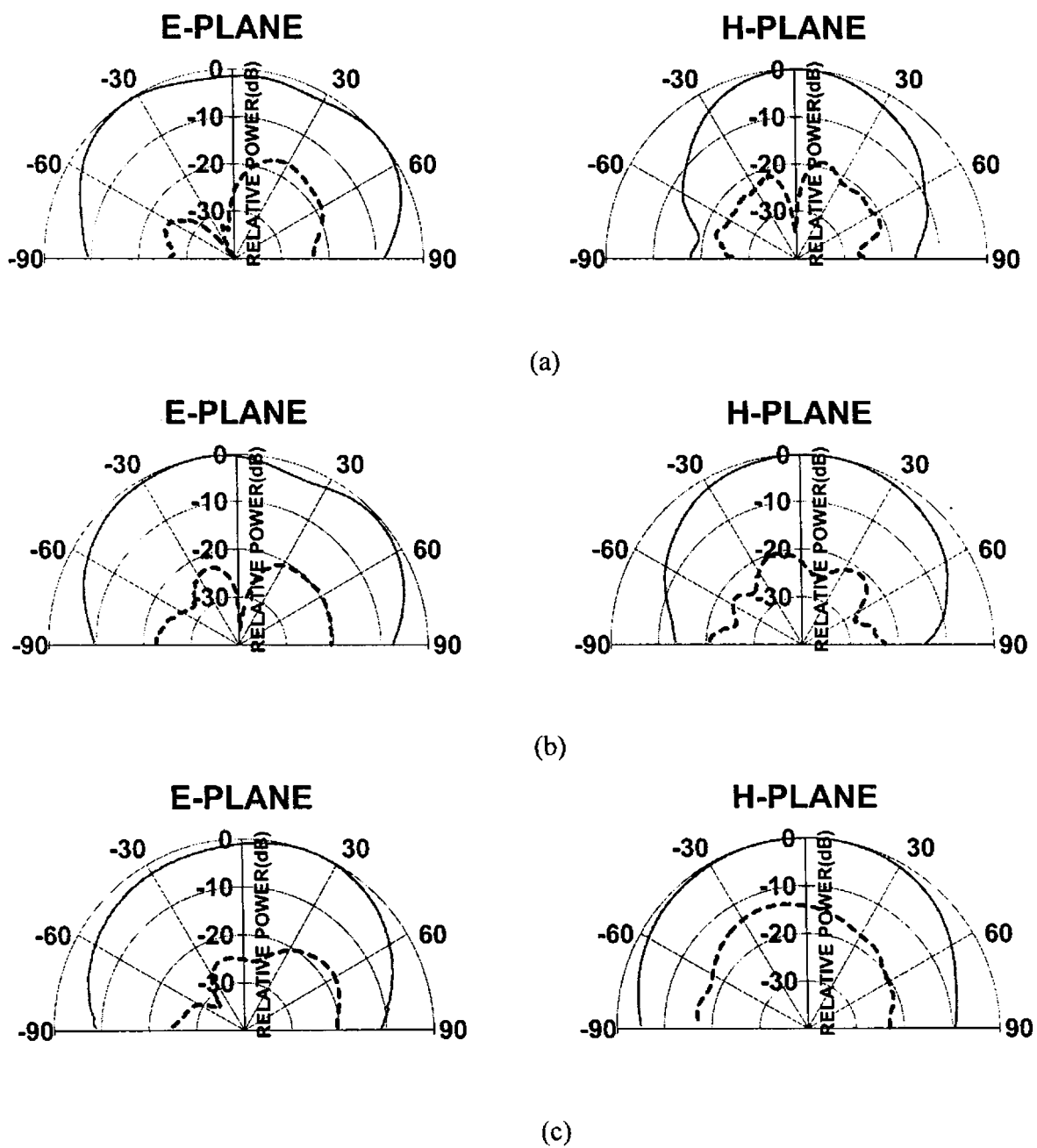


FIGURE 4.12(ii) TM_{10} mode E - and H -plane co and cross polar radiation patterns of different L-band antennas

————— co polar - - - - - cross polar

(a) $L = 3.8$ cm, $B = 2.53$ cm, $W/B = 0.9$

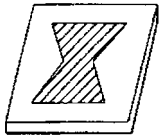
(b) $L = 3.5$ cm, $B = 3.5$ cm, $W/B = 0.5$

(c) $L = 3.5$ cm, $B = 7$ cm, $W/B = 0.5$

TABLE 4.5 Characteristics of TM_{10} mode radiation patterns given in Figure 4.12.

L/B	W/B	Operating band	3 dB beamwidth (deg.)		Peak cross-polar level(dB)	
			E-plane	H-plane	E-plane	H-plane
1.5	0.7	UHF	116	74	-13.64	-11.27
1.0	0.7	UHF	102	76	-13.45	-12.06
0.7	0.7	UHF	95	68	-10.42	-9.650
1.5	0.9	L	133	57	-16.95	-18.81
1.0	0.5	L	128	83	-19.65	-20.23
0.5	0.5	L	102	119	-17.75	-13.30

From the above observations it is found that the new drum-shaped microstrip antenna is acting as a compact antenna without deteriorating the radiation characteristics compared to an equivalent rectangular microstrip antenna. This compact nature of the antenna makes this as an excellent radiating element in systems where size of the antenna is a major concern. In addition, this antenna may be used as a substitute for conventional microstrip patches like rectangular/circular.



THEORETICAL INTERPRETATIONS

5.1 INTRODUCTION

In this chapter complete theoretical analysis of the new compact drum-shaped microstrip antenna is presented. The analysis is based on segmentation technique, cavity model and aperture model. The analysis can predict different antenna characteristics like resonant frequency, mode of operation, radiation pattern, input impedance, etc. The predicted results are validated through experimental results for different antenna geometries.

5.2 ANALYSIS

Configuration of the new drum-shaped compact microstrip antenna along with the coordinate system is shown in Figure 5.1. It consists of a drum-shaped metallic patch on one side of a

dielectric substrate of thickness, h and relative dielectric constant, ϵ_r . The different steps in the analysis are described below.

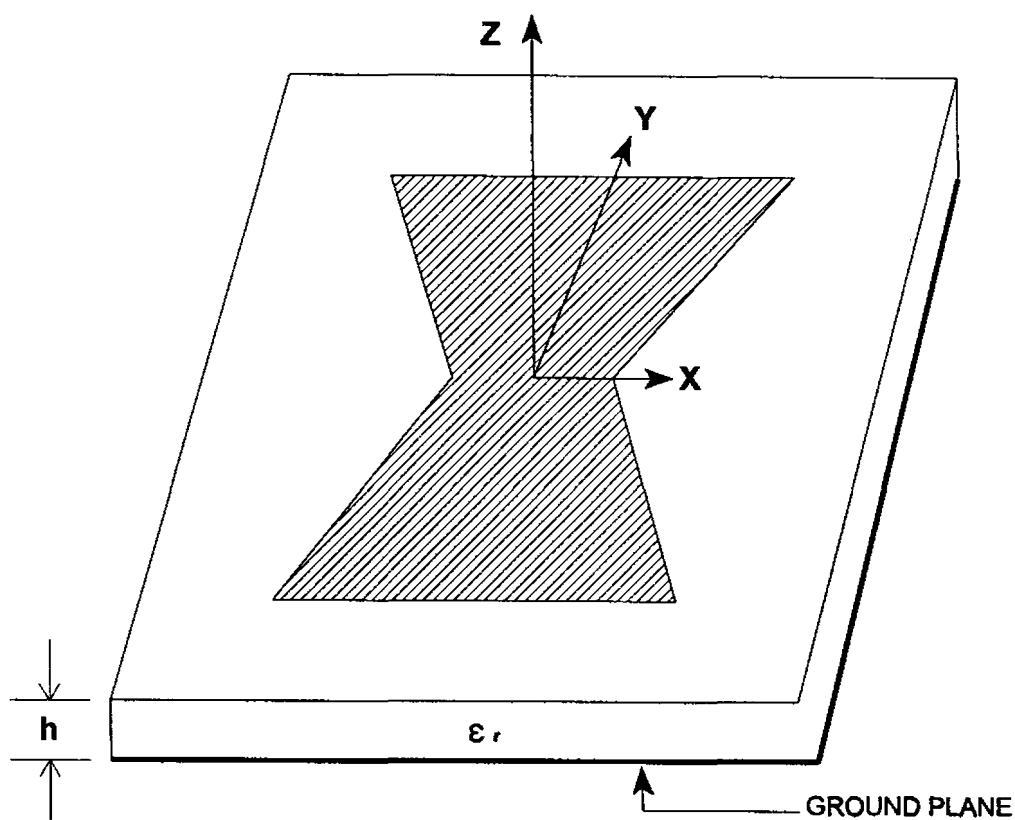


FIGURE 5.1 Configuration of the new drum-shaped compact microstrip antenna

5.2.1 Magnetic wall model formation

The magnetic wall model of the given patch is developed by providing equivalent outward edge extensions terminated in a pure magnetic wall. The edge extensions are to replace the effect of fringing fields at the peripheries of the antenna geometry. These edge extensions depend on the planar dimensions of the patch, relative dielectric constant and substrate thickness. Equivalent edge extensions for the commonly used microstrip radiating geometries like rectangular and circular patches are there in the literature [1, 3, 136]. In the case of arbitrary shaped patches,

sometimes an extension available for the shape closest to the given shape is used. In any case it is desirable to have the same extension all around the patch. An extension of the order of the height of the substrate can be selected as the best approximation [35, 62]. Here also we have chosen an edge extension equal to the height of the substrate all around the periphery. The patch with edge extensions is shown in Figure 5.2. The solid line indicates the actual physical boundary of the patch and the dashed line indicates the virtual periphery of the patch after giving equivalent edge extensions. This virtual patch geometry is used for the calculations in the remaining parts of the thesis.

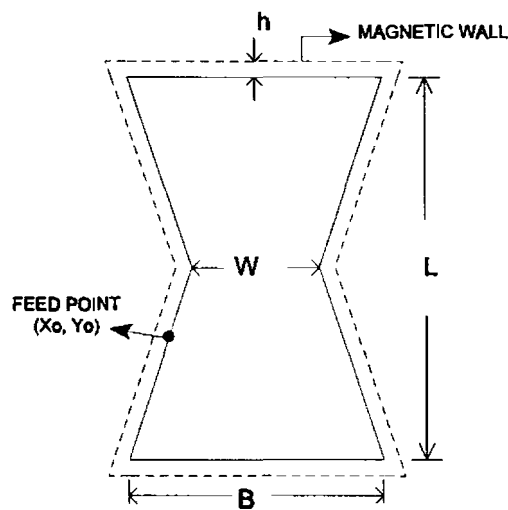


FIGURE 5.2 Geometry of the antenna with edge extensions to incorporate the fringing field effects

5.2.2 Segmentation

The geometry with equivalent edge extensions is divided into different segments for which Green's functions are available. The present antenna is segmented into four triangular and one rectangular shaped segments as shown in Figure 5.3. The Green's functions of rectangular and triangular segments are known. As the Green's functions of 30° - 60° - 90° and 45° - 45° - 90° triangles are available, mainly three symmetric drum-shaped antenna configurations as shown in Figure

5.4 are analysed in detail. These configurations are named for convenience based on the type of triangular segment associated to it. Figure 5.4(a) is named as TSNT antenna indicating Thirty-Sixty-Ninety degree cornered Triangular segments. Here the first letter indicates angle α , second letter indicates angle β and third letter indicates remaining right angle of the triangular segment. Based on this convention the configurations given in Figure 5.4(b) and (c) are named as STNT antenna (antenna with Sixty-Thirty-Ninety degree cornered Triangular segments) and FFNT antenna (antenna with Forty five-Forty five-Ninety degree cornered Triangular segments) respectively. The details of the antenna geometries used in the theoretical study are given in Table 5.1

TABLE 5.1 Details of the antennas used in the theoretical analysis

Name of the antenna configuration	L (cm)	B (cm)	ϵ_r	h (cm)	Type of triangular segments
TSNT ₁	6.9282	6.00	4.5	0.160	30 ⁰ -60 ⁰ -90 ⁰
FFNT ₁	6.9282	8.9282	4.5	0.160	45 ⁰ -45 ⁰ -90 ⁰
STNT ₁	6.9282	14.00	4.5	0.160	60 ⁰ -30 ⁰ -90 ⁰
TSNT ₂	6.9282	6.00	6.0	0.065	30 ⁰ -60 ⁰ -90 ⁰
FFNT ₂	6.9282	8.9282	6.0	0.065	45 ⁰ -45 ⁰ -90 ⁰
STNT ₂	6.9282	14.00	6.0	0.065	60 ⁰ -30 ⁰ -90 ⁰
TSNT ₃	6.9282	8.00	4.5	0.160	30 ⁰ -60 ⁰ -90 ⁰
FFNT ₃	6.9282	10.9282	4.5	0.160	45 ⁰ -45 ⁰ -90 ⁰
STNT ₃	6.9282	16.00	4.5	0.160	60 ⁰ -30 ⁰ -90 ⁰
TSNT ₄	6.9282	8.00	6.0	0.065	30 ⁰ -60 ⁰ -90 ⁰
FFNT ₄	6.9282	10.9282	6.0	0.065	45 ⁰ -45 ⁰ -90 ⁰
STNT ₄	6.9282	16.00	6.0	0.065	60 ⁰ -30 ⁰ -90 ⁰
TSNT ₅	6.9282	6.00	2.21	0.055	30 ⁰ -60 ⁰ -90 ⁰
TSNT ₆	6.9282	8.00	2.21	0.055	30 ⁰ -60 ⁰ -90 ⁰

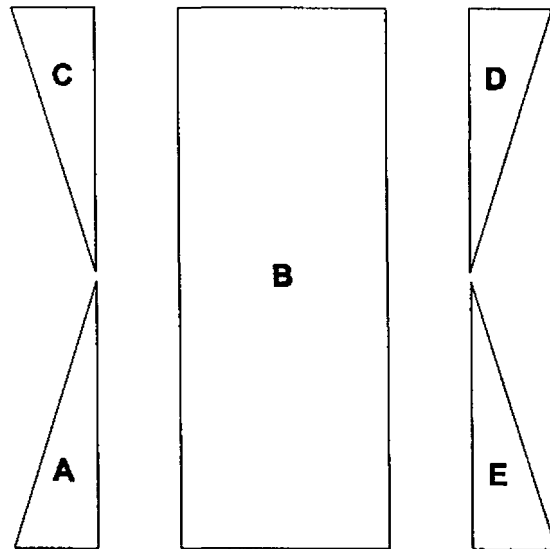


FIGURE 5.3 The picture depicting segmentation into five segments

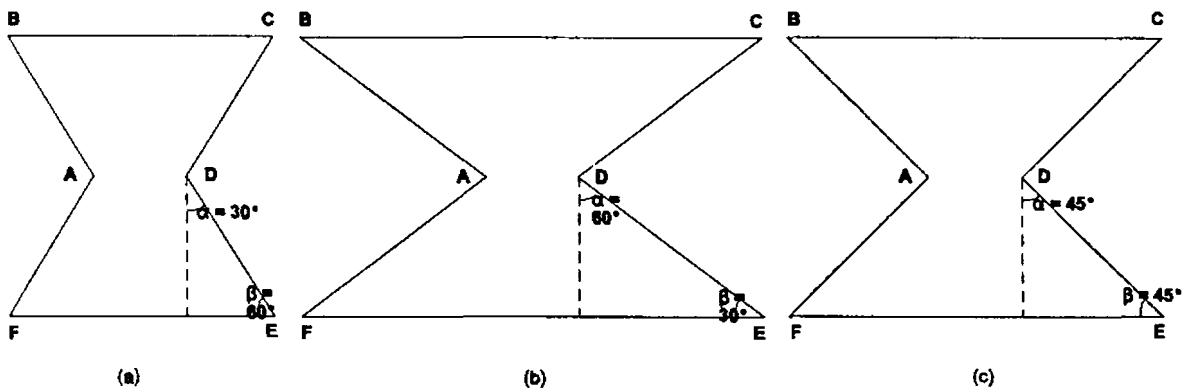


FIGURE 5.4 Three symmetric drum-shaped antenna configurations

- (a) TSNT (antenna with Thirty Sixty Ninety degree cornered Triangular segments)
- (b) STNT (antenna with Sixty Thirty Ninety degree cornered Triangular segments)
- (c) FFNT (antenna with Forty five Forty five Ninety degree cornered Triangular segments)

The continuous connection between segments are now replaced by interconnection at a number discrete points. Now a port is attached to each interconnection point. The width of a port is kept $\leq \lambda_g/20$, where λ_g is the wavelength inside the dielectric medium. This is to ensure

that the current density is uniform over the width of the port.

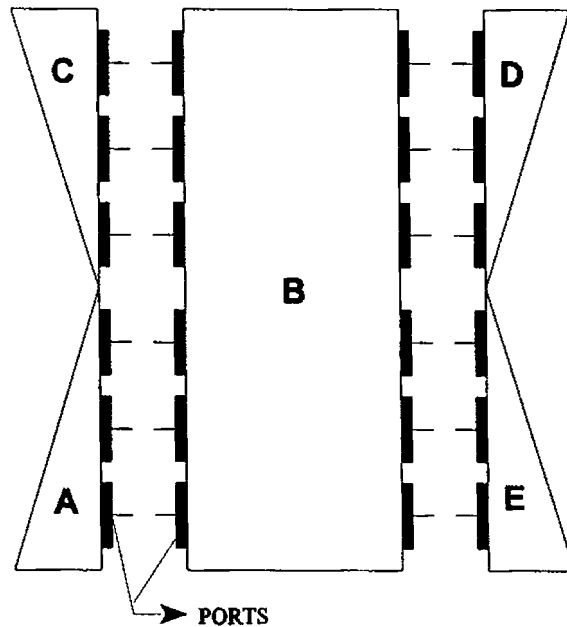


FIGURE 5.4 Segmented antenna geometry showing various ports

Figure 5.4 shows the segmented antenna geometry with ports and interconnection points. The individual segments having regular geometrical shapes (rectangular and triangular) are now treated as multi-port microwave planar circuits and can be analysed by using two dimensional impedance Green's functions available for these shapes. The Z-matrices of the individual segments are obtained from the Green's functions as given in [2, 8, 9]

$$Z_{ij} = \frac{1}{W_i W_j} \int_{\pi_i} \int_{\pi_j} G(x_i, y_i / x_j, y_j) ds_i ds_j \quad (5-1)$$

where (x_i, y_i) denote the locations of the two ports and W_i, W_j represents the corresponding physical port widths. The Green's function G is usually a doubly infinite summation with terms

corresponding to various modes of the planar resonator with magnetic walls as given in [2]

$$G(x,y/x_0,y_0) = j\omega\mu_0h \sum_{m=-\infty}^{\infty} \sum_{n=-\infty}^{\infty} \frac{\Psi_{mn}(x,y) \Psi_{mn}^*(x_0,y_0)}{k_{mn}^2 - k^2} \quad (5-2)$$

where Ψ_{mn} is the eigen function of the mn^{th} mode of the segment and k_{mn} is the corresponding eigen value. The wave number k is given by

$$k = k_0\sqrt{\epsilon_{\text{reff}}} \quad (5-3)$$

where k_0 is the free space wave number and ϵ_{reff} is the effective dielectric constant. For a rectangular segment, it is given as

$$\epsilon_{\text{reff}} = \frac{\epsilon_r + 1}{2} + \frac{\epsilon_r - 1}{2} \frac{1}{\sqrt{1 + \frac{10h}{b}}} \quad (5-4)$$

where b is the width of the rectangular segment.

For a triangular segment ϵ_{reff} is obtained from

$$\epsilon_{\text{reff}} = \frac{\epsilon_r + 1}{2} + \frac{\epsilon_r - 1}{2} \frac{1}{\sqrt{1 + \frac{10h}{a}}} \quad (5-5)$$

where a is the hypotenuse of the triangular segment.

5.2.3 Multi-port connection method

In this method, the Z -matrix of the overall antenna geometry is obtained by combining the Z -matrices of the individual segments one after another. Figure 5.5 shows two segments of a typical drum-shaped antenna with ports designated suitably for this method. To determine the impedance matrix of the combination of the two segments A and B , the ports 1 (feed port), 6 , 7 , 8 , 9 , 10 and 11 are designated as external p ports and the rest as connected ports. The connected ports are subdivided into groups q and r ports. Here q ports are the connected ports of segment A (2 and 3) and r ports are the corresponding ports of segment B (5 and 4).

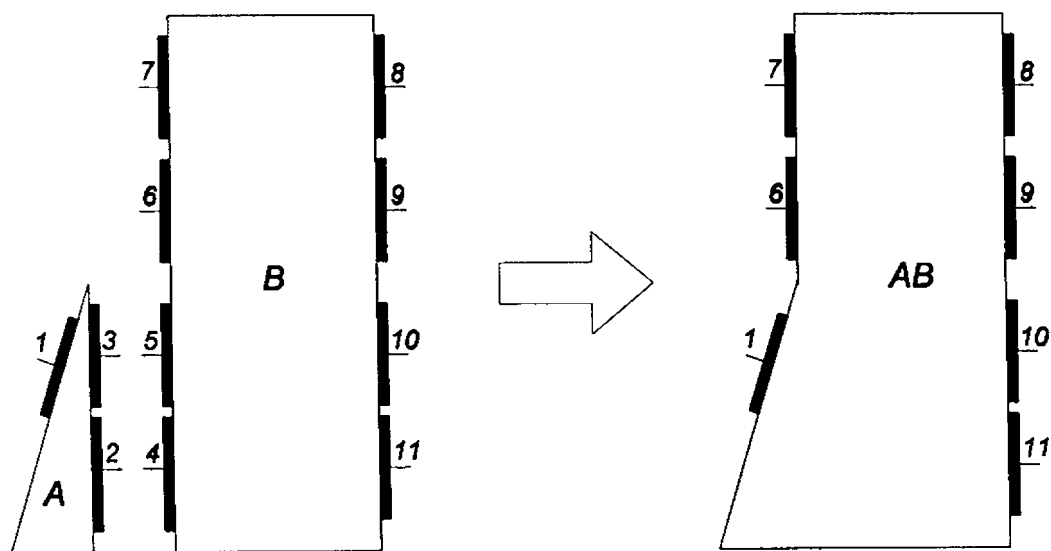


FIGURE 5.5 Two segments of a typical antenna demonstrating the multi-port connection method

The RF port voltages and port currents of segments A and B can be now written generally as [2, 6, 9]

$$\begin{bmatrix} \vec{v}_p \\ \vec{v}_q \\ \vec{v}_r \end{bmatrix} = \begin{bmatrix} Z_{pp} & Z_{pq} & Z_{pr} \\ Z_{qp} & Z_{qq} & Z_{qr} \\ Z_{rp} & Z_{rq} & Z_{rr} \end{bmatrix} \begin{bmatrix} \vec{i}_p \\ \vec{i}_q \\ \vec{i}_r \end{bmatrix} \quad (5-6)$$

i.e.,

$$\begin{bmatrix} \vec{v}_1 \\ \vec{v}_6 \\ \vec{v}_7 \\ \vec{v}_8 \\ \vec{v}_9 \\ \vec{v}_{10} \\ \vec{v}_{11} \\ \vec{v}_2 \\ \vec{v}_3 \\ \vec{v}_4 \\ \vec{v}_5 \end{bmatrix} = \begin{bmatrix} Z_{11} & 0 & 0 & 0 & 0 & 0 & 0 & Z_{12} & Z_{13} & 0 & 0 \\ 0 & Z_{66} & Z_{67} & Z_{68} & Z_{69} & Z_{610} & Z_{611} & 0 & 0 & Z_{64} & Z_{65} \\ 0 & Z_{76} & Z_{77} & Z_{78} & Z_{79} & Z_{710} & Z_{711} & 0 & 0 & Z_{74} & Z_{75} \\ 0 & Z_{86} & Z_{87} & Z_{88} & Z_{89} & Z_{810} & Z_{811} & 0 & 0 & Z_{84} & Z_{85} \\ 0 & Z_{96} & Z_{97} & Z_{98} & Z_{99} & Z_{910} & Z_{911} & 0 & 0 & Z_{94} & Z_{95} \\ 0 & Z_{106} & Z_{107} & Z_{108} & Z_{109} & Z_{1010} & Z_{1011} & 0 & 0 & Z_{104} & Z_{105} \\ 0 & Z_{116} & Z_{117} & Z_{118} & Z_{119} & Z_{1110} & Z_{1111} & 0 & 0 & Z_{114} & Z_{115} \\ Z_{21} & 0 & 0 & 0 & 0 & 0 & 0 & Z_{22} & Z_{23} & 0 & 0 \\ Z_{31} & 0 & 0 & 0 & 0 & 0 & 0 & Z_{32} & Z_{33} & 0 & 0 \\ 0 & Z_{46} & Z_{47} & Z_{48} & Z_{49} & Z_{410} & Z_{411} & 0 & 0 & Z_{44} & Z_{45} \\ 0 & Z_{56} & Z_{57} & Z_{58} & Z_{59} & Z_{510} & Z_{511} & 0 & 0 & Z_{54} & Z_{55} \end{bmatrix} \begin{bmatrix} \vec{i}_1 \\ \vec{i}_6 \\ \vec{i}_7 \\ \vec{i}_8 \\ \vec{i}_9 \\ \vec{i}_{10} \\ \vec{i}_{11} \\ \vec{i}_2 \\ \vec{i}_3 \\ \vec{i}_4 \\ \vec{i}_5 \end{bmatrix} \quad (5-7)$$

Now applying interconnection constraints in the above equation to get the overall impedance matrix of the combination of segments A and B . The interconnection constraints are[2]

$$\begin{aligned} \vec{V}_q &= \vec{V}_r \\ \vec{i}_q + \vec{i}_r &= 0 \end{aligned} \quad \text{and} \quad (5-8)$$

On substituting (5-8) in (5-6) and eliminating V_q, V_r, I_q and I_r , the Z -matrix of the overall structure is obtained as [51]

$$Z_p = Z_{pp} + \begin{bmatrix} Z_{pq} & -Z_{pr} \end{bmatrix} \begin{bmatrix} Z_{qq} & -Z_{qr} & -Z_{rq} & +Z_{rr} \end{bmatrix}^{-1} \begin{bmatrix} Z_{rp} & -Z_{rp} \end{bmatrix} \quad (5-9)$$

Now, from (5-7) one obtains the impedance matrix of the combination of segments A and B (Z_{AB}) by substituting the matrices $Z_{pp}, Z_{pq}, Z_{pr}, Z_{qr}, Z_{qq}, Z_{rr}, Z_{rp}, Z_{qp}, Z_{qr}$ and Z_{rq} in (5-9). The three remaining triangular segments are now attached one by one to get the overall impedance matrix of the new compact microstrip antenna.

5.2.4 Resonant frequency

The resonance in a patch antenna can be considered as a parallel type resonance [137] and hence a large value of input reactance is the indication of resonance of the lossless cavity under the patch. Here, the input reactance of the lossless (as we have not incorporated the losses like

radiation, dielectric, surface wave, etc., here) cavity under the patch is obtained from the overall impedance matrix of the structure as explained in the previous section.

The resonant frequencies of the antenna configurations mentioned in Table 5.1 are computed by evaluating the impedance matrix elements of the different segments using the corresponding impedance Green's functions. Actually the numerical computation of the impedance matrix elements involves the integration of Green's functions over the port widths as given in (5-1). The order of integrations and summations (in the Green's function) can be interchanged and for a rectangular segment, the impedance matrix element z_{ip} corresponding to two ports oriented along the Y -direction (coordinate system is shown in Figure 5.6) namely i and j is given by [2, 8, 9]

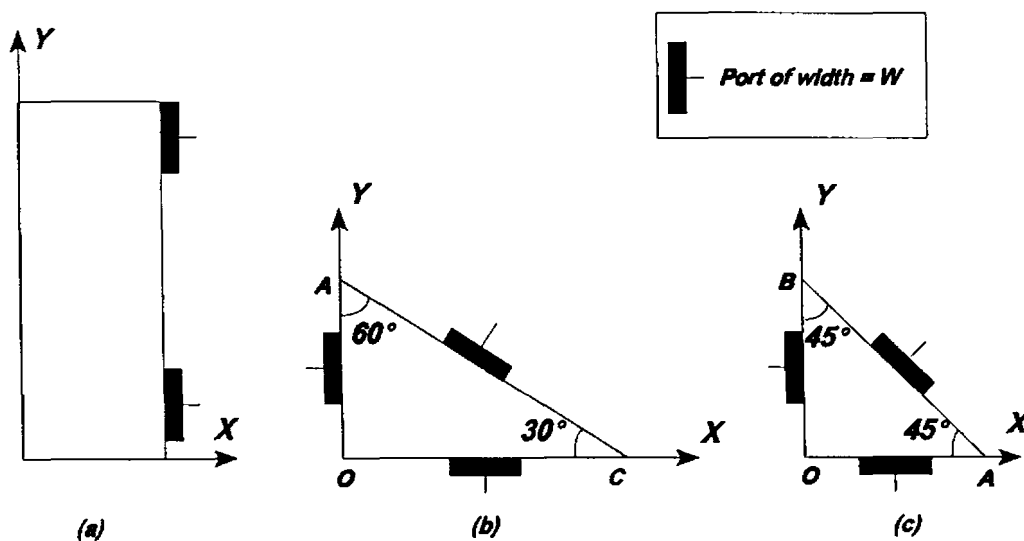


FIGURE 5.6 Coordinate system and orientation of ports for different segments

- (a) Rectangular segment with ports oriented along Y -direction
- (b) 30° - 60° right angled triangle with ports oriented along different sides
- (c) 45° - 45° right angled triangle with ports oriented along different sides

$$\begin{aligned}
Z_{ij} = & -CF \sum_{l=0}^L \sigma_l \cos k_u u_i \cos k_u u_j \cos \gamma_l x_{ga} \cos \gamma_l x_l \frac{\text{sinc}(k_u \frac{W_i}{2}) \text{sinc}(k_u \frac{W_j}{2})}{\gamma_l \sin \gamma_l F} \\
& -jCF \sum_{l=L+1}^{\infty} \cos k_u u_j \cos k_u u_i \sin \frac{k_u W_i}{2} \text{sinc} \frac{k_u W_j}{2} \frac{e^{-j\gamma_l(x_i-x_j)}}{\gamma_l}
\end{aligned} \tag{5-10}$$

where

$$\begin{aligned}
C &= \frac{j\omega \mu h}{ab} & u_i &= y_i & x_g &= \max(x_i, x_j) \\
F &= a & u_j &= y_j & x_i &= \min(x_i, x_j) \\
\gamma_l &= \pm \sqrt{k^2 - k_u^2} & k_u &= \frac{n\pi}{b} & x_{ga} &= x_g - a \\
k &= \omega \sqrt{\mu_0 \epsilon_0 \epsilon_{reff}} & \sigma_l &= \begin{cases} 1 & \text{if } l = 0 \\ 2 & \text{otherwise} \end{cases}
\end{aligned}$$

a and b are the dimensions of the segment and h is the height of the substrate used. The sign of γ_l is selected in such a way that the imaginary part of it is negative. W_i and W_j are the widths of the i^{th} and j^{th} ports. Here the value of L selected is 20 and the maximum value of l used is 50. Ports oriented along the other direction is not relevant here.

For a 30^0 - 60^0 - 90^0 triangular segment, the impedance matrix element Z_{ij} corresponding to the i^{th} and j^{th} ports is given by [8]

$$Z_{ij} = \frac{8j\omega \mu h}{W_i W_j} \sum_{m=-\infty}^{\infty} \sum_{n=-\infty}^{\infty} \frac{I(i)I(j)}{16\sqrt{3} \pi^2 (m^2 + mn + n^2) - 9\sqrt{3} a^2 k^2} \tag{5-11}$$

For ports located along side OC , $I(i)$ is given by

$$\begin{aligned} \frac{I(i)}{W_i} = & (-1)^l \cos \alpha l s \operatorname{sinc} \frac{\alpha l W_i}{2} + (-1)^m \cos \alpha m s \operatorname{sinc} \frac{\alpha m W_i}{2} \\ & + (-1)^n \cos \alpha n s \operatorname{sinc} \frac{\alpha n W_i}{2} \end{aligned} \quad (5-11a)$$

where

$$\alpha = \frac{2\pi}{\sqrt{3}a} \quad 0 < s < 1 \quad l + m + n = 0$$

For ports oriented along side AC (feed port)

$$\begin{aligned} \frac{I(i)}{W_i} = & \cos[\beta(m-n)] \operatorname{sinc}[\alpha(m-n)] + \cos[\beta(n-l)] \operatorname{sinc}[\alpha(n-l)] \\ & + \cos[\beta(l-m)] \operatorname{sinc}[\alpha(l-m)] \end{aligned} \quad (5-11b)$$

where

$$\alpha = \frac{\pi W}{3a} \quad 0 < s < 1 \quad \text{and} \quad \beta = \frac{2\pi s}{3}$$

For ports oriented along side OA

$$\frac{I(i)}{W_i} = (-1)^l \cos[\beta(m-n)] \operatorname{sinc}[\alpha(m-n)] + (-1)^m \cos[\beta(n-l)] \operatorname{sinc}[\alpha(n-l)] \\ + (-1)^n \cos[\beta(l-m)] \operatorname{sinc}[\alpha(l-m)] \quad (5-11c)$$

where

$$\alpha = \frac{\pi W}{3a} \quad \beta = \frac{2\pi s}{3} \quad 0 < s < \frac{1}{2} \quad \text{and } a \text{ is the length of the hypotenuse.}$$

For a $45^\circ-45^\circ-90^\circ$ triangular segment, the impedance matrix element Z_{ij} , corresponding to the i^{th} and j^{th} ports is given by

$$Z_{ij} = \frac{j\omega\mu h}{2W_i W_j} \sum_{m=0}^{\infty} \sum_{n=0}^{\infty} \frac{\sigma_m \sigma_n I(i) I(j)}{(m^2 + n^2)\pi^2 - a^2 k^2} \quad (5-12)$$

For ports oriented along OA , $I(i)$ is given by

$$\frac{I(i)}{W_i} = \cos n\pi s \operatorname{sinc} \frac{n\pi W}{2a} + (-1)^{m+n} \cos m\pi s \operatorname{sinc} \frac{m\pi W}{2a} \quad (5-12a)$$

and for ports oriented along AB (feed port)

$$\frac{I(i)}{W_i} = (-1)^m \cos[(m+n)\pi s] \operatorname{sinc}[(m+n)\alpha] \\ + \cos[(m-n)\pi s] \operatorname{sinc}[(m-n)\alpha] \quad (5-12b)$$

where

$$\alpha = \frac{\pi W}{2\sqrt{2}a} \quad 0 < s < 1 \quad \text{and } a \text{ is the length of any side other than hypotenuse.}$$

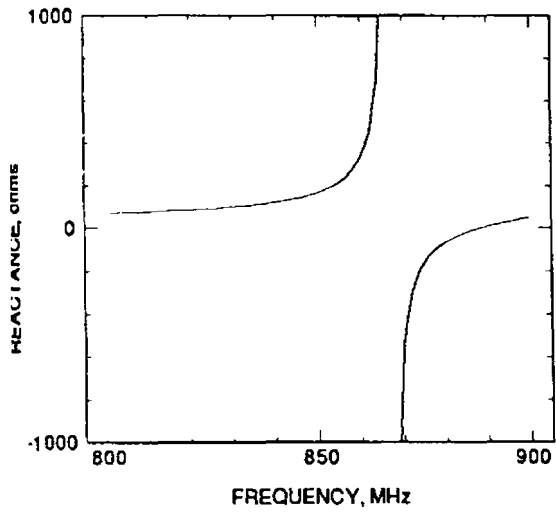
The Z -matrices of different segments are now combined together by means of multi-port connection method as described in section 5.2.3. The input reactance (lossless cavity under the patch) at the feed point is obtained after combining the impedance matrix elements of the five segments. The variation of input reactance with frequency for three typical antenna configurations mentioned in Table 5.1 are shown in Figure 5.7. The number of ports used for the calculation, theoretical resonant frequencies and experimental resonant frequencies obtained for them are shown in Table 5.2. From the table it is found that the present theory can predict the resonant frequency with an error less than 3.5 %.

5.2.5 Electric field variation

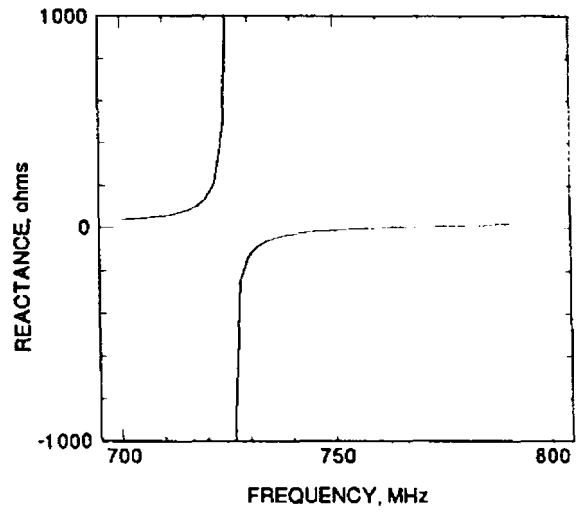
The electric field variation along the periphery of the antenna is required to identify the mode of operation, determination of radiation patterns, power radiated, etc. The electric field variation in a segment can be obtained from the Green's function, $G(s/s_0)$ as [6]

$$E_z = \hat{z} \frac{1}{h} \int G(s/s_0) J(s_0) ds_0 \quad (5-13)$$

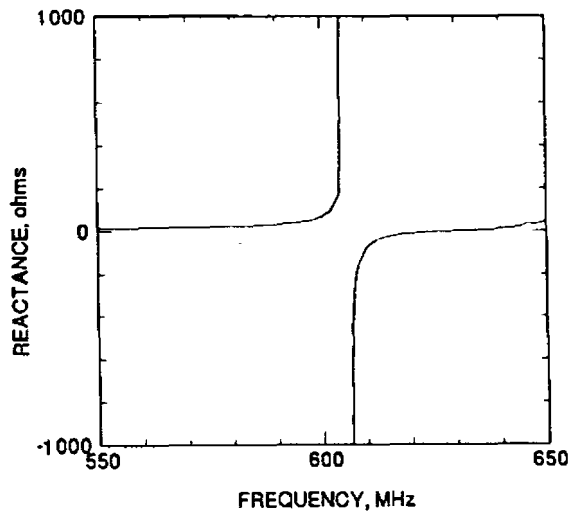
where $J(s_0)$ is the excitation current density along the interconnection. It can be determined from the interconnection point currents which are computed from (5-6) by incorporating the interconnection constraints.



(a)



(b)



(c)

FIGURE 5.7 Variation of input reactance of the lossless cavity under the patch corresponding to three typical antenna configurations

- (a) $TSNT_3$
- (b) $FFNT_3$
- (c) $STNT_3$

TABLE 5.2 The theoretical and Experimental resonant frequencies of the different antenna configurations

Name of the antenna configuration	No. of ports used	Resonant Frequency in MHz		
		Theoretical (f_{TH})	Experimental (f_E)	% Error $(f_E - f_{TH})/f_E * 100$
TSNT ₁	41	824	812	1.48
FFNT ₁	41	695	709	1.97
STNT ₁	41	548	560	2.14
TSNT ₂	41	710	699	1.57
FFNT ₂	41	588	588	0.0
STNT ₂	41	468	477	1.89
TSNT ₃	41	867	872	0.57
FFNT ₃	41	725	750	3.33
STNT ₃	41	606	614	1.30
TSNT ₄	41	726	724	0.28
FFNT ₄	41	610	630	3.17
STNT ₄	41	530	520	1.92
TSNT ₅	41	1224	1230	0.49
TSNT ₆	41	1249	1262	1.03

The RF currents at the interconnecting q ports are given by [2, 9]

$$\vec{i}_q = \left(Z_{qq} + Z_{rr} \right)^{-1} \left(Z_{rp} - Z_{rp} \right) \vec{i}_p \quad (5-14)$$

$J(s_0)$ is given by [138]

$$J(s_0) = \frac{-1}{L} \sum_{k=1}^p a_k \cos \frac{(k-1)\pi s_0}{L} \quad (5-15)$$

where L is the interconnection length, s_0 is the running coordinate along the interconnection, a_k is the expansion coefficient for the k^{th} mode and p represents the number of modes in the segment, which is equal to the number of ports along the interconnection. The expansion coefficients are determined by equating the p interconnection point currents to the excitation current along the interconnection. i.e.,

$$i(s_0) = L J(s_0) \quad (5-16)$$

Now a set of p simultaneous equations are obtained and which could be solved for getting the expansion coefficients.

For the segment shown in Figure 5.8, the electric field at a point (x, y) will contain contributions from both interconnecting sides. It is given by

$$E_z(x, y) = \hat{z} \frac{1}{h} \int_0^L G(x, y/x_0, y_0) J_1(y_0) dy_0 + \hat{z} \frac{1}{h} \int_0^L G(x, y/x_0, y_0) J_2(y_0) dy_0 \quad (5-17)$$

where $J_1(y_0)$ is the excitation current density along interconnection *side 1* and $J_2(y_0)$ is the same along *side 2*. They are obtained as

$$J_1(y_0) = \frac{-1}{L} \sum_{k=1}^6 a_k \cos \frac{(k-1) \pi y_0}{L} \quad (5-18)$$

a similar expression can be used for $J_2(y_0)$.

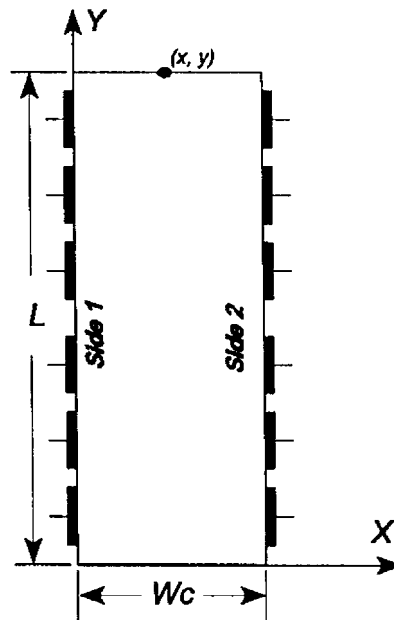


FIGURE 5.8 Rectangular segment with various dimensions for computing electric field at any point (x, y)

The electric field variation in other segments can be evaluated in a similar manner and hence we can compute the field variation along the periphery of the antenna. To get the radiation pattern and the effective loss tangent, the Z-directed electric field along the patch periphery is to be determined.

For the rectangular middle segment (see the coordinate system assigned in Figure 5.6), the Green's function used is given by [2, 8]

$$G(x, y/x_0, y_0) = \frac{j\omega\mu h}{ab} \sum_{n=0}^{\infty} \sum_{m=0}^{\infty} \frac{\sigma_m \sigma_n \cos k_x x_0 \cos k_y y_0 \cos k_x x \cos k_y y}{k_x^2 + k_y^2 - k^2} \quad (5-19)$$

where

$$k_x = \frac{m\pi}{a} \quad \text{and} \quad k_y = \frac{n\pi}{b}$$

$$\sigma_l = \begin{cases} 1 & \text{if } l = 0 \\ 2 & \text{otherwise} \end{cases}$$

For the 30° - 60° - 90° triangular segments for the coordinate system shown in Figure 5.6, the Green's function used is given by [2, 8]

$$G(x,y/x_0,y_0) = 8j\omega\mu h \sum_{m=-\infty}^{\infty} \sum_{n=-\infty}^{\infty} \frac{T(x_0,y_0) T(x,y)}{16\sqrt{3}\pi^2(m^2+mn+n^2) - 9\sqrt{3}a^2k^2} \quad (5-20)$$

where

$$\begin{aligned} T(x,y) = & (-1)^{(m+n)} \cos \frac{2\pi(-m-n)x}{\sqrt{3}a} \cos \frac{2\pi(m-n)y}{3a} \\ & + (-1)^m \cos \frac{2\pi mx}{\sqrt{3}a} \cos 2\pi(2n+m)\frac{y}{3a} \\ & + (-1)^n \cos \frac{2\pi nx}{\sqrt{3}a} \cos 2\pi(-2m-n)\frac{y}{3a} \end{aligned} \quad (5-20a)$$

For the 45° - 45° - 90° triangular segments, the Green's function used is given by [2, 8]

$$G(x,y/x_0,y_0) = \frac{j\omega\mu h}{2} \sum_{m=0}^{\infty} \sum_{n=0}^{\infty} \frac{\sigma_m \sigma_n T(x_0,y_0) T(x,y)}{(m^2+n^2)\pi^2 - a^2 k^2} \quad (5-21)$$

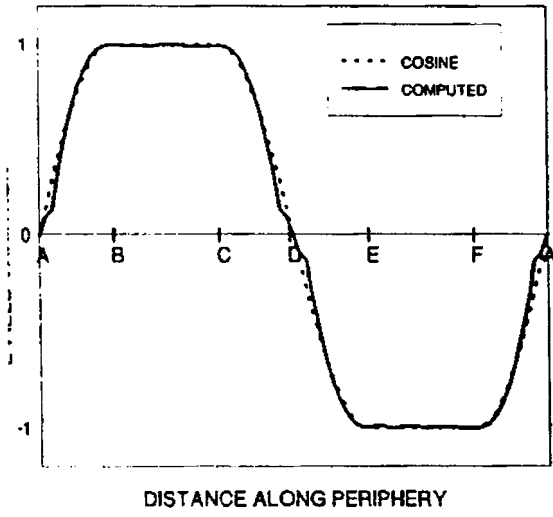
where

$$T(x,y) = \cos \frac{m\pi x}{a} \cos \frac{n\pi y}{a} + (-1)^{m+n} \cos \frac{n\pi x}{a} \cos \frac{m\pi y}{a} \quad (5-21a)$$

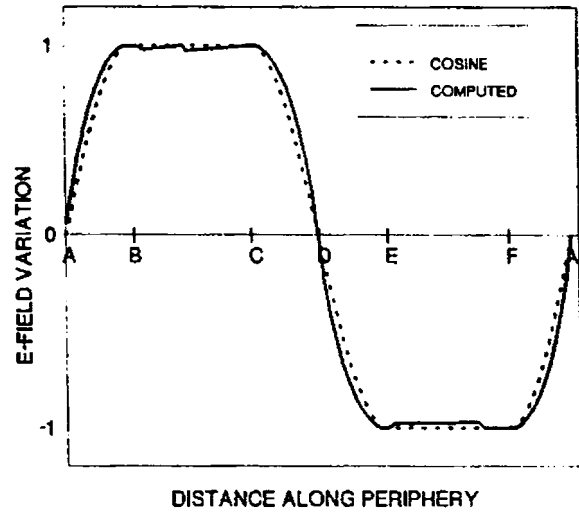
The computed electric field variation along the periphery of some antenna configurations given in Table 5.1 are normalised and plotted in Figure 5.9. From these field variations the mode is identified as TM_{01} , as there is no field variation along X -direction and one half wave variation along Y -direction. The computed electric field variations in Figure 5.9 are associated with cosine quarter wave variations from A to B , constant field from B to C , cosine quarter wave variation from C to D , again cosine quarter wave variation from D to E , constant field from E to F and cosine quarter wave variation from F to A . From the Figure it is clear that the cosine field variation approximations are accurate. These approximations are useful for the computation of radiation pattern of the antenna.

5.2.6 Aperture model development

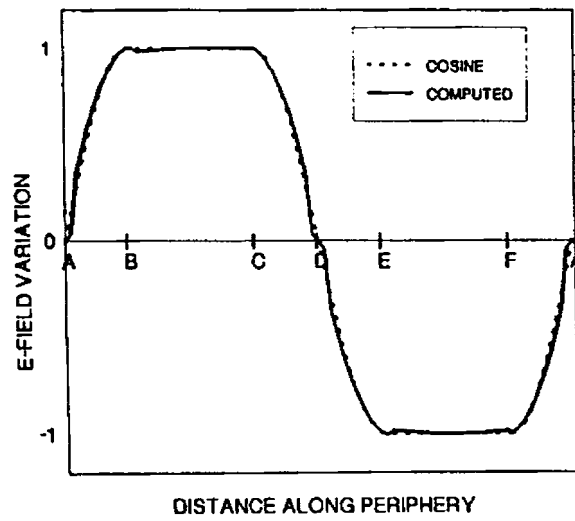
In this model, the microstrip antenna is converted into an equivalent aperture antenna and the radiation characteristics are determined with the spatial Fourier transform of the aperture electric field [35].



(a)



(b)



(c)

FIGURE 5.9 Computed electric field variation along the periphery of three typical antenna configurations

- (a) TSNT₃
- (b) FFNT₃
- (c) STNT₃

Figure 5.10 shows the geometry of the antenna and the coordinate system. The radiation field in the half space $z > 0$ is completely determined by the tangential component of electric field in the plane $z = 0$. The tangential component of electric field is zero on the patch metallisation (as it is assumed to be perfectly conducting) and at large distances from the patch in the plane $z = 0$. However, tangential component of electric field will exist in the close vicinity of the patch. Thus we can say that the radiation is due to this tangential component of electric field in an aperture extending along the entire periphery of the antenna.

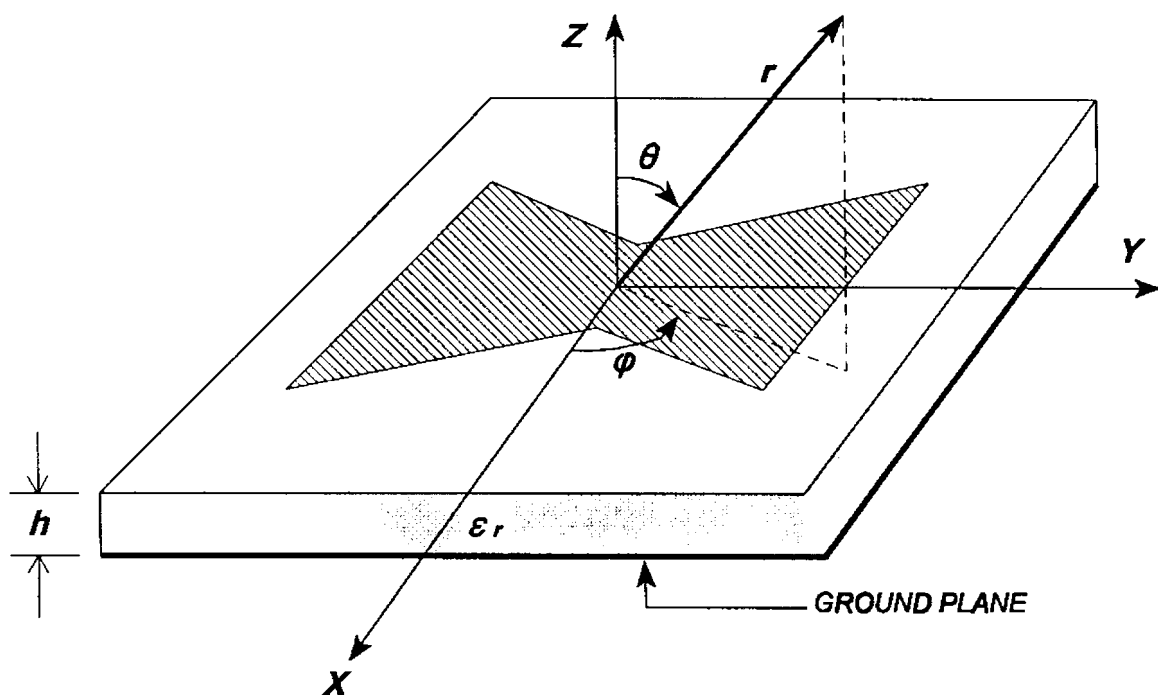


FIGURE 5.10 The coordinate system of the new drum-shaped antenna

One can simplify this approach on the basis of the fact that, the variation of tangential field in the radiating aperture along direction perpendicular to the edges of the patch has no important influence on the radiation field [35]. In the simplified model the aperture field is assumed to be a constant, E_a , over a small distance Δ from the edge of the resonator. The already computed Z -directed electric field along the periphery can be taken as equal to E_a and Δ can be equated to h , the dielectric thickness. This can be justified because, the electric field at the

periphery of the antenna gives rise to fringing fields which are responsible for radiation [1]. These fields are accounted by giving an equivalent outward edge extension equal to the height of the substrate as described in the magnetic wall model.

The aperture model of the antenna contains an infinite conducting plane at $z = 0$ with slots of width h around the surface of the patch excited by an electric field E_a as shown in Figure 5.11.

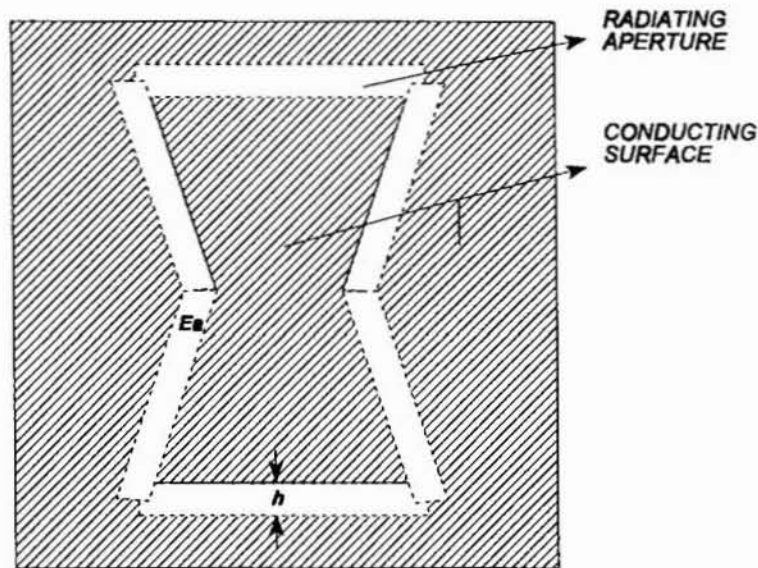


FIGURE 5.11 Aperture model of the antenna. The widths of the slots are selected to be equal to the height of the substrate used, h and the excitation field is E_a .

5.2.7 Determination of radiation pattern

The radiating aperture constructed as described earlier can be considered to be made up of 6 radiating aperture slots (S_1, S_2, S_3, S_4, S_5 and S_6) as shown in Figure 5.12. The slots are assumed to be having a width equal to the dielectric thickness (h). From Figure 5.9 it is found that the assumed cosine and computed electric field variations along the periphery closely resembles and

the former is used as the aperture excitations for the computation of radiation patterns as given below.

The aperture excitation fields E_1 and E_4 corresponding to slots S_1 and S_4 are given by

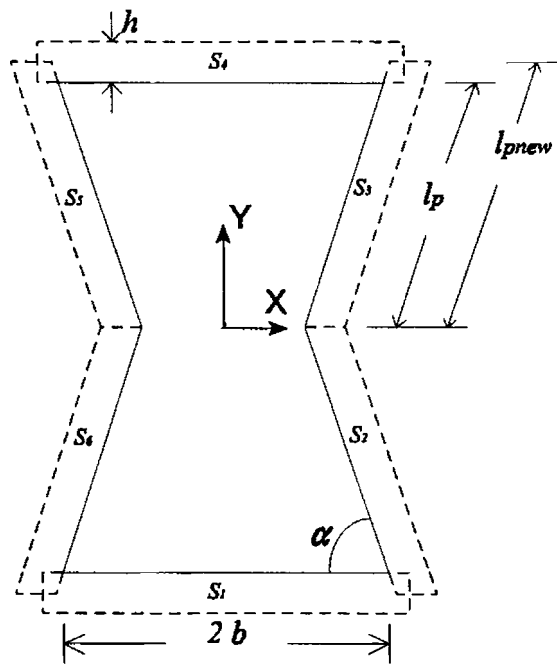


FIGURE 5.12 Configuration of radiating slots for computing the far field

$$E_1 = E_4 = E_0 \cos \left[\frac{m \pi (b + \frac{h}{2} + x)}{2(b + \frac{h}{2})} \right] \quad - (b + \frac{h}{2}) \leq x \leq (b + \frac{h}{2}) \quad (5-22)$$

The aperture excitation fields E_2 and E_6 corresponding to slots S_2 and S_6 are given by

$$E_2 = E_6 = E_0 \cos \left[\frac{n \pi}{2l_{pnew}} (l_{pnew} + \frac{y}{\sin \alpha}) \right] \quad - (l_{pnew} \sin \alpha) \leq y \leq 0 \quad (5-23)$$

The aperture excitation fields E_3 and E_5 corresponding to slots S_3 and S_5 are given by

$$E_3 = E_5 = E_0 \cos \left[\frac{n\pi}{2l_{pnew}} \left(l_{pnew} + \frac{y}{\sin \alpha} \right) \right] \quad 0 \leq y \leq (l_{pnew} \sin \alpha) \quad (5-24)$$

where $l_{pnew} = (l_p + \frac{h}{2})$

m, n are the mode numbers and E_0 is the maximum amplitude of aperture excitation.

The far field components produced by these aperture excitations are determined by taking their spatial Fourier transforms [35] as given below

$$\mathcal{F}(E_a) = \int_{x_{min}}^{x_{max}} \int_{y_{min}}^{y_{max}} E_a e^{jk_x x} e^{jk_y y} dx dy \quad (5-25)$$

where

$$k_x = k_0 \sin\theta \cos\phi$$

$$k_y = k_0 \sin\theta \sin\phi$$

$$k_0 = \frac{2\pi}{\lambda_0}$$

and λ_0 is the free space wavelength

The aperture excitation field E_a and the limits of integration varies according to the radiating slots. For TM_{01} mode (fundamental mode in our case), the far field contributions from

E_1 and E_4 have only Y -directed components, where as E_2, E_3, E_5 and E_6 have got both X - and Y -directed components. We can write the Fourier transform of the complete excitation field as

$$\vec{E}_{total} = \vec{i}_x E_x + \vec{i}_y E_y \quad (5-26)$$

where E_x and E_y are obtained by vectorially adding the X - and Y - directed components after incorporating the spatial phase shifts as below

$$E_x = E_{3yf} e^{jk_x s_{3x}} e^{jk_y s_{3y}} + E_{6yf} e^{jk_x s_{6x}} e^{jk_y s_{6y}} - E_{2yf} e^{jk_x s_{2x}} e^{jk_y s_{2y}} - E_{5yf} e^{jk_x s_{5x}} e^{jk_y s_{5y}} \quad (5-27)$$

$$E_y = E_{1yf} e^{jk_x s_{1x}} e^{jk_y s_{1y}} + E_{4yf} e^{jk_x s_{4x}} e^{jk_y s_{4y}} - E_{2yf} e^{jk_x s_{2x}} e^{jk_y s_{2y}} - E_{3yf} e^{jk_x s_{3x}} e^{jk_y s_{3y}} \\ - E_{5yf} e^{jk_x s_{5x}} e^{jk_y s_{5y}} - E_{6yf} e^{jk_x s_{6x}} e^{jk_y s_{6y}} \quad (5-28)$$

where E_{1f} and E_{4f} are the Y -directed far field components produced by slot excitations E_1 and E_4 respectively. $E_{2xf}, E_{3xf}, E_{5xf}$ and E_{6xf} are the X -directed far field components produced due to aperture excitations E_2, E_3, E_5 and E_6 respectively. $E_{2yf}, E_{3yf}, E_{5yf}$ and E_{6yf} are the corresponding Y -directed far field components. $(S_{1x}, S_{1y}), (S_{2x}, S_{2y}), \dots, (S_{6x}, S_{6y})$ are the co-ordinates of the centre points of the slots S_1, S_2, \dots, S_6 respectively. The total far field produced can be written as [35]

$$E(r, \theta, \phi) = \frac{jk_0 e^{-jk_0 r}}{2\pi r} (\hat{i}_\theta E_1 + \hat{i}_\phi E_2) \quad (5-29)$$

where

$$E_1 = E_x \cos \phi + E_y \sin \phi$$

$$E_2 = -E_x \sin \phi \cos \theta + E_y \cos \phi \cos \theta$$

The two principal plane patterns (E - and H -plane) are obtained by taking $|E_\theta|$ in $\phi = 90^\circ$ plane and $|E_\phi|$ in $\phi = 0^\circ$ plane respectively.

The computed and measured radiation patterns of different antenna configurations mentioned in Table 5.1, in the two principal planes (E - and H -plane) are shown in Figure 5.13. From the above figures it is clear that the computed and experimental patterns are in good agreement.

5.2.8 Determination of power radiated

Total power radiated from the microstrip antenna fed at the periphery as shown in Figure 5.2 can be determined by normalising the input voltage at the feed point (x_0, y_0) to 1 V. i.e.,

$$h E_z(x_0, y_0) = 1 \quad (5-30)$$

for TM_{01} mode

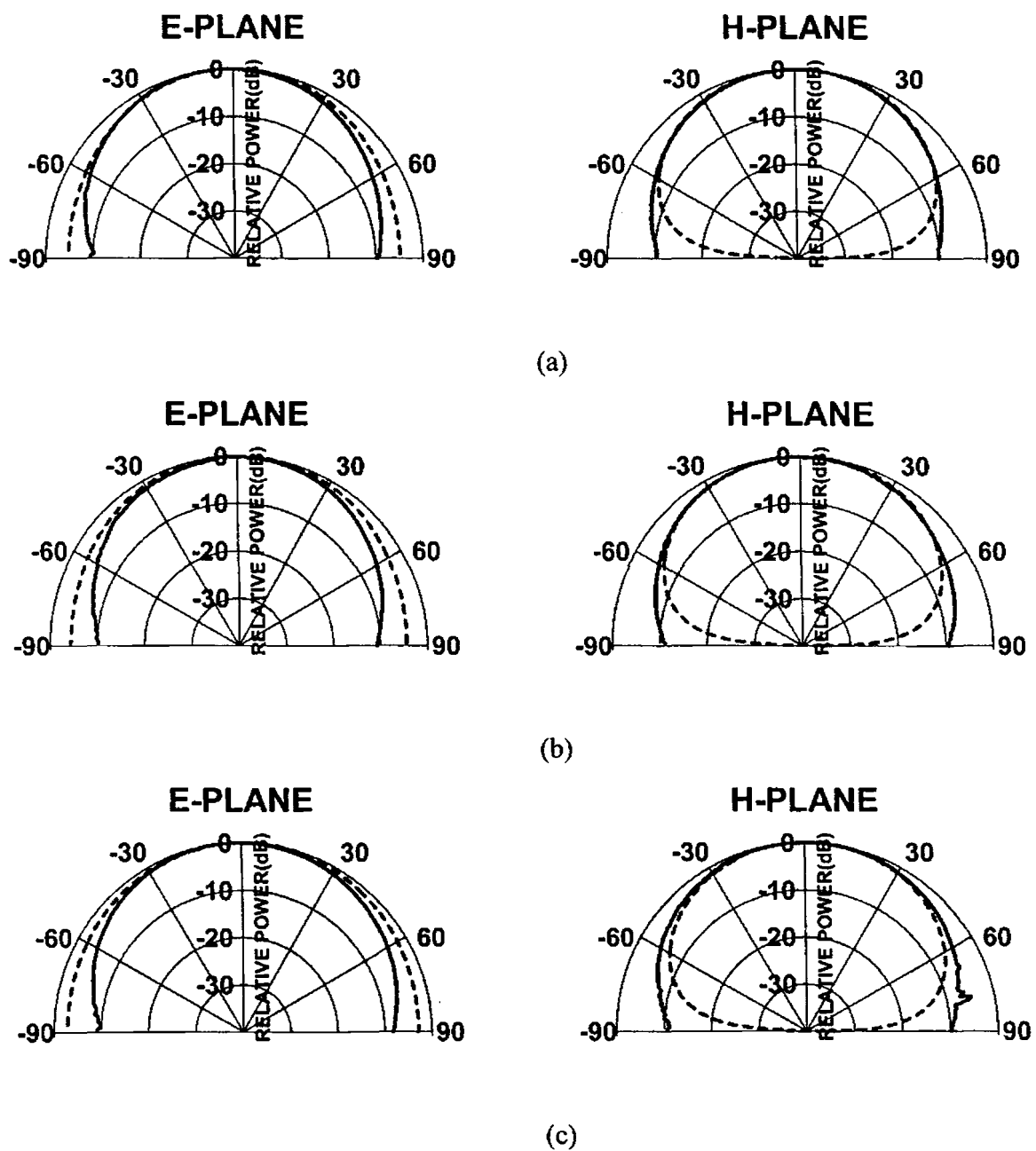
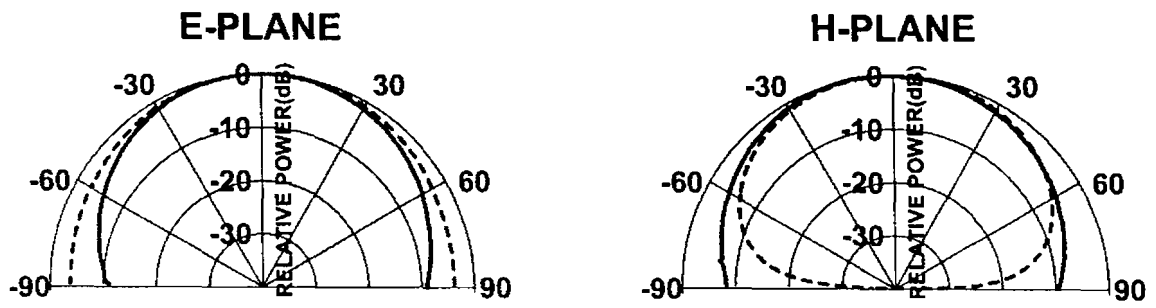


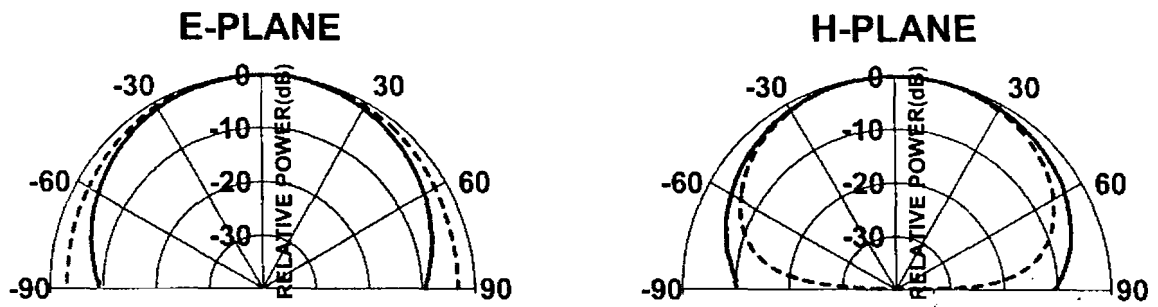
FIGURE 5.13(i) Computed and measured radiation patterns of different drum-shaped antenna configurations

————— measured - - - - - computed

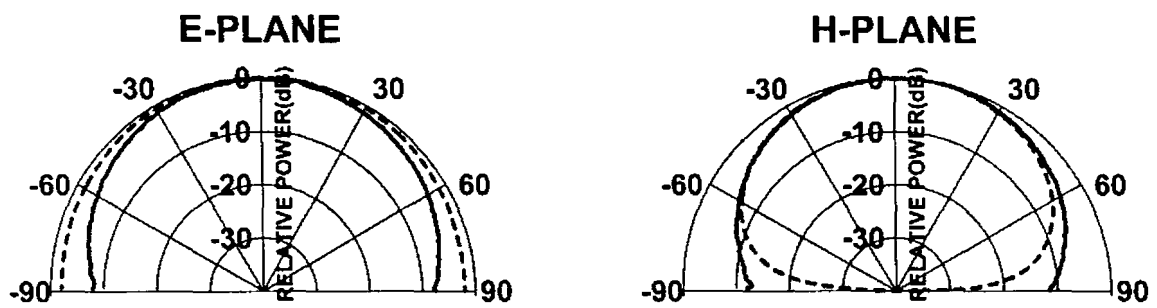
- (a) TSNT,
 (b) FFNT,
 (c) STNT,



(a)



(b)

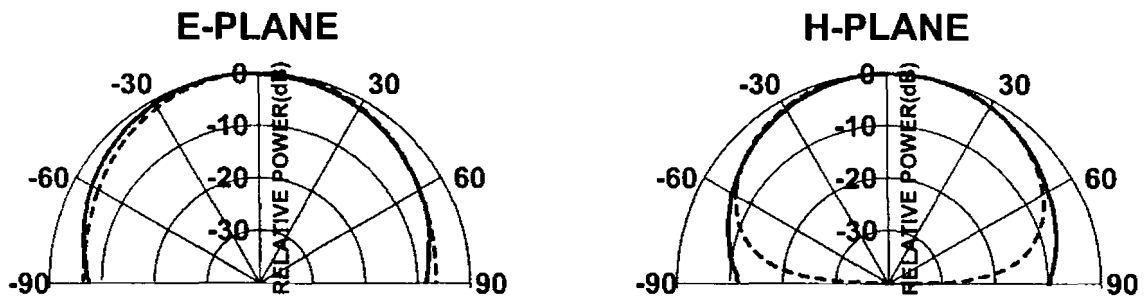


(c)

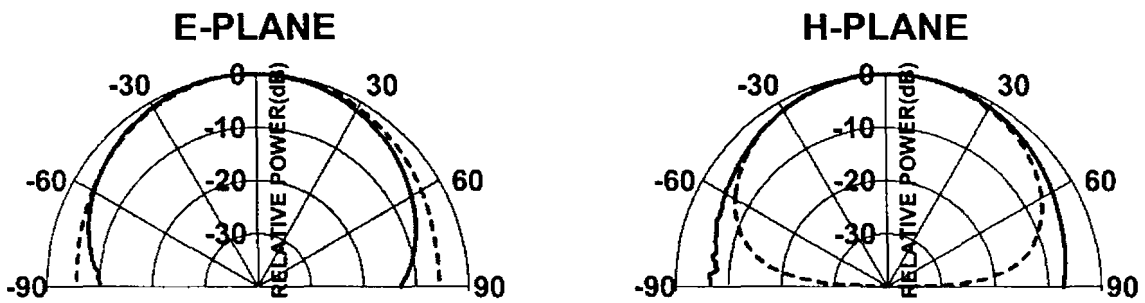
FIGURE 5.13(ii) Computed and measured radiation patterns of different drum-shaped antenna configurations

————— measured - - - - - computed

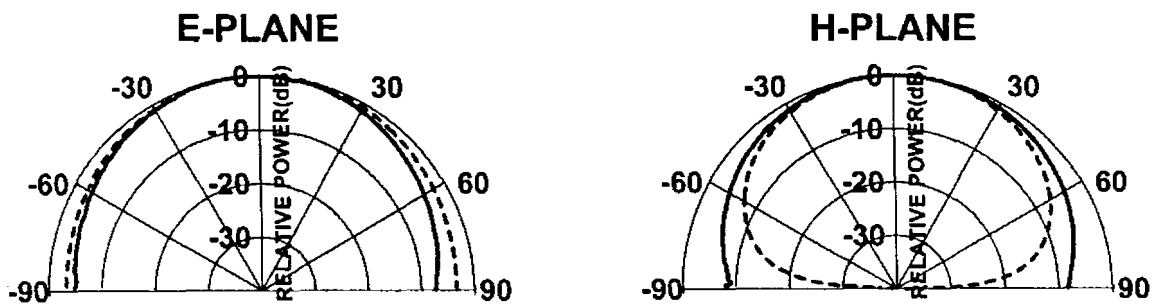
- (a) TSNT₂
- (b) FFNT₂
- (c) STNT₂



(a)



(b)



(c)

FIGURE 5.13(iii) Computed and measured radiation patterns of different drum-shaped antenna configurations

———— measured - - - - - computed

- (a) TSNT₃
- (b) FFNT₃
- (c) STNT₃

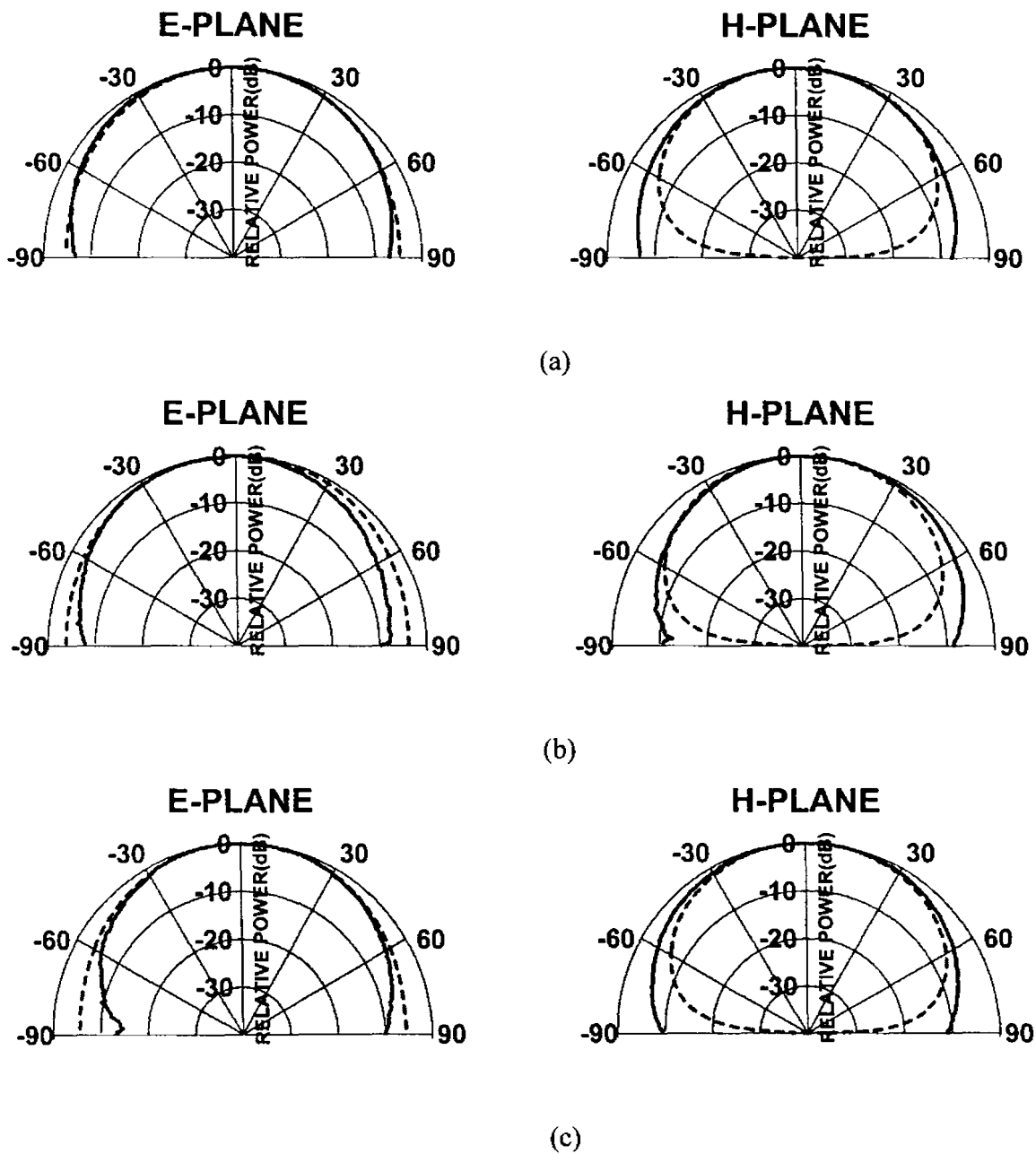


FIGURE 5.13(iv) Computed and measured radiation patterns of different drum-shaped antenna configurations

———— measured - - - - - computed

- (a) $TSNT_4$
- (b) $FFNT_4$
- (c) $STNT_4$

$$h E_0 \cos \left[\frac{n\pi}{2l_p} \left(l_p + \frac{y_0}{\sin \alpha} \right) \right] = 1 \quad (5-31)$$

l_p and α have got the same meanings as in the previous section (see Figure 5.12). E_0 obtained from the above equation will be used for the evaluation of E_θ and E_ϕ and which in turn will be used for the computation of the total radiated power as given below

$$P_r = \frac{1}{Z_0} \int_0^{\frac{\pi}{2}} \int_0^{2\pi} (|E_\theta|^2 + |E_\phi|^2) \sin\theta r^2 d\phi d\theta \quad (5-32)$$

where Z_0 is the wave impedance of free space

5.2.9 Stored energy in the cavity

The total stored energy (W_{total}) in the cavity formed by the microstrip patch on one side, ground plane on the other side and magnetic walls along the periphery of the patch at resonance is determined by adding the time averaged electric and magnetic field energy under each segment.

The stored energy under a segment is generally given by

$$W_s = \frac{1}{2} \epsilon_0 \epsilon_{eff} \iiint_v |E_z|^2 dv \quad (5-33)$$

E_z is given by (5-18) and v is the volume of the cavity constituted by the segment.

As explained earlier, for the rectangular segment, the electric field along Y -direction varies in a cosine manner and constant field along Z and X -directions, we can simplify (5-33) as,

$$W_{rect} = \frac{1}{2} \epsilon_0 \epsilon_{reff} h w_r \int_{rl} |E_{zy}|^2 dy \quad (5-34)$$

where E_{zy} is the Z -directed field variation along Y -direction, w_r is the width of the rectangular segment and rl represents the integration path along the length of the segment.

For a triangular segment, the stored energy is numerically equal to half of the stored energy under a rectangle having length and breadth equal to the base and altitude of the right-angled triangular segment. Assuming cosine quarter wave variation along Y -direction and constant field along X and Z -directions, the stored energy under the newly formed rectangular segment ($W_{newrect}$) is calculated using (5-34). Stored energy under the triangular segment ($W_{triangle}$) is given by

$$W_{triangle} = \frac{W_{newrect}}{2} \quad (5-35)$$

So total stored energy, W_{total} is given by

$$W_{total} = W_{rect} + 4 W_{triangle} \quad (5-36)$$

5.2.10 Quality factor

The quality factor of the antenna can be computed by knowing the total power lost (P_{lost}) and the total stored energy (W_{total}) as

$$Q = \frac{\omega_r W_{total}}{P_{lost}} \quad (5-37)$$

where $\omega_r = 2\pi f_{01}$ and f_{01} is the TM_{01} mode resonant frequency.

The total power lost is the sum of the power loss due to radiation (P_r), power loss due to the finite conductivity of the copper walls (P_c), dielectric loss (P_d) and surface wave loss (P_{sw}).

i.e.,

$$P_{lost} = P_r + P_c + P_d + P_{sw} \quad (5-38)$$

$$\approx P_r$$

as P_c , P_d and P_{sw} are not significant at lower frequencies and for lower order modes. P_r and W_{total} are obtained as described earlier.

5.2.11 Input impedance

The actual input impedance of the antenna is evaluated by incorporating the total energy lost as an effective loss tangent, δ_{eff} . This effective loss tangent modifies the dielectric constant to a

complex value. This complex permittivity is given by

$$\epsilon_{renv} = \epsilon_{reff} (1 - j\delta_{eff}) \quad (5-39)$$

where δ_{eff} is given by

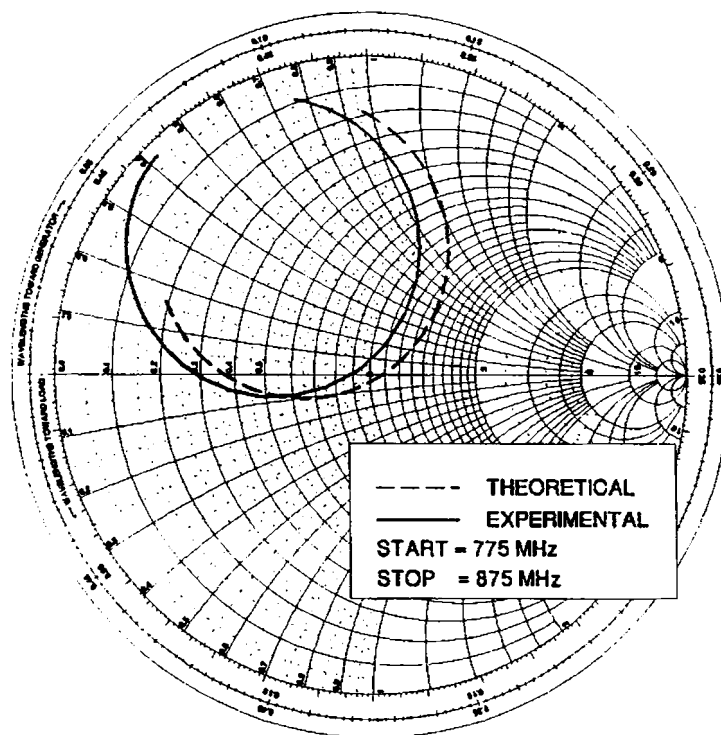
$$\delta_{eff} = \frac{1}{Q} \quad (5-40)$$

This new value of dielectric constant modifies the wave number to an effective value, k_{eff} , given by

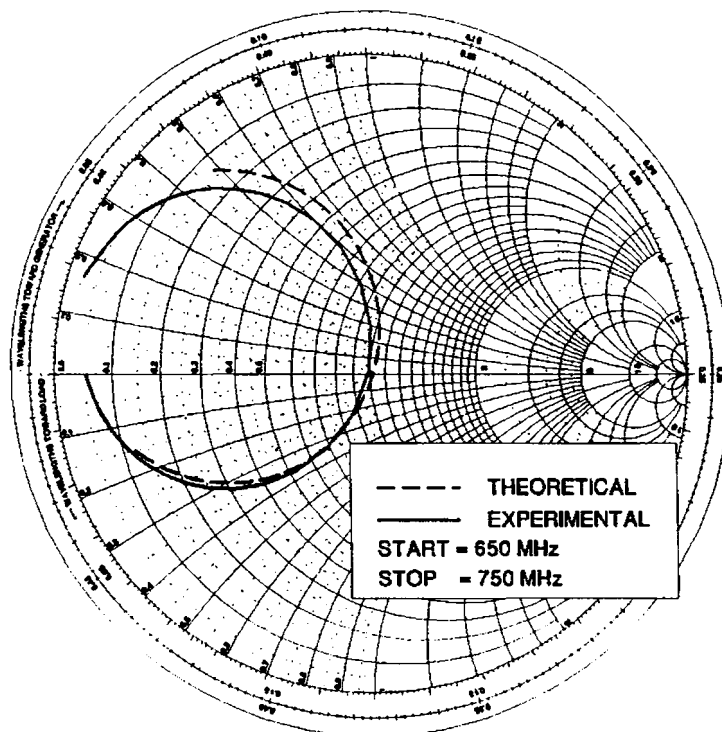
$$k_{eff} = k_0 \sqrt{\epsilon_{renv}} \quad (5-41)$$

The impedance matrix elements of the various segments will be now computed once again. The effective wavenumber, k_{eff} , will be used in the evaluation of the Green's functions. The impedance matrix elements of the different segments are now combined together by multi-port connection method as explained earlier in section 5.2.3 to get the complex input impedance of the antenna. Now a purely real value of the input impedance indicates resonance.

The computed and measured input impedance in and around the resonant frequency for different antenna configurations given in Table 5.1 are shown in Figure 5.14. The theoretical and experimental impedance loci are in close agreement for different dielectric substrates and antenna dimensions.



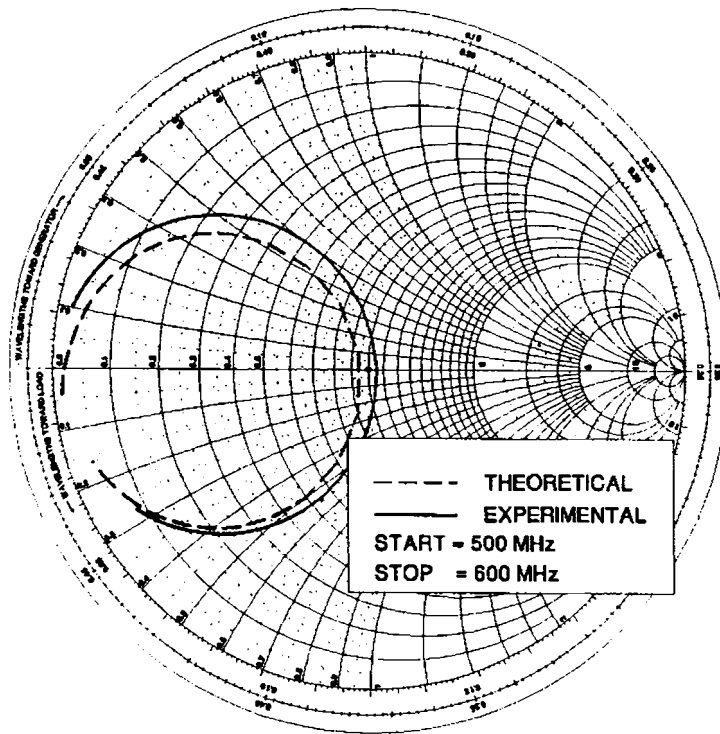
(a)



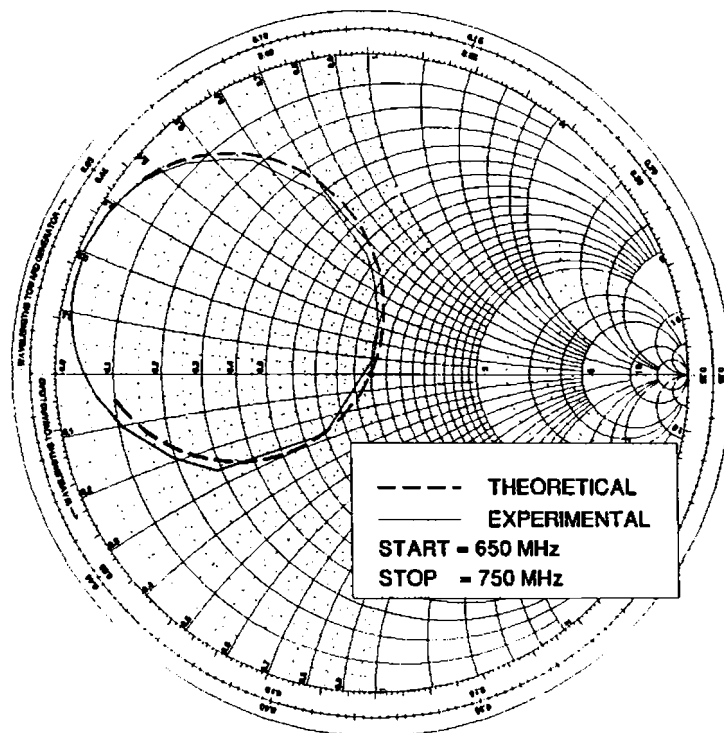
(b)

FIGURE 5.14(i) Computed and measured input impedance variations of different drum-shaped antenna configurations in and around the resonance frequency (increasing frequency is clockwise)

- (a) TSNT₁
 (b) FFNT₁



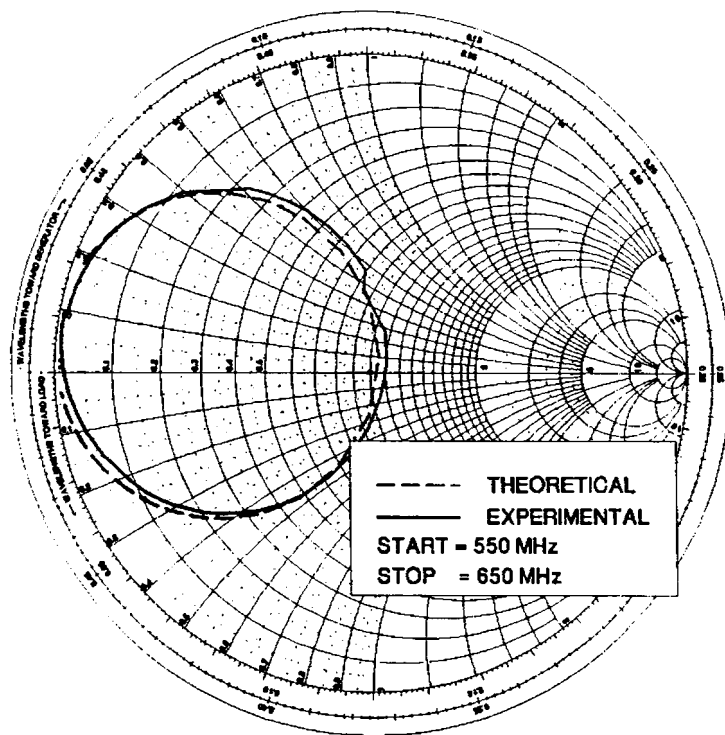
(a)



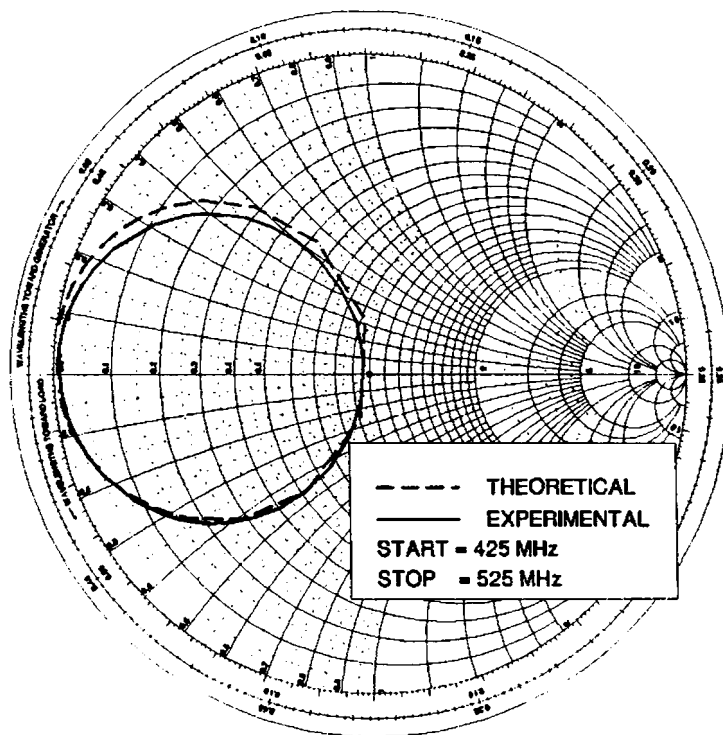
(b)

FIGURE 5.14(ii) Computed and measured input impedance variations of different drum-shaped antenna configurations in and around the resonance frequency (increasing frequency is clockwise)

- (a) STNT₁
 (b) TSNT₂



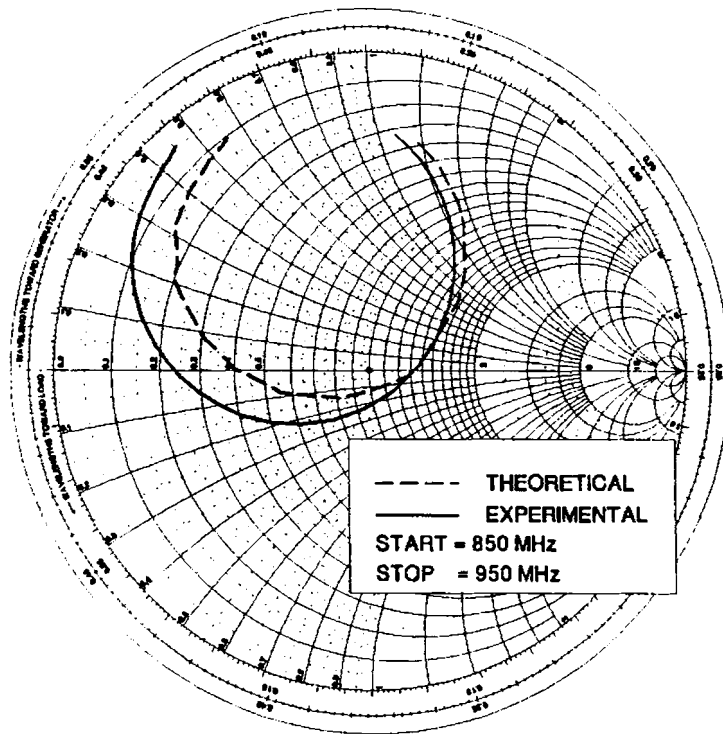
(a)



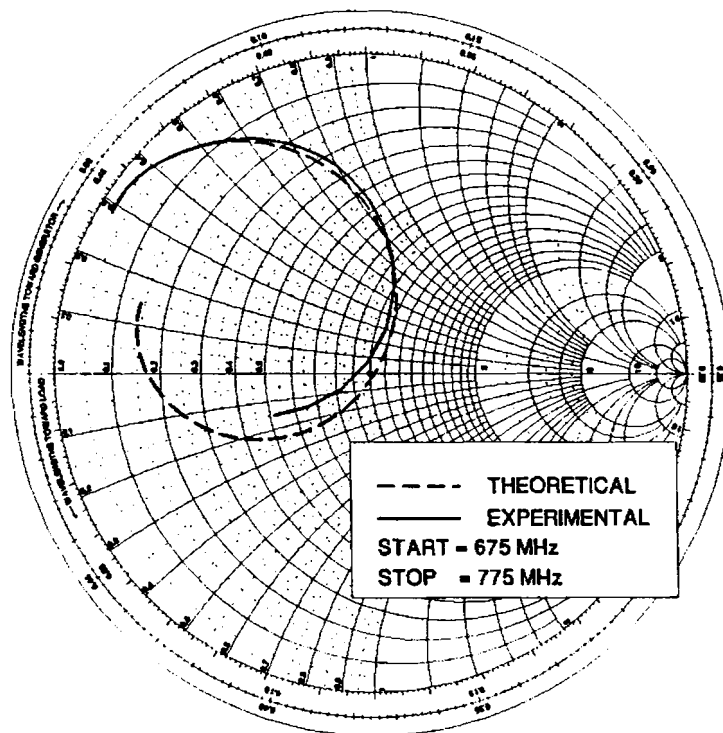
(b)

FIGURE 5.14(iii) Computed and measured input impedance variations of different drum-shaped antenna configurations in and around the resonance frequency (increasing frequency is clockwise)

- (a) FFNT₂
 (b) STNT₂



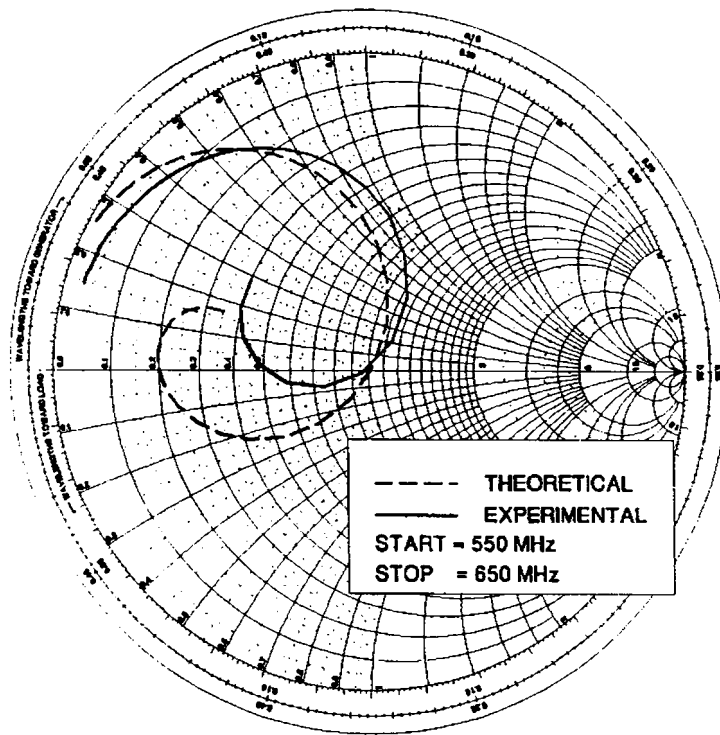
(a)



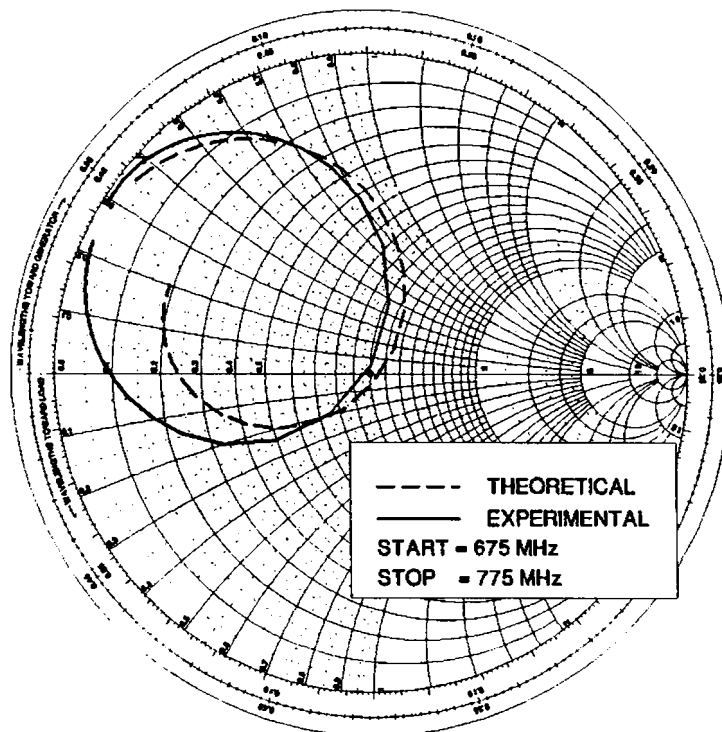
(b)

FIGURE 5.14(iv) Computed and measured input impedance variations of different drum-shaped antenna configurations in and around the resonance frequency (increasing frequency is clockwise)

- (a) $TSNT_3$
 (b) $FFNT_3$



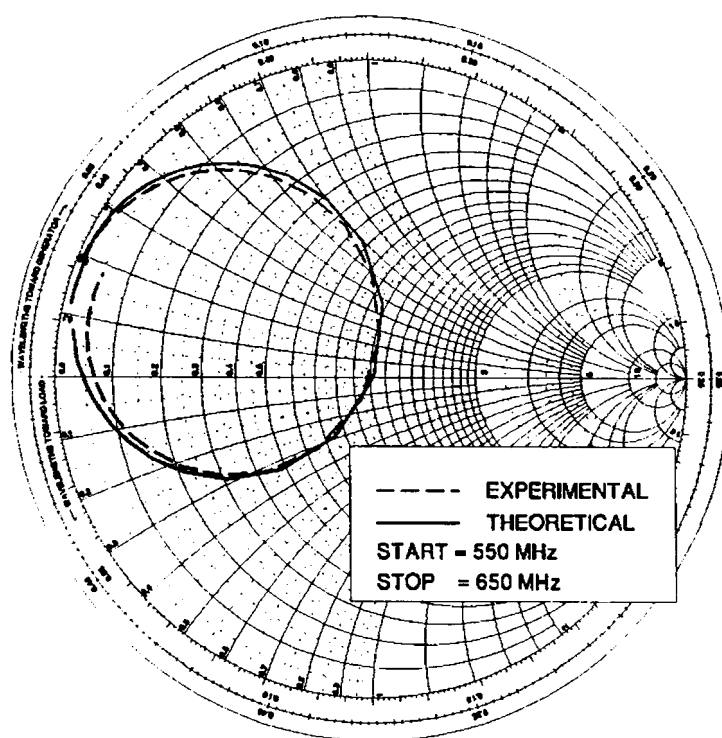
(a)



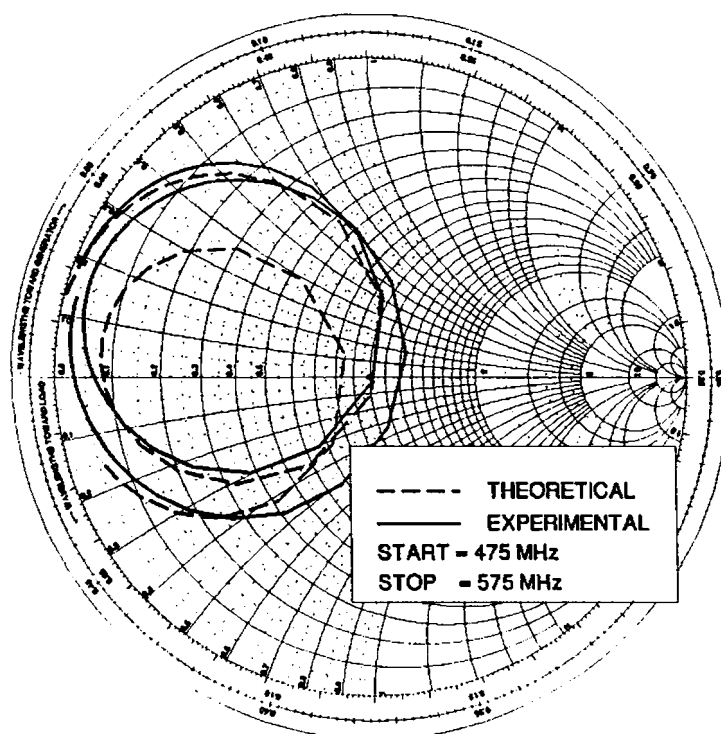
(b)

FIGURE 5.14(v) Computed and measured input impedance variations of different drum-shaped antenna configurations in and around the resonance frequency (increasing frequency is clockwise)

- (a) STNT₃
- (b) TSNT₄



(a)

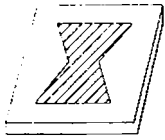


(b)

FIGURE 5.14(vi) Computed and measured input impedance variations of different drum-shaped antenna configurations in and around the resonance frequency (increasing frequency is clockwise)

- (a) FFNT₄
 (b) STNT₄

The new compact drum-shaped antenna has been analysed for different characteristics like resonant frequency, mode of operation, field variation along the periphery, radiation pattern, input impedance, bandwidth, etc. The analysis can be performed only on those antenna configurations, which could be divided into a combination of rectangular and triangular segments. The triangular segments should be of the 30° - 60° - 90° or 45° - 45° - 90° type. Different antenna configurations satisfying the above condition have been analysed completely and the results obtained were compared with experimental results. Excellent agreement between them is observed. The slight difference between them could be attributed to fabrication tolerances and/or poor modelling of fringing fields.



CONCLUSIONS

This chapter presents the conclusions drawn from the experimental and theoretical investigations carried out on the drum-shaped compact microstrip antenna. The conclusions drawn from experimental and theoretical investigations are considered separately. Suggestions for further work in the field are given at the end of the chapter.

6.1 INFERENCES FROM EXPERIMENTAL INVESTIGATIONS

The characteristics of three possible types ($L/B < 1$, $L/B = 1$, $L/B > 1$) of drum-shaped antennas are studied in the UHF- and L-bands. From the exhaustive experimental investigations it is found that the drum-shaped antenna is resonating at a lower frequency compared to a conventional microstrip antenna having same surface area. It is observed that the resonant frequency of the

drum-shaped antenna due to electric field variation along the length of the patch is found to be decreasing with the central width. Figure 4.5 indicates clearly this shift of resonant frequency with respect to central width. From Table 4.1 it is clear that the effect is true for all types of drum-shaped microstrip antennas in both the bands.

The area requirement of different drum-shaped antennas have been presented and compared in Table 4.2 with the commonly used rectangular patches. From these observations, it is clear that the drum-shaped antenna requires very less area compared to an ordinary rectangular patch antenna operating at the same frequency and fabricated on the same substrate.

The drum-shaped microstrip antenna possess an easy method for frequency tuning. Frequency tuning through reduction of resonant frequency can be achieved by slightly reducing the central width. Whereas, in the case of rectangular microstrip antennas, the reduction in frequency is achieved only by increasing the length and which in turn requires the fabrication of a new antenna. Frequency tuning through increase of resonant frequency can also be achieved through the reduction of resonant length as in the case of rectangular patches. Hence without fabricating a new antenna, increasing or decreasing of resonant frequency can be achieved by suitably trimming the length or central width of the antenna.

The radiation pattern characteristics have been studied in detail. From Figure 4.7. and Table 4.3, it is clear that the pattern of the antenna is almost similar to those of rectangular patches. The cross-polar levels in most of the cases are found to be better than 12 dB.

Gain of the antenna has been compared with gain of an equivalent rectangular patch fabricated on the same substrate. Figure 4.8 gives a comparison between the two. It is observed that, in all the cases, in both the bands the gain is not much affected when the central width is greater than 50% of the radiating edge width for TM_{01} mode.

The presence of the mode due to the field variation along the length of the patch is confirmed by measuring the electric field variation under the patch at the resonant frequency.

Figure 4.9 shows that there is half wave variation of electric field amplitude along the length of the patch and virtually no variation along the width of the antenna.

Finally, the mode due to field variation along the other side is studied and observed that the resonant frequency increases with a decrease in central width. The study of this mode opens the possibility of using this as a dual frequency orthogonally polarised antenna. The frequency ratio between the two frequencies is found to be increasing with the decrease in central width. This is demonstrated in Figure 4.11. Here also frequency ratio tuning can be performed by trimming the central width.

6.2 INFERENCES FROM THEORETICAL INVESTIGATIONS

A method based on segmentation technique, cavity model and spatial Fourier transform technique is used for the analysis of the antenna configurations. The analysis could predict the characteristics like resonant frequency, electric field variation along the periphery of the patch, radiation pattern, input impedance, etc., of the antenna.

For the analysis, the antenna geometry is divided into four triangular and one rectangular segments. The fringing fields, which are responsible for the radiation are accounted by giving equivalent edge extensions equal to the height of the substrate. The continuous interconnection between the segments are now discretised. A port is associated with each of these points whose width is kept $\leq \lambda_g/20$ to enable us to assume that there is no field variation over the width of a port. The impedance matrix elements of different segments are now computed and combined together to get the overall impedance matrix of the antenna. From the study of the reactance variation with respect to frequency as shown in Figure 5.7, we can determine the resonant frequency of the antenna.

The different port currents are computed at resonant and the discrete port currents are converted into a continuous current density along the interconnection length. This continuous

current density is used for the determination of the field variation along the periphery of the antenna. A typical field variation along the periphery is shown in Figure 5.9. From the nature of this field variation we can identify the mode of excitation of the antenna.

Aperture model of the antenna is now developed as explained in Section 5.2.6 and the radiation patterns are computed. The power radiated is computed from the radiation pattern expression. The total stored energy under the cavity is determined using the field variation under the patch. The quality factor of the cavity under the patch is calculated and is used for the determination of the complex dielectric constant. This value is then used for the evaluation of the impedance matrix elements to get the actual input impedance of the antenna.

The theoretical analysis can predict the resonant frequency, impedance of the antenna, the radiation pattern, mode of operation, field variation along the periphery within a tolerable limits. The slight difference in the theoretical and experimental values may be attributed to the fabrication tolerances and/or the poor modelling of fringing fields.

6.3 SOME POSSIBLE APPLICATIONS OF THE PROPOSED ANTENNA

The drum-shaped antenna may find applications in areas, where antenna size is a major constraint. The size of the antenna is very crucial if it is to be integrated with active devices in a GaAs substrate in the case of Monolithic Microwave Integrated Circuits (MMICs). Being a compact microstrip antenna, the proposed antenna may be a suitable candidate in such applications.

The development of compact, conformal low-cost antennas have received much attention in recent years due to the demand from personal communication systems, global positioning system etc. The most important requirement for an antenna element to be used in such applications is the compact size. The drum-shaped antenna, being a simple compact

microstrip antenna element may find applications in such systems.

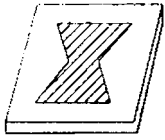
This antenna can effectively replace conventional rectangular and circular patches in applications like phased arrays as there is no deterioration in gain compared to an equivalent rectangular patch antenna till the central width reaches 50% of the radiating edge width.

6.4 SCOPE FOR FURTHER WORK IN THE FIELD

Like other microstrip antenna elements, this also suffers from poor impedance bandwidth. The bandwidth enhancement of this new compact microstrip antenna would be an interesting topic for further work. The bandwidth of the antenna may be improved by parasitic loading of the antenna, by using proper superstrates, or by loading with suitable dielectric resonators.

The effect of impedance bandwidth using different feeding techniques like proximity coupling, aperture coupling, superstrate loading etc. also may be an interesting field of study.

Different geometrical modifications of the drum-shaped antenna obtained by altering the irregular side periphery using circular, parabolic, logarithmic, etc., curves can be studied in detail for enhancing the impedance bandwidth.



COMPACT DUAL FREQUENCY MICROSTRIP ANTENNA

A.1 INTRODUCTION

Compact dual frequency microstrip antennas are getting more and more attention due to the fast developments in the area of communication. A microstrip antenna could be made compact through different methods. Some of the methods involve the use of a shorting pin [110, 119, 120, 121] and some others involve the geometrical modification [97, 115, 143]. In this appendix, we present a dual frequency microstrip antenna by adding a shorting pin to a compact drum-shaped microstrip antenna. The shorting pin provided dual frequency operation along with further reduction of the resonant frequency. The range of frequency ratio of the antenna can be varied by changing the aspect ratio.

A.2 DESIGN DETAILS AND EXPERIMENTAL SETUP

The schematic diagram of the proposed miniature dual frequency microstrip antenna is shown in Figure A.1. The configuration consists of a drum-shaped patch [143] etched on a substrate of thickness h and dielectric constant ϵ_r . L is the length, B is the width and W is the central width of the antenna. The feed point and shorting pin positions are specified in terms of coordinates (x_f, y_f) and (x_s, y_s) respectively.

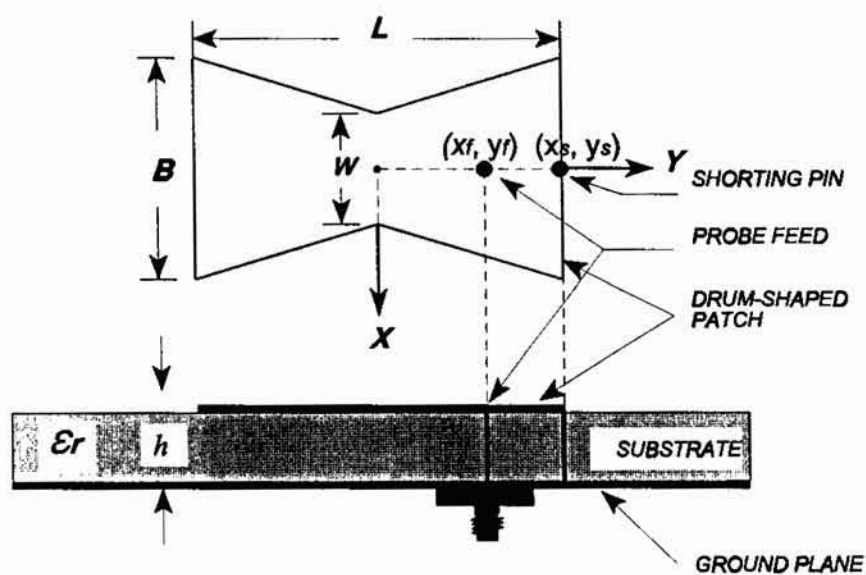


FIGURE A.1 Geometry of the proposed miniature dual frequency drum-shaped microstrip antenna

The different characteristics of the antenna like resonance frequency, input impedance, radiation pattern, etc., are measured as explained in Chapter 3.

A.3 EXPERIMENTAL RESULTS AND DISCUSSION

It is noted that the maximum reduction in size of the antenna is achieved if the shorting pin is

placed at the centre of the radiating edge. With a prudent selection of the feed point along the Y -axis, matching without the excitation of TM_{10} mode can be achieved. Here, the antenna is found resonating with the first two frequencies having the same polarisation by eliminating TM_{10} mode.

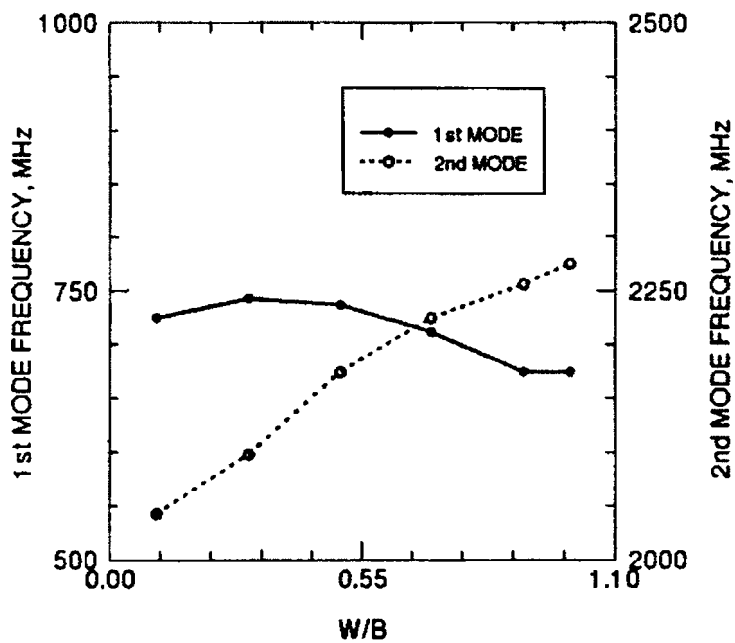


FIGURE A.2 Variation of first and second mode resonant frequencies with central width

Figure A.2 shows the variation of first and second resonance frequencies with central width W for a typical drum-shaped antenna with length $L = 3.8$ cm, width $B = 2.53$ cm, fabricated on a substrate of $\epsilon_r = 4.5$ and $h = 0.16$ cm. From the graph, it is observed that the first resonance frequency increases from 675 MHz to 743 MHz and the second resonance frequency decreases from 2275 MHz to 2043 MHz with decreasing W/B . i.e., the frequency ratio varies from 3.37 to 2.75. The variation of frequency ratio with W is maximum when $L/B < 1$ and decreases as we increase the L/B ratio. Figure A.3 shows the frequency ratio variation with respect to W/B , for

different L/B values. From the observations it is found that a frequency ratio of about 5 is achieved when L/B is 0.5. Hence the frequency ratio can be varied by trimming L/B and/or W/B .

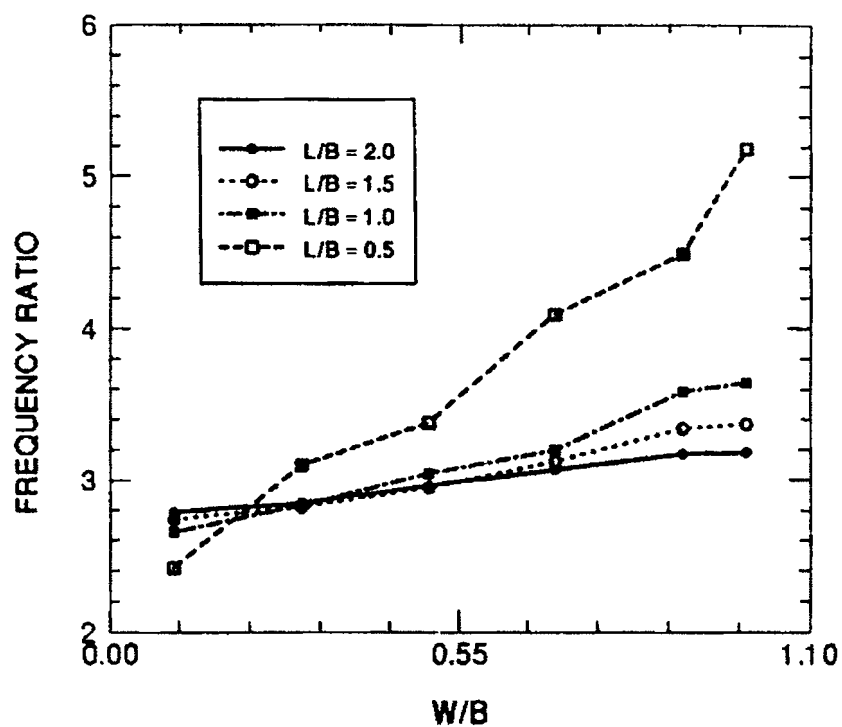


FIGURE A.3 Variation of frequency ratio with central width for different aspect ratios

In a particular drum-shaped antenna configuration, there exists a feed point along the central line at which both the resonance frequencies can be excited with good matching. When $W = 0.7 B$, for the typical antenna mentioned above, the feed point is found at (1.75 cm, 0 cm)

when the shorting pin is at $(L/2, 0 \text{ cm})$. Figure A.4 shows the return loss variation of the antenna. The antenna is resonating at 701.8 MHz and 2201 MHz. The percentage bandwidths are 1.19% and 1.59% respectively. Figure A.5 shows the E - and H -plane co and cross polar patterns at the central frequencies of the two bands. The gain of the antenna has been studied by using rectangular microstrip antennas fabricated on the same substrate and resonating at the same frequencies. For the second resonance, no deterioration in antenna gain is observed till the central width reaches $0.5B$ and beyond that the gain decreases. For the first mode, the gain in all the cases is found less than that of the corresponding rectangular patch antennas. Here the reduced gain may be compensated by integrating amplifiers on the substrate or by superstrate technique [121, 133].

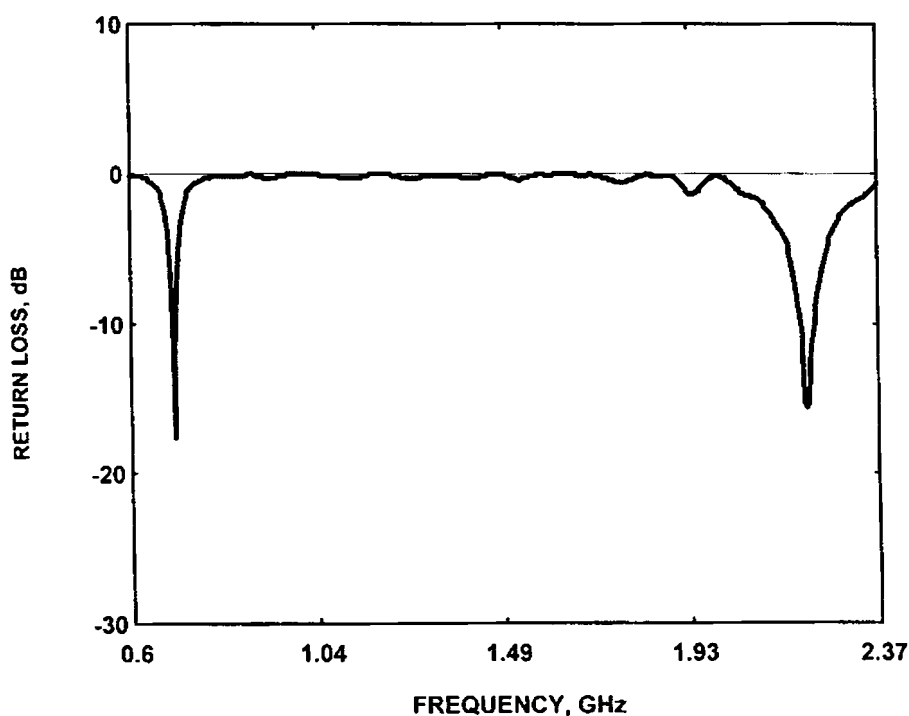


FIGURE A.4 Variation of return loss with frequency for the typical antenna configuration

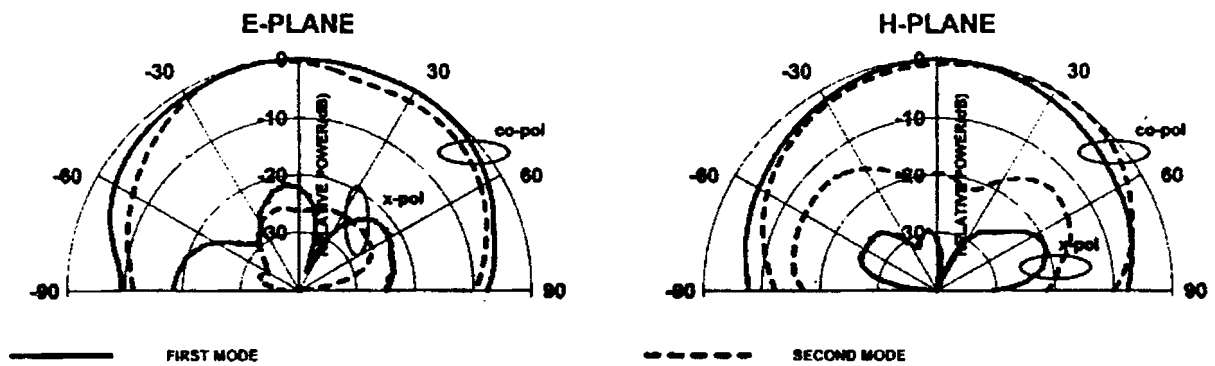


FIGURE A.5 *E* and *H*-plane co and cross polar patterns of the antenna

A.4 CONCLUSIONS

A new dual frequency compact microstrip antenna configuration with wide range of variation of frequency ratio is presented. The new configuration takes advantage of the compactness of drum-shaped microstrip antennas along with dual frequency operation provided through putting a shorting pin. This new configuration may find applications in mobile satellite communication systems.



BROADBAND DUAL FREQUENCY MICROSTRIP ANTENNA

B.1 INTRODUCTION

Microstrip antennas are offering many advantages like, low profile, light weight, conformal nature, etc., over the conventional radiating elements and attracted great attention for the past few years. Commonly used microstrip radiators are circular or rectangular patches. Radar and advanced communication applications like synthetic aperture radar (SAR), Global position system (GPS) and vehicular communication requires a low profile antenna capable of dual frequency dual polarisation operation with sufficiently large bandwidth and good isolation between its ports. In the literature only limited number of methods are available for dual frequency operation [139, 140] at the ports. Most of these techniques provide small impedance

bandwidth that limits their fields of application.

In this appendix, a new microstrip antenna geometry that provides two independent ports with orthogonal polarisation and comparable gain to that of a standard circular patch antenna is presented. Corresponding to its two ports, the new structure resonates at two frequencies with large impedance bandwidths. Energy is coupled electromagnetically to these ports using two perpendicular microstrip feed lines. The new antenna offers excellent isolation between its ports that is essential to avoid any crosstalk. A formula for calculating the resonant frequencies of the two ports is also presented.

B.2 DESIGN AND EXPERIMENTAL DETAILS

The antenna geometry is defined by the intersection of two circles of the same radius r with their centres c_1 and c_2 displaced by a small distance d and fed by proximity coupling using two 50Ω perpendicular microstrip lines as shown in Figure B. 1.

The test antenna is fabricated on a substrate (RT/Duroid) with dielectric constant $\epsilon_{r1} = 2.21$ and thickness $h_1 = 0.08$ cm (substrate 1). Intersection of two circular patches of radius $r = 2$ cm each with their centres displaced by a distance $d = 0.4 r$ cm (optimised experimentally for maximum bandwidth and good isolation) is etched on the above substrate and fed as shown in Figure B. 1. The microstrip feedlines are fabricated on a substrate of dielectric constant $\epsilon_r = 4.5$ and thickness $h_2 = 0.16$ cm (substrate 2). The optimised feed locations are $f_{p1} = 0.6$ cm and $f_{p2} = 0.5$ cm (these are the distances from the edges of the feed lines from *port 1* and *port 2* to the centre point c).

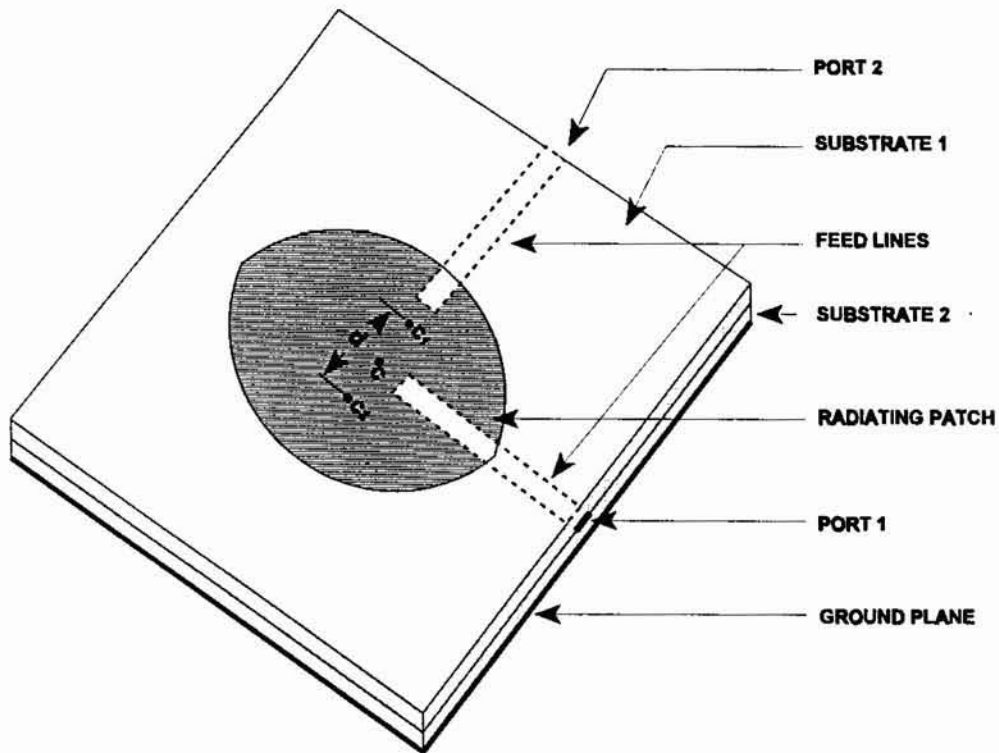


FIGURE B.1 Geometry of the proposed microstrip antenna with feeding technique

B.3 RESULTS

The antenna resonates at two frequencies, 2.635 GHz and 3.05 GHz for *port 1* and *port 2* respectively. The variation of return loss with frequency is given in Figure B. 2. The 2:1 VSWR bandwidths corresponding to *port 1* and *port 2* are 3% and 5.3 % respectively. These values are quite higher than that of a conventional circular patch antenna [1]. The frequency separation between the resonances is found to be increasing with d . The radiation from the antenna is linearly polarised and the polarisations of the two ports are orthogonal to each other. Figure B.3 clearly shows that, the antenna offers an isolation better than 30 dB between the ports in the operating frequency range (2.595 - 3.13 GHz). The E - and H -plane radiation patterns for the *port 1* and *port 2* are given in Figure B. 4. The 3 dB beamwidths along E -plane are 96.3° and 101.6°

for port 1 and port 2 respectively. The corresponding beamwidths along H -plane are 65.9° and 94.5° . The cross polar levels are found to be better than 25 dB for these ports. The gain of the new antenna is found to be nearly equal (with a difference of < 0.5 dB) to that of a corresponding standard circular microstrip patch operating at the same frequencies.

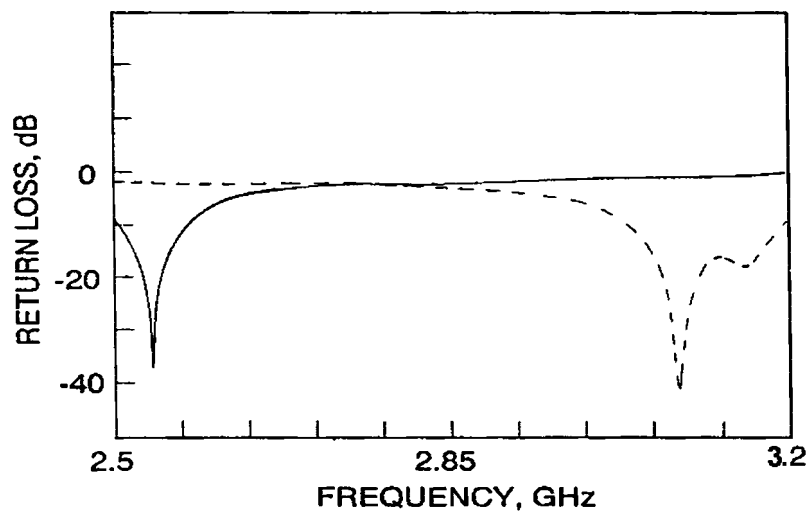


FIGURE B.2 Variation of return loss with frequency

— port 1
 - - - port 2

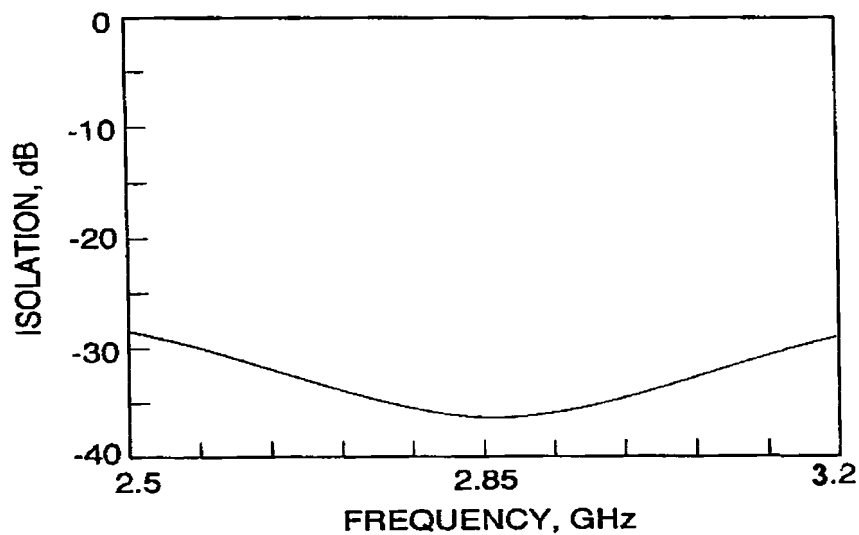


FIGURE B.3 Measured isolation between port 1 and port 2

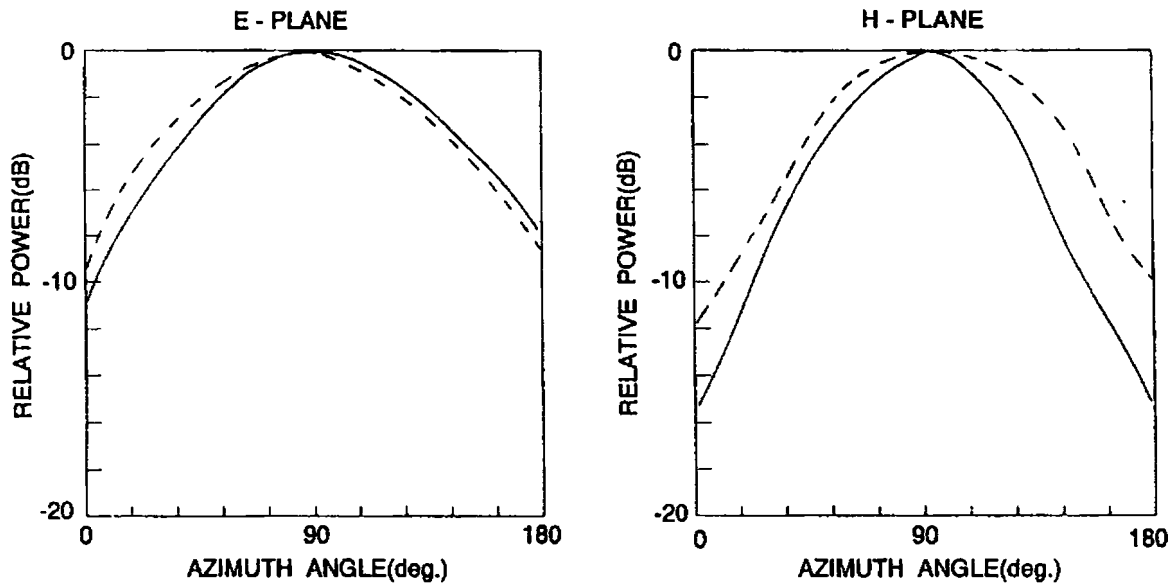


FIGURE B.4 *E*- and *H*-plane radiation patterns of the antenna at the centre frequencies of the two ports

———— *port 1*
 - - - - - *port 2*

B.4 THEORETICAL ANALYSIS

The two resonant frequencies of the present antenna configuration can be calculated using the following procedure as given in [7].

The TM_{11} mode resonant frequency of a circular microstrip antenna of radius r fabricated on a substrate of dielectric constant ϵ_r and thickness h is given as

$$f_r = \frac{1.841 c}{2 \pi r \sqrt{\epsilon_r}} \quad (\text{B-1})$$

where 're' is

$$r_s = r \left[1 + \frac{2h}{\pi r \epsilon_r} \left(\ln \frac{\pi r}{2h} + 1.7726 \right) \right]^{\frac{1}{2}}$$

Now the two frequency offset values are suitably modified as,

$$\left. \begin{aligned} \Delta f_1 &= -f_r \frac{0.4185}{2} \frac{ds}{s} \\ \Delta f_2 &= f_r \frac{0.4185}{2} \frac{ds}{s} \end{aligned} \right\} \text{for } \epsilon_r < 4.5 \quad (\text{B-2})$$

$$\left. \begin{aligned} \Delta f_1 &= -f_r \frac{0.4185}{2} \frac{ds}{s} \\ \Delta f_2 &= f_r \frac{0.4185}{2} \frac{ds}{s} \end{aligned} \right\} \text{for } \epsilon_r \geq 4.5 \quad (\text{B-3})$$

The resonant frequencies corresponding to *port 1* and *port 2* respectively are given by

$$f_1 = f_r + \Delta f \quad (\text{B-4})$$

$$f_2 = f_r + \Delta f_2 \quad (\text{B-5})$$

where c is the velocity of light in free space, $s = \pi r^2$ (area of the original circle) and $(s - \Delta s)$ is the overlapping area of the two circles. The theoretical resonant frequencies for *port 1* and *port 2* are 2.609 and 3.129 GHz respectively. The experiment has been repeated with substrates of different thickness and dielectric constant. The agreement between theoretical and experimental resonance frequencies is found to be good, except for a slight error that could be due to tolerances in dielectric constant, fabrication etc. Generally, the above analysis can predict the resonance frequencies with an error of less than 5%.

B.5 CONCLUSION

A novel dual port broadband microstrip antenna resonating at two frequencies and providing orthogonal polarisations with very good isolation between the two ports is presented. The gain of the antenna is comparable to that of a standard circular patch microstrip antenna. This antenna may find applications in systems where dual frequency operation with large bandwidth is required.



DIELECTRIC RESONATOR LOADED MICROSTRIP ANTENNA FOR ENHANCED IMPEDANCE BANDWIDTH AND EFFICIENCY

C.1 INTRODUCTION

Microstrip antennas find far reaching applications in the current communication scenario due to their unique properties like light weight, ease of fabrication, low production cost, low profile, etc. The fields of application of these antennas are mainly limited by their inherent disadvantage of low impedance bandwidth. Two commonly used microstrip radiating geometries are rectangular and circular. Techniques are available in the literature for improving the impedance band width of microstrip antennas [72, 98, 141, 142]. However, these methods will increase the complexity of the system or in most of the cases reduces the antenna gain.

In this Appendix, a method for improving the impedance bandwidth of a microstrip antenna using a Dielectric Resonator (DR) attached on the surface of the patch is presented. This technique improves the impedance bandwidth, to more than 10% for a rectangular Microstrip Antenna.

C.2 DESIGN DETAILS AND EXPERIMENTAL SETUP

The schematic diagram of a typical antenna configuration is shown in Figure C.1. The configuration consists of a rectangular patch of length L and width W on a substrate of thickness h and dielectric constant ϵ_r . The antenna is loaded with a cylindrical dielectric resonator of diameter d , height H and dielectric constant ϵ_{dr} . The patch is fed by a probe at the position (X_p, Y_p) . The operating frequency of the antenna is selected to be close to the $TE_{01\delta}$ mode resonant frequency of the dielectric resonator.

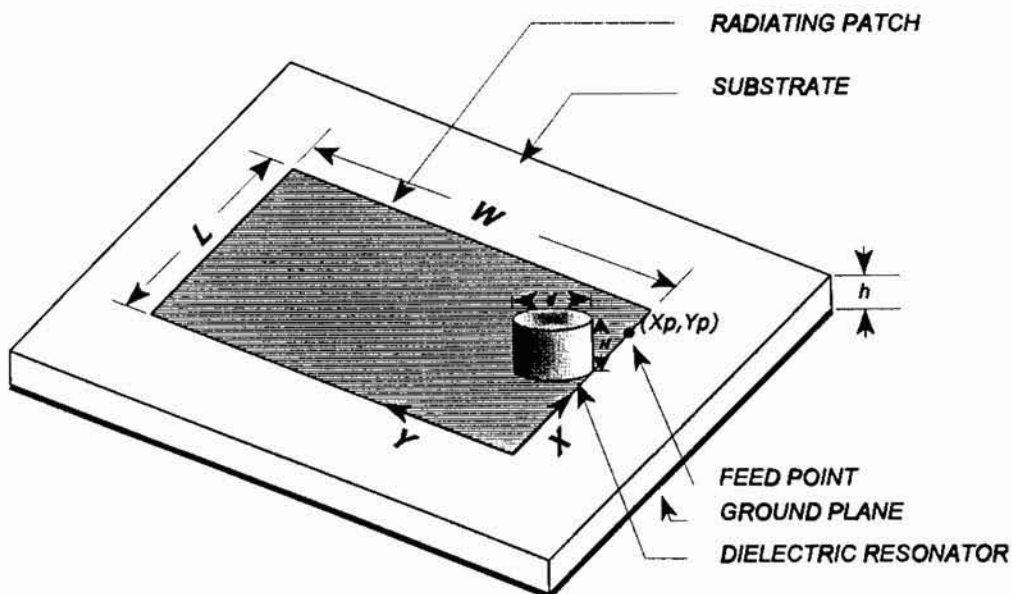


FIGURE C.1 Schematic diagram of a typical antenna configuration

The different characteristics of the antenna are measured by using the method described in Chapter 3.

C.3 EXPERIMENTAL RESULTS AND DISCUSSION

A rectangular microstrip antenna resonating at 2.70 GHz ($L = 2.58$ cm, $W = 3.35$ cm, $h = 0.16$ cm and $\epsilon_r = 4.5$) is designed for optimum radiation performance [1]. A cylindrical DR ($H = 0.9$ cm, $d = 1.4$ cm and $\epsilon_{dr} = 58$) having $TE_{01\delta}$ mode frequency close to the resonating frequency of the above antenna is suitably positioned on the patch surface. The patch width, position of the DR on the patch and the feed point are optimised experimentally for maximum impedance bandwidth and the DR is pasted at this position using a thin layer of conducting epoxy. This typical configuration is giving a maximum bandwidth of 274 MHz at 2.63 GHz when $L = 2.58$ cm, $W = 2.94$ cm, $X_p = 1.98$ cm, $Y_p = 0.0$ cm and the DR is placed at the middle of the non-radiating edge in such a way that its surface is just gracing the radiating patch edge as shown in Figure C.1. The variation of percentage bandwidth with feed location is shown in Table C.1. When the patch is fed at (2.58 cm, 0.0 cm), the system was not at all matched. But on loading with DR the antenna is found to be matched and providing an impedance band-width of more than 8%. This shows that this technique can be used for the impedance tuning of microstrip antennas.

The experiment is repeated on a circular microstrip antenna resonating at 4.01 GHz (radius = 1.42 cm, $\epsilon_r = 2.2$ and $h = 0.08$ cm) with a DR ($H = 0.565$ cm, $d = 0.979$ cm, $\epsilon_{dr} = 63$ and $TE_{01\delta}$ mode frequency 4.0 GHz). Here the position of the DR on the patch surface and the feed point are experimentally optimised for maximum bandwidth. The configuration is giving a maximum bandwidth of 239 MHz at 3.92 GHz when the feed point is at a distance of 1.00 cm and DR centre is at a distance of 1.21 cm from the patch centre. The sector angle formed between two

radial vectors, one passing through the DR centre and the other through the feed point, is 135° .

The different characteristics for the above optimum antenna configurations are given in Table C. 2 for a comparative study.

TABLE C.1 Variation of impedance bandwidth with respect to feed location for the experimentally tuned rectangular microstrip antenna configuration

Feed point ($X_p, Y_p=0$) X_p cm	% Bandwidth	
	Before DR loading	After DR loading
2.58	*	8.90%
2.43	*	8.15%
2.28	*	8.10%
2.13	*	10.10%
1.98	2.2%	10.41%
1.83	2.2%	8.20%
1.68	3.3%	7.21%
1.53	3.3%	6.84%

* *Not Matched.*

TABLE C.2 Characteristics of the DR loaded rectangular and circular microstrip antenna configurations

Characteristic	Rectangular patch	Circular patch
Substrate dielectric constant	4.5	2.2
Resonant frequency without DR	2.70 GHz	4.01 GHz
% bandwidth (VSWR ≤ 2) without DR	2.2%	1.1%
% bandwidth (VSWR ≤ 2) with DR	10.41%	6.1%
Central frequency with DR	2.63 GHz	3.92 GHz
3dB beamwidth		
<i>E</i> -plane	128.7°	109.8°
<i>H</i> -plane	71.2°	79.5°

The variation of VSWR with frequency for the two configurations are shown in Figure C.2. The *E*- and *H*-Plane radiation patterns of the antenna systems at the corresponding central frequencies are shown in Figure C.3. In both the cases the *E*-Plane patterns differ slightly from those of conventional microstrip antennas. *H*-Plane patterns are similar to those of conventional ones. Figure C.4 shows the variation of S_{21} with frequency for the configuration shown in Figure C.1. This figure shows that compared to ordinary microstrip antennas the present configuration is giving an increased gain of >1 dB. This may be due to the reradiation from the DR.

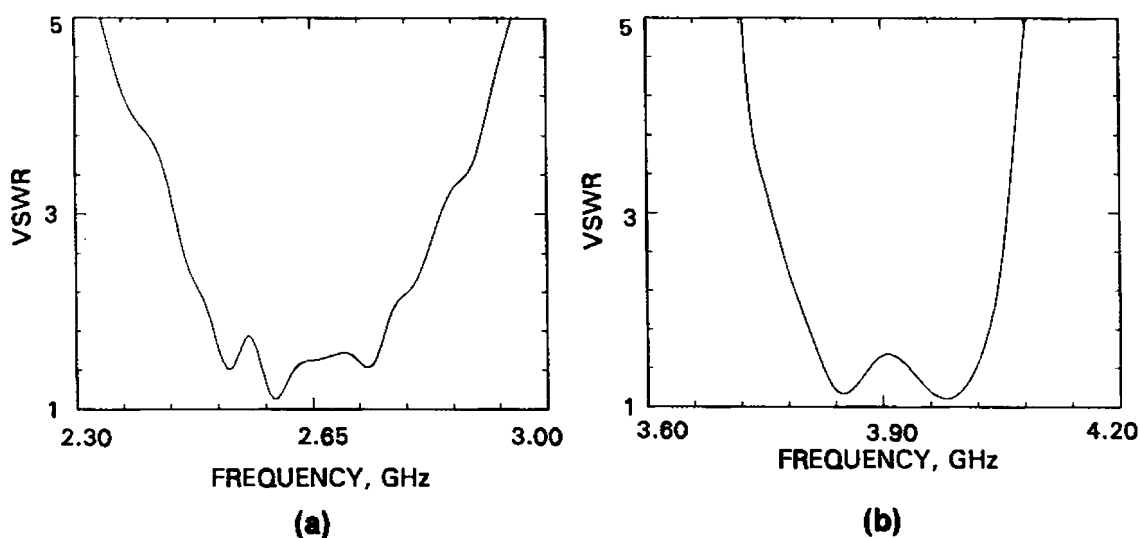


FIGURE C.2 Variation of VSWR with frequency for the two proposed antenna configurations

- (a) Rectangular patch configuration
- (b) Circular patch configuration

C.4 CONCLUSIONS

A new Method for enhancing the impedance bandwidth of microstrip antennas is proposed. This approach enhances the gain of the antenna as well as enables impedance tuning. Optimum rectangular (bw >10%) and circular (bw >6%) antenna configurations are demonstrated. These configurations may find applications in wideband phased arrays.

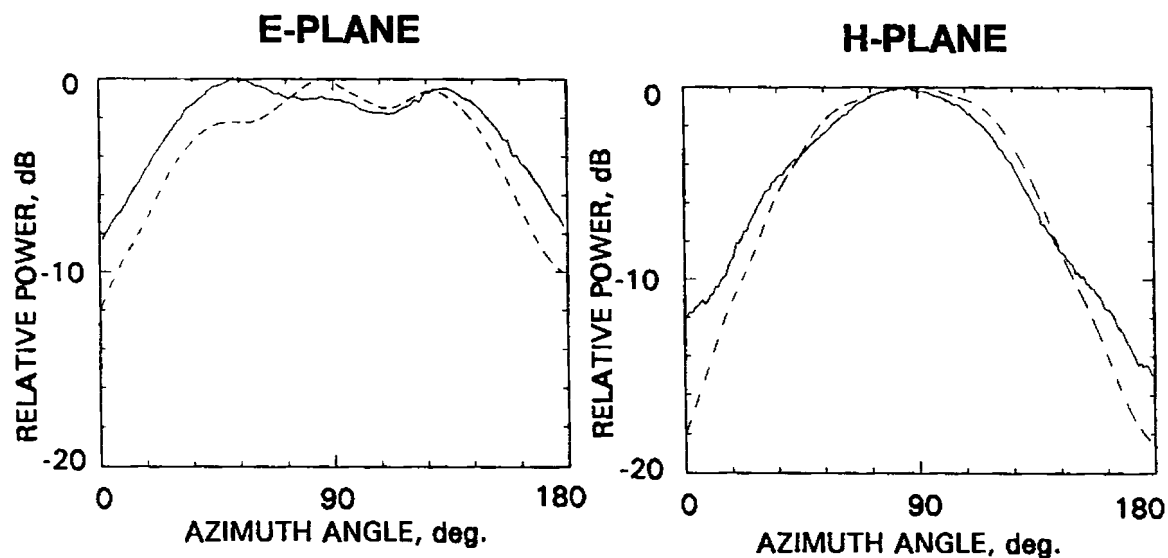


FIGURE C.3 *E*- and *H*-plane radiation patterns of the two antenna configurations at the corresponding central frequencies.

— rectangular patch configuration
 - - - circular patch configuration

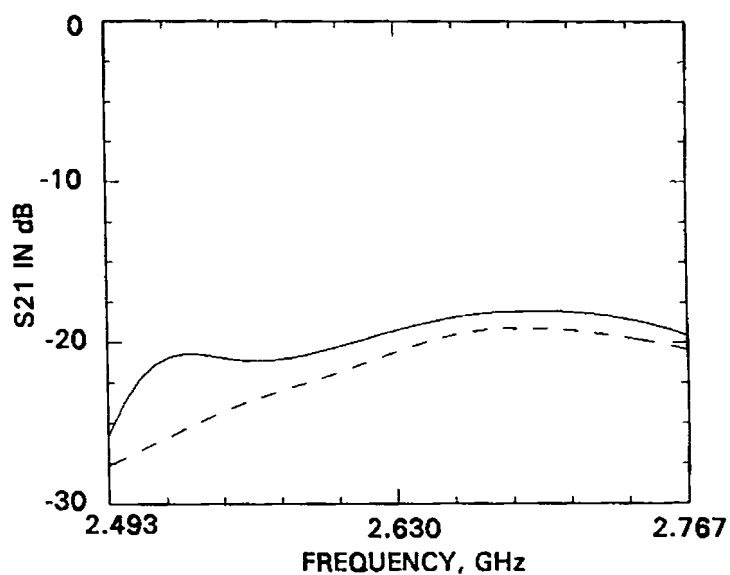
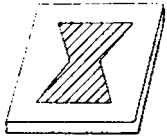


FIGURE C.4 Variation of S_{21} with frequency for the optimum rectangular patch configuration

— after DR loading
 - - - before DR loading



REFERENCES

BOOKS

1. I.J. Bahl and P. Bhartia, "Microstrip antennas, " Artech House, Dedham, MA, 1980
2. K.C. Gupta, R. Garg, and R. Chadha, "Computer-aided design of microwave circuits, " Artech House, Norwood, MA, 1981
3. J.R. James, P.S. Hall, and C. Wood, "Microstrip antenna - theory and design, "London, UK: Peter Peregrinus Ltd., IEE, 1981.
4. C.A. Balanis, "Antenna theory: analysis and design, " Harper and Row, Publishers, New York, 1982.
5. J.D. Kraus, "Antennas," McGraw-Hill, New York, 1988.
6. K.C. Gupta and Abdelaziz Benalla, "Microstrip antenna design, "Artech House, Norwood, MA, 1988.
7. J.R. James and P.S. Hall, "Hand book of microstrip antennas, " Peter Peregrinus Ltd., IEE Engineers IV series, 1989

8. T. Itoh, "Numerical techniques for microwave and millimeter-wave passive structures, " John Wiley & Sons, Inc., New York, 1989
9. K.C. Gupta, M.D. Abouzahara and Vijai K. Tripathi "CAD of microstrip circuits and antennas - Volume I and II, " Short course conducted in connection with the 4th International symposium on recent advances in microwave technology, New Delhi, India, 1993.
10. F. Gardiol, "Microstrip circuits, " John Wiley & Sons, Inc., New York, 1994.
11. Stephen Wolfram, "The *MATHEMATICA* book, "Wolfram Research Inc,Champaign, USA, 1996

JOURNAL/SYMPOSIUM PAPERS

12. J.F. Ramsay, "Microwave antenna and waveguide technique before 1900, " *Proc. IRE*, vol. 46, pp. 405-415, Feb. 1958
13. J.H. Richmond, "A wire-grid model for scattering by conducting bodies, " *IEEE Trans. Antennas Propagat.*, vol. AP-14, pp. 782-786, Nov. 1966.
14. W.E. Gordon, "A hundred years of radio propagation, " *IEEE Trans. Antennas Propagat.*, vol. AP-33, pp. 126-130, Feb. 1985.
15. J.D. Kraus, "Antennas since Hertz and Marconi, " *IEEE Trans. Antennas Propagat.*, vol. AP-33, pp. 131-137, Feb. 1985.
16. H.A. Wheeler, "Antenna topics in my experience, " *IEEE Trans. Antennas Propagat.*, vol. AP-33, pp. 144-151, Feb. 1985.
17. R.E. Munson, "Conformal microstrip antennas, " *Microwave Journal.*, pp. 91-109, Mar. 1988.
18. J.D. Kraus, "Antennas: our electronic eyes and ears, " *Microwave Journal.*, pp. 77-92, Jan. 1989.
19. G.A. Deschamps, "Microstrip microwave antennas, " presented at the 3rd USAF Symp. on Antennas, 1953.
20. H. Gulton and G. Bassinot, "Flat aerial for ultra high frequencies, " French Patent No. 703113, 1955.
21. E.V. Byron, "A new flush-mounted antenna element for phased array applications, " in *Proc. Phased-Array Antenna Symp.*, pp. 187-192, 1970.
22. J.Q. Howell, "Microstrip antennas, " in *Dig. Int. Symp. Antennas Propagat. Soc.*, Williamsburg, VA, pp. 177-180, Dec. 1972.

23. R.E. Munson, "Conformal microstrip antennas and phased arrays," *IEEE Trans. Antennas Propagat.*, vol. AP-22, pp. 74-77, 1974.
24. G.G. Sanford, "Conformal microstrip phased array for aircraft tests with ATS-6," *Proc. Nat. Electronic Conf.*, vol. 29, pp. 252-257, 1974.
25. H.D. Weinschel, "Cylindrical array of circularly polarised microstrip antennas," *IEEE Antennas Propagat. Soc. Int. Symp.*, pp. 177-180, 1975.
26. A.G. Derneryd, "Linear microstrip array antenna," *Chalmer Univ. Technol., Goteborge, Sweden, Tech. Report.*, TR 7505, 1975.
27. A.G. Derneryd, "Linearly polarised microstrip antennas," *IEEE Trans. Antennas Propagat.*, vol. AP-24, pp. 846-851, 1976.
28. J.R. James and C.J. Wilson, "Microstrip antennas and arrays Part-I: Fundamental action and limitations," *IEE Proc. Microwaves, Opt. and Antennas*, vol. 1, pp. 165-174, 1977.
29. P.K. Agarwal and M.C. Bailey, "An analysis technique for microstrip antennas," *IEEE Trans. Antennas Propagat.*, vol. AP-25, pp. 756-759, 1977.
30. Y.T. Lo, D. Solomon, and W.F. Richards, "Theory and experiment on microstrip antennas," *IEEE Antennas Propagat. Soc. Int. Symp.*, pp. 53-55, 1978.
31. Y.T. Lo, W.F. Richards, and D.D. Harrison, "Improved theory for microstrip antennas," *Electron. Lett.*, vol.15, pp. 42-44, 1979.
32. Y.T. Lo, D. Solomon, and W.F. Richards, "Theory and experiments on microstrip antennas," *IEEE Trans. Antennas Propagat.*, vol. AP-27, pp.137-145, 1979.
33. E.L. Newman, "Strip antennas in a dielectric slab," *IEEE Trans. Antennas Propagat.*, vol. AP-26, pp. 647-653, 1978.
34. E.L. Newman and D.M. Pozar, "Electromagnetic modelling of composite wire and surface geometries," *IEEE Trans. Antennas Propagat.*, vol. AP-26, pp. 784-787, 1978.
35. P. Hammer, D. Van Bouchante, D. Verschraevan, and A. Van de Capelle, "A model for calculating the radiation field of microstrip antennas," *IEEE Trans. Antennas Propagat.*, vol. AP-27, pp. 267-270, 1979.
36. K.R. Carver and E.L. Coffey, "Theoretical investigation of the microstrip antenna," *Physic. and Sci. Lab., New Mexico State Univ., Las Cruces, Tech. Report PT 00929*, 1979.
37. J.L. Kerr, "Microstrip antenna developments," in *Proc. Workshop Printed Circuit Antenna Tech., New Mexico State Univ., Las Cruces*, pp. 3/1-20, 1979.
38. D.H. Schaubert and F.G. Farrar, "Some conformal printed circuit antenna designs," in *Proc. Workshop Printed Circuit Antenna Tech., New Mexico State Univ., Las Cruces*, pp. 5/1-21, 1979.

39. J. McIlvenna and N. Kernweis, "Variations on the circular microstrip antenna element, "in *Proc. Workshop Printed Circuit Antenna Tech., New Mexico State Univ., Las Cruces*, pp. 25/1-15, 1979.
40. S. Bartely and D. Huebner, "A dual beam low sidelobe microstrip array, " *IEEE Antennas Propagat. Soc. Int. Symp.*, pp. 399-402, 1979.
41. J. Yee and W. Furlong, "An extremely light weight fuselage integrated phased array for airborne applications, " *Proc. Workshop on Printed Circuit Antenna Tech.*, pp.15, Oct. 1979.
42. F. Cipolla, "A 7.5 GHz microstrip phased array for aircraft to satellite communications, " *Proc. Workshop on Printed Circuit Antenna Tech.*, pp.19, Oct. 1979.
43. L. Murphy, "SEASAT and SIR-A microstrip antennas, " *Proc. Workshop on Printed Circuit Antenna Tech.*, pp.18, Oct. 1979.
44. M. Weiss and R. Cassel, "Microstrip millimeter wave antenna study, " *Tech. Rept., CORADCOM - 77-0158 F*, Apr. 1979.
45. C. Wood, "Curved microstrip lines as compact wideband circularly polarised antennas, " *IEE Journal of Microwaves, Optics and Acoustics*, vol. 3, pp. 5-13, 1979
46. J.W. Mink, "Circular ring microstrip antenna elements, " *IEEE Antennas Propagat. Soc. Int. Symp.*, Quebec City, Canada, June 1980.
47. R. Chadha and K.C. Gupta, "Green's functions for triangular segments in planar microwave circuits, " *IEEE Trans. Microwave Theory Tech.*, vol. MTT-28, pp. 1139-1143, Oct. 1980.
48. L.C. Shen, "The elliptical microstrip antenna with circular polarisation, " *IEEE Trans. Antennas Propagat.*, vol. AP-29, pp. 95-99, 1981.
49. S.A. Long, L.C. Shen, D.H. Schaubert, and F.G. Farrar, "An experimental study of the circular polarised elliptical printed circuit antenna, " *IEEE Trans. Antennas Propagat.*, vol. AP-29, pp. 267-270, 1981.
50. R. Chadha and K.C. Gupta, "Green's functions for circular sectors, annular rings, and annular sectors in planar microwave circuits, " *IEEE Trans. Microwave Theory Tech.*, vol. MTT-29, pp. 68-71, Jan. 1981.
51. R. Chadha and K.C. Gupta, "Segmentation technique using impedance matrices for analysis of planar microwave circuits, " *IEEE Trans. Microwave Theory Tech.*, vol. MTT-29, pp. 71-74, Jan. 1981.
52. P.C. Sharma and K.C. Gupta, "Desegmentation method for analysis of two-dimensional microwave circuits, " *IEEE Trans. Microwave Theory Tech.*, vol. MTT-29, pp. 1094-1098, Oct. 1981.

53. E.H. Newman and P. Tulyathan, "Analysis of microstrip antennas using moment methods," *IEEE Trans. Antennas Propagat.*, vol. AP-29, pp. 47-53, 1981.
54. K.R. Carver and J.W. Mink, "Microstrip antenna technology," *IEEE Trans. Antennas Propagat.*, vol. AP-29, pp. 2-24, 1981
55. T. Itoh and W. Menzel, "A full-wave analysis method for open microstrip structures," *IEEE Trans. Antennas Propagat.*, vol. AP-29, pp. 63-68, 1981
56. K.C. Gupta, "Two-dimensional analysis of microstrip circuits and antennae," *J. IEEE* vol. 28, no. 7, pp. 346-364, 1982.
57. C. Wood, "Improved bandwidth of microstrip antennas using parasitic elements," *IEE Proc. Pt. H*, vol. 127, pp. 231-234, 1980.
58. M.D. Deshpande and M.C. Bailey, "Input impedance of microstrip antennas," *IEEE Trans. Antennas Propagat.*, vol. AP-30, pp. 645-650, Jul. 1982.
59. D.R. Poddar, J.S. Chatterjee, and S.K. Choudhary, "On some broadband microstrip resonators," *IEEE Trans. Antennas Propagat.*, vol. AP-31, pp. 193-194, 1983.
60. N. Das and J.S. Chatterjee, "Conically depressed microstrip patch antenna," *IEE Proc. Pt. H.*, vol. 130, pp. 193-196, 1983.
61. M.S. Lee and S.S. Lee, "Design of wideband quasi-log-periodic microstrip antenna," *J. Korean Inst. Electron. Eng.*, vol. 20, pp. 40-44, 1983.
62. E. Lier and K.R. Jakobsen, "Rectangular microstrip patch antennas with Infinite and Finite Ground Plane Dimensions," *IEEE Trans. Antennas Propagat.*, vol. AP-31, pp. 978-984, Nov. 1983.
63. P.C. Sharma and K.C. Gupta, "Analysis and optimised design of single feed circularly polarised microstrip antennas," *IEEE Trans. Antennas Propagat.*, vol. AP-31, pp. 949-955, Nov. 1983.
64. Y. Suzuki and T. Chiba, "Computer analysis method arbitrarily shaped microstrip antenna with multiterminals," *IEEE Trans. Antennas Propagat.*, vol. AP-32, pp. 585-590, Jun. 1984
65. W.F. Richards, Jai-Dong Ou, and S.A. Long, "A theoretical and experimental investigation of annular, annular sector and circular sector microstrip antennas," *IEEE Trans. Antennas Propagat.*, vol. AP-32, pp. 864-867, Aug. 1984.
66. H. Poes and Van De Capelle, "Accurate transmission-line model for the rectangular microstrip antenna," *IEE Proc.*, vol. 131, pt. H., pp. 334-340, 1984.
67. V. Palanisamy and R. Garg, "Rectangular ring and H-shaped microstrip antennas-alternatives to rectangular patch antenna," *Electron. Lett.*, vol.21, no. 19, pp. 874-876, 1985.

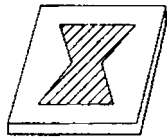
68. P.S. Bhatnagar, J.P. Daniel, K. Mahdjoubi, and C. Terret, Experimental study on stacked triangular microstrip antennas, "*Electro. Lett.*", vol. 22, pp. 864-865, 1985.
69. K.S. Fong, H.F. Pues, and M.J. Withers, "Wideband multilayer coaxial fed microstrip antenna element, "*Electro. Lett.*", vol. 21, pp. 497-499, 1985.
70. C.J. Prior and P.S. Hall, "Microstrip disc antenna with a short circuited annular ring, "*Electro. Lett.*", vol. 21, pp. 719-721, 1985.
71. J.R. Mosig and F.E. Gardiol, "The effect of parasitic elements on microstrip antennas, "*IEEE Antennas Propagat. Soc. Int. Symp.*, Vancouver, pp. 397-400, June 1985.
72. G. Kumar and K.C. Gupta, "Non-radiating edges and four edges gap coupled multiple resonator broadband microstrip antennas, "*IEEE Trans. Antennas Propagat.*, vol. AP-33, pp. 173-178, 1985.
73. G. Kumar and K.C. Gupta, "Directly coupled multiple resonator wideband microstrip antennas, "*IEEE Trans. Antennas Propagat.*, vol. AP-33, pp. 588-593, 1985.
74. V. Palanisamy and R. Garg, "Analysis of arbitrary shaped microstrip patch antennas using segmentation technique and cavity model, "*IEEE Trans. Antennas Propagat.*, vol. AP-34, pp. 1208-1213, Oct. 1986.
75. V. Palanisamy and R. Garg, "Analysis of circularly polarised square ring and crossed strip microstrip antennas, "*IEEE Trans. Antennas Propagat.*, vol. AP-34, pp. 1340-1346, Nov. 1986.
76. C. K. Aanandan and K. G. Nair, "Compact broadband microstrip antenna, "*Electron. Lett.*", vol. 22, no. 20, pp. 1064-1065, 1986.
77. P.S. Hall, "Multioctave bandwidth log-periodic microstrip antenna array, "*IEE Proc.*, vol. 133, pt. H, pp. 127-136, 1986.
78. A. Benalla and K.C. Gupta, "Transmission-line model for two-port rectangular microstrip patches with ports at the nonradiating edges, "*Electron. Lett.* vol. 23pp. 882-884, 1987
79. D.M. Pozar and B. Kaufman, "Increasing the bandwidth of a microstrip antenna through proximity coupling, "*Electron. Lett.*, vol. 23, pp. 368-369, Apr. 1987.
80. D.M. Pozar and S.M. Voda, "A rigorous analysis of a microstripline fed patch antenna, "*IEEE Trans. Antennas Propagat.*, vol. AP-35, pp. 1343-1350, 1987
81. H.Y. Yang and N.G. Alexopoulos, "Gain enhancement methods for printed circuit antennas through multiple superstrates, "*IEEE Trans. Antennas Propagat.*, vol. AP-35, pp. 860-863, Jul. 1987.
82. A. Reineix and B. Jecko, "Analysis of microstrip patch antennas using finite difference time domain method, "*IEEE Trans. Antennas Propagat.*, vol. AP-37, pp. 1361-1369, Nov. 1989.

83. A. Benalla and K.C. Gupta, "Multiport network approach for modelling the mutual coupling effects in microstrip patch antennas and arrays, "*IEEE Trans. Antennas Propagat.*, vol. AP-37, pp. 148-152, Feb. 1989
84. J.L. Drewniak and P.E. Mayes, "ANSERLIN: a broadband, low-profile circularly polarised antenna, "*IEEE Trans. Antennas Propagat.*, vol. AP-37, pp. 281-288, Mar. 1989.
85. J.J.H. Wang and V.K. Tripp, "Design of multioctave spiral mode microstrip antennas, "*IEEE Trans. Antennas Propagat.*, vol. AP-39, pp. 332-335, Mar. 1991.
86. A.J. Svitak, D.M. Pozar, and R.W. Jackson, "Optically fed aperture coupled microstrip patch antennas, "*IEEE Trans. Antennas Propagat.*, vol. AP-40, pp. 85-90, Jan. 1992.
87. A.A. Kishk, "Analysis of spherical annular microstrip antennas, "*IEEE Trans. Antennas Propagat.*, vol. AP-41, pp. 338-343, Mar. 1993.
88. T. Kashiwa, T. Onishi, and I. Fukai, "Analysis of microstrip antennas on a curved surface using the conformal grids FDTD method, "*IEEE Trans. Antennas Propagat.*, vol. AP-42, pp. 423-427, Mar. 1994.
89. K.F. Lee, S.R. Chebolu, W. Chen, and R.Q. Lee, "On the role of substrate loss tangent in the cavity model theory of microstrip patch antennas, "*IEEE Trans. Antennas Propagat.*, vol. AP-42, pp. 110-112, Jan. 1994.
90. H. An, B.K.J.C. Nauwelaens, and A.R. Van de Capelle, "Broadband active microstrip antenna design with the simplified real frequency technique, "*IEEE Trans. Antennas Propagat.*, vol. AP-42, pp. 1612-1619, Dec. 1994.
91. S.A. Bokhari, J.F. Zucher, J.R. Mosig, and F.E. Gardiol, "Near fields of microstrip antennas, "*IEEE Trans. Antennas Propagat.*, vol. AP-43, pp. 188-197, Feb. 1995.
92. X.H. Shen, G.A.E. Vandenbosch, and A.R. Van de Capelle, "Study of gain enhancement method for microstrip antennas using moment method, "*IEEE Trans. Antennas Propagat.*, vol. AP-43, pp. 227-231, Mar. 1995.
93. H. Iwasaki, "A circularly polarised rectangular microstrip antenna using single-fed proximity couple method, "*IEEE Trans. Antennas Propagat.*, vol. AP-43, pp. 895-896, Aug. 1995.
94. D.M. Pozar and S.M. Duffy, "A dual-band circularly polarised aperture coupled stacked microstrip antenna for Global positioning satellite "*IEEE Trans. Antennas Propagat.*, vol. AP-45, pp. 1618-1625, Nov. 1997
95. C.R. Rowell and R.D. Murch, "A capacitively loaded PIFA for compact mobile telephone handsets "*IEEE Trans. Antennas Propagat.*, vol. AP-45, pp. 837-841, May 1997.
96. H. Ohmine, Y. Sunahara, and M. Matsunaga, "An annular-ring microstrip antenna fed by a co-planar feed circuit for mobile satellite communication use, "*IEEE Trans. Antennas Propagat.*, vol. AP-45, pp. 1001-1008, Jun. 1997.

97. V. Palanisamy and R. Garg, "Rectangular ring and H-shaped microstrip antennas-alternatives to rectangular patch antenna," *Electron. Lett.*, vol.21, no. 19, pp. 874-876, 1985.
98. C. K. Aanandan and K. G. Nair, "Compact broadband microstrip antenna," *Electron. Lett.*, vol. 22, no. 20, pp. 1064-1065, 1986.
99. G. Kossiavas, A. Papiernik, J. P. Boisset, and M. Sauvan, "The C-patch: A small microstrip element," *Electron. Lett.*, vol. 25, no. 4, pp. 253-254, 1989.
100. J. L. Volakis and J. M. Jin, "A scheme to lower the resonant frequency of the microstrip patch antenna," *IEEE Microwave and Guided Wave Lett.*, vol. 2, pp. 292-293, Jul. 1992.
101. E. K. N. Yung, W. W. S. Lee, and K. M. Luk, "A dielectric resonator on a microstrip antenna," *IEEE Antennas Propagat. Soc. Int. Symp.*, Michigan, pp. 1504-1507, June 1993.
102. Supriyo Dey, C. K. Aanandan, P. Mohanan, and K. G. Nair, "A new compact circular patch antenna," *IEEE Antennas Propagat. Soc. Int. Symp.*, Washington, pp. 822-825, June 1994.
103. M. Sanad, "Effect of the shorting posts on short circuit microstrip antennas," *IEEE Antennas Propagat. Soc. Int. Symp.*, Washington, pp. 794-797, June 1994.
104. Y. Hwang, Y. P. Zhang, G. X. Zheneg, and T. K. C. Lo, "Planar inverted F antenna loaded with high permittivity material," *Electron. Lett.*, vol. 31, pp. 1710-1712, 1995.
105. Y. Zhang, T. K. Lo, and Y. Hwang, "A dielectric-loaded miniature antenna for microcellular and personal communications," *IEEE Antennas Propagat. Soc. Int. Symp.*, California, pp. 1152-1155, June 1995.
106. S. Dey, S. Chebolu, R. Mittra, I. Park, T. Kobayashi, and M. Itoh, "A compact microstrip antenna for CP," *IEEE Antennas Propagat. Soc. Int. Symp.*, California, pp. 982-985, June 1995.
107. M. G. Douglas and R. H. Johnston, "A compact two way diversity microstrip U-patch antenna," *IEEE Antennas Propagat. Soc. Int. Symp.*, California, pp. 978-981, June 1995.
108. Mohamed Sanad, "Double C-patch antennas having different aperture shapes," *IEEE Antennas Propagat. Soc. Int. Symp.*, California, pp. 2116-2119, June 1995.
109. Jacob George, P. Mohanan, and K. G. Nair, "A broadband low profile microstrip circular patch antenna," *IEEE Antennas Propagat. Soc. Int. Symp.*, California, pp. 700-703, June 1995.
110. R. Waterhouse, "Small microstrip patch antenna," *Electron. Lett.*, vol. 31 no. 8, pp. 604-605, 1995.
111. R. B. Waterhouse, "Performance of microstrip patches incorporating a single shorting post," *IEEE Antennas Propagat. Soc. Int. Symp.*, Maryland, pp. 29 - 32, July 1996.

112. M. Sanad, "A compact dual-broadband microstrip antenna having both stacked and planar parasitic elements, " *IEEE Antennas Propagat. Soc. Int. Symp.*, Maryland, pp. 6 - 9, July 1996.
113. I. Park and R. Mittra, "Aperture-coupled quarter-wave microstrip antenna, " *IEEE Antennas Propagat. Soc. Int. Symp.*, Maryland, pp.14-17, July 1996.
114. M. Sanad, "Non-planar shorted double C-patch antennas for portable communication equipment, " *IEEE Antennas Propagat. Soc. Int. Symp.*, Maryland, pp. 738 - 741, July 1996.
115. S. Dey and R. Mittra, "Compact microstrip patch antenna, " *Microwave Optical Technol. Lett.*, vol. 13, no. 1, pp. 12-14, Sept 1996.
116. T. K. Lo, C. O. Ho, Y. Hwang, E. K. W. Lam, and B. Lee, "Miniature aperture-coupled microstrip antenna of very high permittivity, " *Electron. Lett.*, vol. 33, no. 1, pp. 9-10, 1997.
117. K. L. Wong and S. C. Pan, "Compact triangular microstrip antenna, " *Electron. Lett.*, vol. 33, no. 6, pp. 433-434, 1997.
118. K. L. Wong and W. S. Chen, "Compact microstrip antenna with dual frequency operation, " *Electron. Lett.*, vol. 33, no. 8, pp. 646-647, 1997.
119. K. L. Wong and Y. F. Lin, "Small broadband rectangular microstrip antenna with chip-resistor loading, " *Electron. Lett.*, vol. 33, no. 9, pp. 11593-1594, 1997.
120. C. L. Tang, H. T. Chen, and K. L. Wong, "Small circular microstrip antenna with dual frequency operation, " *Electron. Lett.*, vol. 33, no. 13, pp. 1112-1113, 1997.
121. D. Singh, P. Gardner and P. S. Hall, "Miniaturised microstrip antenna for MMIC applications, " *Electron. Lett.*, vol. 33, no. 22, pp. 1830-1831, 1997.
122. R. B. Waterhouse, "Printed antenna suitable for mobile communication handsets, " *Electron. Lett.*, vol. 33, no. 22, pp. 1831-1832, 1997.
123. K. L. Wong and J. Y. Wu, "Single-feed small circularly polarised square microstrip antenna, " *Electron. Lett.*, vol. 33, no. 22, pp. 1833-1834, 1997.
124. R. B. Waterhouse, "Small printed antennas with low cross-polarised fields, " *Electron. Lett.*, vol. 33, no. 15, pp. 1280-1281, 1997.
125. K. L. Wong and K. P. Yang, "Small dual-frequency microstrip antenna with cross slot, " *Electron. Lett.*, vol. 33, no. 23, pp. 1916-1917, 1997.
126. D. M. Kokotoff, R. B. Waterhouse, and J. T. Aberle, "An annular ring coupled to a shorted patch, " *IEEE Trans. Antennas Propagat.*, vol. AP- 45, no. 5, pp. 913-914, May 1997.
127. K. L. Wong, C. L. Tang, and H. T. Chen, "A compact meandered circular microstrip antenna with a shorting pin, " *Microwave Optical Technol. Lett.*, vol. 15, no. 3, pp. 147-149, June 1997.

128. H.T. Chen, "Experimental results of compact microstrip antennas, " *IEEE Antennas Propagat. Soc. Int. Symp.*, pp. 932 - 935, July 1997.
129. R.B. Waterhouse, S.D. Targonski, and D.M. Kokotoff, "Improving the mechanical tolerances and radiation performance of shorted patches, " *IEEE Antennas Propagat. Soc. Int. Symp.*, pp. 1852 - 1855, July 1997.
130. J. H. Lu, C. L. Tang, and K. L. Wong, "Slot-coupled small triangular microstrip antenna, " *Microwave Optical Technol. Lett.*, vol. 16, no. 6, pp. 371-374, Dec. 1997.
131. K. L. Wong and K. P. Yang, "Modified planar inverted F antenna, " *Electron. Lett.*, vol. 34, no. 1, pp. 7-8, 1998.
132. S. K. Satpathy, K. P. Ray, and G. Kumar, "Compact shorted variations of circular microstrip antennas, " *Electron. Lett.*, vol. 34, no. 2, pp. 137-138, Jan. 1998.
133. C. Y. Huang, J. Y. Wu, C. F. Yang, and K. L. Wong, "Gain-enhanced compact broadband microstrip antenna, " *Electron. Lett.*, vol. 34, no. 2, pp. 138-139, Jan. 1998.
134. A. S. Vaello and D. S. Hernandez, "Printed antennas for dual-band GSM/DCS 1800 mobile handsets, " *Electron. Lett.*, vol. 34, no. 2, pp. 140-141, Jan. 1998.
135. J.S. Dahele and A.L. Cullen, "Electric probe measurements on microstrip, " *IEEE Trans. Microwave Theory Tech.*, vol. MTT-28, pp. 752-755, Jul. 1980.
136. W.C. Chew and J.A. Kong, "Effect of fringing fields on the capacitance of circular disc, " *IEEE Trans. Microwave Theory Tech.*, vol. MTT-28, pp. 98-104, Feb. 1980.
137. D.M. Pozar, "Considerations for millimeterwave printed antennas, " *IEEE Trans. Antennas Propagat.*, vol. AP-31, pp. 740-747, 1985.
138. T. Miyoshi and S. Miyauchi, "The design of planar circulators for wideband operation, " *IEEE Trans. Microwave Theory Tech.*, vol. MTT-28, pp. 210-214, Mar. 1980.
139. H. Iwasaki, "Proximity coupled linearly polarised patch antenna for dual frequency use, " *Electron. Lett.*, vol. 31, pp. 1212-1213, 1995.
140. C. Salvador, L. Borselli, A. Falciani, and S. Maci, "Dual frequency planar antenna at S and X bands, " *Electron. Lett.*, vol. 31, pp. 1706-1707, 1995.
141. H. Iwasaki and Y. Suzuki, "Electromagnetically coupled circular-patch antenna consisting of multilayered configuration, " *IEEE Trans. Antennas Propagat.*, Vol. AP-44, No. 6, pp. 777-780, June 1996.
142. Supriyo Dey, C. K. Aanandan, P. Mohanan and K. G. Nair, "A New Broadband Circular Patch Antenna, " *Microwave Optical Technol. Lett.*, Vol. 7, No. 13, pp. 604-605, Sep. 1994.
143. J. George, M. Deepukumar, C.K. Aanandan, P. Mohanan, and K.G. Nair, "New compact microstrip antenna, " *Electron Lett.*, vol. 32, no. 6, pp. 508-509, 1996.



INDEX

Aanandan, C.K	22, 26	active antennas	24
Agarwal	16	aperture coupling	7
Alexopoulos, N.G	23	aperture model	16
An, H	24	arbitrary shaped antennas	11
Analysis	93	bandwidth enhancement	8, 22
aperture model	113	bandwidth improvement	19
electric field variation	107	basic configuration	3
input impedance	127	boundary conditions	9
magnetic wall model formation	94	broadband microstrip antennas	7
multi-port connection method	100	broadside direction	4
power radiated	120	bunny antenna	17
quality factor	127	buried feed	6
radiation pattern	116	C-shaped	26
resonant frequency	102	cavity model	8, 9, 16
segmentation	95	circular	3, 8
stored energy	125	coaxial feed	5
Antennas	1	compact microstrip antenna	8, 26, 29, 32
array antennas	2	desegmentation technique	20
digital beam forming	2	dielectric constant	19
electromagnetic horn	2	dielectric losses	19
electronic eyes and ears	1	dielectric substrate	3
helices	2	drawbacks	3
linear conductor	2	drum-shaped microstrip antenna	32
loops	2	dual frequency operation	17
reflectors	2	electric walls	9
wire antennas	2	electric surface currents	9
Antennas; microstrip antennas	2, 19	elliptical antenna	18

excitation techniques	4	Bhatnagar	21
finite difference time domain	8, 10, 23	Bokhari, S.A	24
finite element method	8, 10, 17	Books	160
generalised transmission line model	24	Bose, J.C	1
Green's function	10, 20	short waves	1
ground plane	20	Broadband dual frequency microstrip antenna	147
H-shaped	21, 26	comparable gain	148
ideal transmission line	9	electromagnetically	148
impedance bandwidth	18, 23	intersection of Two circles	148
integral equation	9	isolation	149
log-periodic	20	linearly polarised	149
magnetic wall	9, 16	proximity coupling	148
Maxwell's curl equations	10	radiation patterns	149
method of moments	9, 16, 24, 25	return loss	149
microstrip antenna	2, 3	RT/Duroid	148
microstrip feed	4, 6	theoretical	151
modelling	15	two frequencies	149
models/techniques	8	Byron	15
multiport network approach	23	Carver	17, 18
new geometrical shapes	8	Cavity model	138
parasitic element	19, 22, 25	Chadha, R	18
parasitic patch	7	Chen, H.T	31
personal communication systems	8	Chen, W.S	29
phased arrays	25	Chiba, T	20
piggy back antenna	17	Cipolla	17
proximity coupled	7, 25	Circular microstrip antenna	156
radiating slots	9	Compact dual frequency microstrip antenna	141
radiation	3	central width	143
radiation fields	16	centre of the radiating edge	143
radiation losses	11	co and cross polar patterns	145
radiation mechanism	4	experimental setup	142
rectangular	3, 8, 9	gain	145
rectangular ring	26	miniature dual frequency	142
Richmond's reaction theorem	16	resonant frequencies	143
segmentation technique	8, 11, 23	shorting pin	141, 142
shorting posts	8, 27	Computed electric field	113
slot feed	7	area requirement	137
spherical annular microstrip	24	cavity model	138
square	9	central width	137
substrate thickness	19	electric field amplitude	138
surface currents	16	experimental investigation	136
surface waves	8	field variation along the periphery	139
thicker substrates	7	frequency tuning	137
transmission line model	8, 9, 21	gain	137
trapezoidal shaped patch	17	impedance	139
triangular	29	less area	137
U patch antenna	27	mode of operation	139
wire grid model	16	port currents	138
Aperture model	113	possible applications	139
aperture field	115	power radiated	139
equivalent aperture antenna	113	radiation pattern	137, 139
infinite conducting plane	116	rectangular	138
magnetic wall model	116	resonant frequency	139
radiation	116	resonating	136
spatial fourier transform	113	segmentation technique	138
Bailey	16	shift of resonant frequency	137
Bandwidth	44	spatial fourier transform	138
Bandwidth enhancement	140	theoretical investigation	138
Bartely	17	triangular	138
Benalla, A	22, 23	Cosine quarter wave	113, 126

Cylindrical dielectric resonator	155	field variation along the periphery	111
Das	20	Green's function	107
Derneryd	9, 15	rectangular	111
Deschamps	2, 15	simultaneous equations	110
Deshpande, M.D	19	Z-directed electric field	111
Dey, S	27, 29	Excitation current density	110
Dielectric resonator loaded microstrip antenna	154	Excitation techniques	36
antenna configuration	155	coaxial feed	36
circular microstrip antenna	156	microstrip feed	36
cylindrical dielectric resonator	155	Fabrication of microstrip antenna	33
cylindrical DR	156	dimensional tolerance	33
impedance bandwidth	154, 155	fast fabrication process	34
radiation patterns	158	photolithographic technique	34, 35
rectangular microstrip	155	FFNT	96
VSWR	158	Fong	21
Douglas, M.G	27	Frequency band	43
Drewniak, J.L	23	Frequency tuning	137
Drum-shaped microstrip antenna	32, 42	Fringing fields	94
analysis	93	Furlong	17
antenna configurations	97	Gain	39, 78, 137, 145
aperture model	41	comparative measurement	39
bandwidth	44	gain transfer method	78
compact microstrip antenna	42	network analyzer	39
electric field variation	41	rectangular antenna	39
frequency tuning	58	relative gain	39
gain	78	wideband ridged horn	78
geometry	42	Gardiol	21
global positioning system	42	Garg, R	21, 22, 26
impedance bandwidth	63	George, J	28
impedance matrix	40	Green's function	103, 107, 111, 112
Japanese drum	42	30°-60°-90° triangular segment	112
mobile satellite communication	42	45°-45°-90° triangular segment	112
personal communication system	42	middle segment	111
phased arrays	42	Green's functions	18, 98
power radiated	41	Guglielmo marconi	2
Q-factor	41	transatlantic communication	2
radiation pattern	41, 44, 63	wireless signal	2
rectangular	40	Gulton	15
resonant frequency	43	Gupta, K.C	18, 19, 22, 23
stored energy	41	Hall	22
theoretical	93	Hammer	16
TM ₀₁ mode	43	Heinrich rudolph hertz	1
TM ₁₀ mode	44	end loaded half-wave dipole	1
triangular	40	square loop antenna	1
UHF and L-bands	42	Hernandez, D.S	32
Duffy, S.M	25	Howell	3, 15
Earlier work in the field	14	Huang, C.Y	32
Effective dielectric constant	99	Hwang, Y	27
rectangular segment	99	Impedance bandwidth	87
triangular segment	99	Impedance matrix element	103, 106
Electric field intensity	39	30°-60°-90° triangular segment	104
network analyzer	39	45°-45°-90° triangular segment	106
probe assembly	39	rectangular segment	103
probe plate	39	Input impedance	127
semirigid cable	39	complex permittivity	128
Electric field variation	107	effective loss tangent	127
computed electric field	113	impedance matrix elements	128
cosine quarter wave	113	energy lost	127
electric field at a point	110	wave number	128
excitation current density	110	Interconnection constraints	102

Intersection of two circles	148	Newman	16, 18
Itoh, T	19	Ohmine, H	25
Iwasaki, H	25	Palanisamy, V	21, 22, 26
James	16	Pan, S.C	29
Jecko, B	23	Park, I	28
Jin, J.M	26	Personal communication systems	2
Johnston, R.H	27	Poddar, D.R	20
Journal/symposium papers	161	Possible applications	139
Kashiwa, T	24	global positioning system	139
Kaufman, B	22	MMICs	139
Kerr	17	personal communication systems	139
Kishk, A.A	24	Power radiated	120
Kokotoff, D.M	30	computation	125
Kossiavas, G	26	radiated power	125
Kraus, J.D	2	Pozar, D.M	22, 25
Kumar, G	22	Principal plane patterns	120
Lee	20	Prior	21
Lee, K.F	24	Proximity coupling	148
Lier, E	20	Pues, H	21
Lin, Y.F	29	Quality factor	127
Linearly polarised	149	total power lost	127
Lo	16	total stored energy	127
Lo, T.K	29	Radiating aperture	116
Long	18	Radiation pattern	37, 87, 116, 137
Lu, J.H	31	aperture excitation fields	117
Magnetic wall model	94, 116	computation of radiation patterns	117
fringing fields	94	far field components	118
height of the substrate	95	field variations along the periphery	116
outward Edge extensions	94	Fourier transform	119
virtual patch geometry	95	<i>MERL soft</i>	38
<i>MATHEMATICA</i>	41	network analyzer	38
Mayes, P.E	23	positioner controller	38
Mcilvenna	17	principal plane patterns	120
Merl soft	36, 37	radiating aperture	116
Methodology	33	ridged horn	37
analysis of the antenna	40	spatial fourier transforms	118
bandwidth	36	total far field	119
electric field intensity	39	Radiation patterns	44
excitation techniques	36	Ramsay	2
fabrication of microstrip antenna	33	Rayleigh-ritz method	20
gain	39	Rectangular microstrip	155
radiation pattern	37	References	160
resonant frequency	36	Reineix, A	23
return loss measurement	36	Resonant frequency	44, 49, 82, 102, 136
Miniature dual frequency	142	cavity under the patch	103
Mink	18	Green's function	103
Mitra, R	28, 29	input reactance	102
Mobile satellite communication systems	2	Return loss	36
Modeling of fringing field	135	setup for the measurement	37
Mosig	21	RF currents	109
Multi-port connection method	100	Richards, W.F	21
connected ports	100	Richmond's reaction method	9
external	100	Rowell, C.R	25
interconnection constraints	102	Sanad, M	27-29
Munson	3, 9, 15	Sanford	15
Murch, R.D	25	Satpathy, S.K	31
Murphy	17	Schaubert	17
Nair, K.G	22, 26	Segmentation	95
Near field probing	78	Green's function	95
Network analyzer	36	rectangular	95

segmentation into five segments	97	Z-matrices	98, 100, 102, 107
segmented antenna Geometry	98	Green's functions	98
triangular	95	Zhang, Y	27
Sharma, P.C	18, 20		
Shen	18		
Shen, X.H	25		
Shorting pin	141, 142		
Singh, D	30		
Spatial fourier transform	113, 118, 138		
Stnt	96		
Stored energy	125, 126		
cosine quarter wave variation	126		
electric and magnetic field energy	125		
rectangular segment	126		
stored energy under a segment	125		
total stored energy	125		
triangular segment	126		
Suzuki, Y	20		
Svitak, A.J	24		
Tang, T.L	30		
Theoretical interpretations	93		
Theoretical investigation	138		
TM ₀₁ mode	49		
central width	49		
frequency tuning	58		
gain	78		
gain transfer method	78		
impedance bandwidth	63		
linearly polarised	49		
mode identification	78		
near field probing	78		
percentage bandwidth	63		
physical area	58		
radiated fields	49		
radiation pattern	63		
resonant frequency	49, 58		
TM ₁₀ mode	82, 92		
central width	82		
impedance bandwidth	87		
radiation pattern	87		
resonant frequency	82		
unmodified side	82		
Tripp, V.K	23		
Tsnt	96		
Uhf and l-bands	42		
Vaello, A.S	32		
Volakis, J.L	26		
Wang, J.J.H	23		
Waterhouse, R	28		
Waterhouse, R.B	28, 30		
Weinschel	15		
Weiss	17		
Wilson	16		
Wong, K.L	29-31		
Wood	17, 19		
Wu, J.Y	30		
Yang, H.Y	23		
Yang, K.P	30, 31		
Yee	17		
Yung, E.K.N	26		



LIST OF PUBLICATIONS OF THE AUTHOR

INTERNATIONAL JOURNAL

1. New Compact Microstrip Antenna, *Electronics Letters*(U.K), vol.32, No. 6, pp. 508-509, 1996
2. Broadband Dual Frequency Microstrip Antenna, *Electronics Letters*(U.K), vol. 32, No. 17, pp.1531-1532, 1996
3. Dielectric Resonator loaded Microstrip Antenna for Enhanced Impedance Bandwidth and Efficiency, *Microwave and Optical Technology Letters* (USA), vol. 17, No.3, pp.205-207, 1998
4. Dual Frequency Miniature microstrip antenna (accepted for publication in *Electronics Letters*, UK, Issue No. 12, 1998)
5. Analysis of a compact microstrip antenna (accepted for publication in *IEEE Transactions on Antennas and propagation*)

SEMINAR / SYMPOSIA

1. A Broadband Low Profile Microstrip Circular Patch Antenna, *Proc. IEEE AP-S*

- International Symposium (USA), 700-703, 1995*
2. A method for Lowering the Resonant Frequency of a Rectangular Microstrip Antenna, *IEEE AP-S International Symposium (USA), 1996*
 3. A Peripherally fed Broadband Modified Circular Microstrip Antenna, *IEEE AP-S International Symposium (USA), 1996*
 4. Investigations on the band-width enhancement effect of dielectric resonator loaded microstrip antenna, *presented in the Asia Pacific Microwave Conference APMC-96*
 5. A broad band microstrip antenna for dual frequency operation, *presented in the Asia Pacific Microwave Conference APMC-96*
 6. Microwave Dielectric Properties of $\text{Ba}(\text{B}'_{1/2}\text{Nb}_{1/2})\text{O}_3$ {B'=La, Pr, Nd, Sm, Eu, Gd, Tb, Dy, Er, Y & In} Ceramics, *Proc. of Advances in Microwaves and Light waves, New Delhi, 1998.*
 7. A modified compact circular patch antenna, *Proc. of the National Symposium on Antennas and Propagation (APSYM - 94), Cochin 682 022, 1994.*
 8. Design and development of a high Tc superconducting low pass filter at microwave frequencies, *Proc. of the National Symposium on Antennas and Propagation (APSYM - 94), Cochin 682 022, 1994.*
 9. Dielectric resonator loaded compact microstrip circular patch antenna, *Proc. of the National Symposium on Antennas and Propagation (APSYM - 96), Cochin 682 022, 1996.*

BIO-DATA OF JACOB GEORGE

Department of Electronics
 Cochin University of Science and Technology, Cochin 682 022
 Kerala, India
 Phone: 91 484 532161, Fax: 91 484 532800
 E-mail: cusatdoe@md2.vsnl.net.in

OBJECTIVE

To involve in Research and Development activities in the field of Antennas, numerical modeling and biomedical applications of electromagnetics.

AREAS OF INTEREST

Computer aided design and development of Microstrip Antennas, biomedical applications of electromagnetics and high frequency measurements.

EDUCATION

a) Master of Science in Electronics Science

Specialization in Artificial Intelligence and Robotics, Cochin University of Science and Technology, Cochin, India (April 1993).

Score Obtained - 1965 / 2400 (Fist rank with distinction)

Project and Thesis

Design and Implementation of a Microprocessor based Distributed Digital Control System for Robotics and Industrial Process Control Applications.

b) Bachelor of Science in Physics

Mahatma Gandhi University, Kottayam , Kerala, India (July 1990).

Score Obtained - 900 / 1000. (Fist class with distinction)

POST GRADUATE LEVEL COURSES

a) M.Sc Electronics Science

System Theory & Circuit Analysis

Artificial Intelligence

Electronic Circuits

Robotics

Applied Quantum Electronics

Physics of Semiconductor Devices

Communication Electronics

Numerical Methods

Electromagnetic Theory

IC Technology & Transducers

Control System

Microprocessors

b) Ph.D. course work

Microwave Network and Devices

Microwave Antennas

COMPUTER PROFICIENCY

Operating Systems	DOS, WINDOWS 95/NT, UNIX
General Applications	Proficient in MS OFFICE.
Technical Applications	MATHEMATICA, MATLAB, PUFF, LIBRA
Languages	HP BASIC, VISUAL BASIC, FORTRAN , C, LISP, PROLOG, PASCAL.

RESEARCH AND WORK EXPERIENCE

1. Currently working as a **Senior Research Fellow** in the Department of Electronics, Cochin University of Science and Technology, Cochin, India. Present area of research is the theoretical simulation of the characteristics of microstrip antennas (NOV 1996 onwards).
2. Worked as a **Junior Research Fellow** in Department of Electronics, Cochin University of Science and Technology, Cochin, India. Was engaged in full time research in Microstrip antenna design and evaluation. Results include two novel Microstrip patch antenna configurations. (AUG. 1993 - OCT 1996).
3. Worked as a **co-op engineer** at Allied Electronics, Madras, India.(SEPT. 92 - JUNE 93)

TECHNICAL SEMINARS ATTENDED

1. Attended and presented technical papers in the VIII ASIA PACIFIC MICROWAVE CONFERENCE (APMC '96) held at New Delhi.

PROJECTS COMPLETED

1. Conceived, fabricated and tested one new Microstrip antenna geometry for broadband, multi-port, dual frequency operation (please see the list of publications).
2. Conceived, fabricated and tested one new Compact Microstrip antenna geometry for applications which demand compact antennas (please see the list of publications).
3. Designed a Microprocessor Based DC Servomotor Control System with Optical Encoder.
4. Designed, fabricated and successfully tested a Shared Memory Data Transfer Scheme for Inter-Processor communication in a Parallel Processing environment using multiple microprocessors.
5. Designed and fabricated a Distributed Digital Control System for Robotic actuator control.
6. Developed Visual BASIC code for the automatic radiation pattern measurement using *hp* 8510B Network Analyzer
7. Worked towards the development of a computer controlled antenna positioner for the automatic radiation pattern measurement

ACADEMIC HONORS

1. First Class with Distinction (equivalent to highest honor) in B.Sc. (Bachelor of Science)
2. First Class with Distinction and First Rank (equivalent to highest honor) in M.Sc. (Master of Science)

AWARDS & FELLOWSHIPS

1. First rank in the Msc Degree Examination, Cochin University of Science and Technology, Cochin, India
2. Qualified in the National Eligibility Test for Lectureship and Research fellowship (*University Grants Commission, Govt. of India*)
3. Senior Research Fellowship (*Council of Scientific and Industrial Research, Govt. of India*)